IMPLEMENTATION OF A VECTOR CONTROLLED INDUCTION MOTOR DRIVE

A THESIS SUBMITTED TO
THE GRADUATE SCHOOL OF NATURAL AND APPLIED SCIENCES
OF
THE MIDDLE EAST TECHNICAL UNIVERSITY

BY

AKIN ACAR

IN PARTIAL FULFILMENT OF THE REQUIREMENTS FOR THE DEGREE OF
MASTER OF SCIENCE
IN
THE DEPARTMENT OF ELECTRICAL AND ELECTRONICS ENGINEERING

JANUARY 2004

Approval of the Graduate School of Natural and Applied Sciences

_____

Prof. Dr. Canan ÖZGEN
Director

I certify that this thesis satisfies all the requirements as a thesis for the degree of Master of Science.

_____

Prof. Dr. Mübeccel DEMİREKLER
Head of the Department

This is to certify that we have read this thesis and that in our opinion it is fully adequate, in scope and quality, as a thesis for the degree of Master of Science.

_____

Prof. Dr. H. Bülent ERTAN
Supervisor

Examining Committee Members

Prof. Dr. Muammer ERMİŞ(chairman) _____

Prof. Dr. H.Bülent ERTAN _____

Prof. Dr. Yıldırım ÜÇTUĞ _____

Assist. Prof. Dr. Ahmet M. HAVA _____

Tolga ÇAMLIKAYA(Msc) _____

ABSTRACT

IMPLEMENTATION OF A VECTOR CONTROLLED INDUCTION MOTOR DRIVE

ACAR, Akın
M.Sc., Department of Electrical and Electronics Engineering
Supervisor: Prof. Dr. H. Bülent ERTAN

January 2004, 138pages

High dynamic performance, which is obtained from dc motors, became achievable from induction motors with the recent advances in power semiconductors, digital signal processors and development in control techniques. By using field oriented control, torque and flux of the induction motors can be controlled independently as in dc motors. The control performance of field oriented induction motor drive greatly depends on the correct stator flux estimation. In this thesis voltage model is used for the flux estimation. Stator winding resistance is used in the voltage model. Also leakage inductance, mutual inductance and referred rotor resistance values are used in vector control calculations.

Motor control algorithms use motor models, which depend on motor parameters, so motor parameters should be measured accurately. Induction motor parameters may be measured by conventional no load and locked rotor test.

However, an intelligent induction motor drive should be capable of identifying motor parameters itself.

In this study parameter estimation algorithms are implemented and motor parameters are calculated. Then these parameters are used and rotor flux oriented vector control is implemented. Test results are presented.

Keywords: Field oriented control, parameter estimation, induction motor drive.

ÖZ

VEKTÖR KONTROLLU ASENKRON MOTOR SÜRÜCÜ UYGULAMASI

ACAR, Akın
Yüksek Lisans, Elektrik Elektronik Mühendisliği Bölümü
Tez Danışmanı: Prof. Dr. H. Bülent ERTAN

Ocak 2004, 138 sayfa

Doğru akım motorlarından elde edilebilen yüksek dinamik performans, güç yarı iletkenleri, dijital sinyal işleyicileri ve kontrol tekniklerindeki gelişmelerle birlikte, asenkron motorlarla ulaşılabilir olmuştur. Asenkron motorlarda alan yönlendirmeli kontrolun kullanılmasıyla, dc motorlarda olduğu gibi , akı ve moment bağımsız olarak control edilebilir. Alan yönlendirmeli indüksiyon motorunun performansı stator akısının doğru tahminine bağlıdır. Bu tezde stator akısının tahmini için gerilim modeli kullanılmıştır. Gerilim modelinde stator sargı direnci kullanılmaktadır. Ayrıca vektör kontrol hesaplamalarında kaçak indüktans, ortak indüktans ve rotor direncide kullanılmaktadır.

Motor kontrol algoritmaları motor parametrelerine bağımlı motor modelleri kullanır. Motor parametreleri kilitli rotor testi ve boşta çalışma testi ile elde edilebilir. Ancak akkıllı bir asenkron motor sürücüsü, motor parametrelerini kendi başına belirleme yeteneğine sahip olmalıdır.

Bu çalışmada parametre tahmini ile ilgili kodlar denenmiş ve motor parametreleri hesaplanmıştır. Daha sonar bu parametreler kullanılarak alan yönlendirmeli vektör kontrol uygulaması yapılmıştır. Test sonuçları sunulmuştur.

Anahtar Kelimeler: Alan yönlendirmeli kontrol, parametre tahmini, asenkron motor sürücü.

ACKNOWLEDGEMENTS

I would like to thank my family for their continuous support, confidence and reassurance.

I would like to express my sincere gratitude to Prof. Dr. H. Bülent ERTAN for his guidance, patient supervision and support that made this study possible.

I would like to thank Tolga ÇAMLIKAYA, Erdal BİZKEVELCİ, Arif YILMAZ, Mustafa AYDIN, Barış ÇOLAK, Çağlar OZYURT, Levent YALÇINER Ertan MURAT, Cüneyt KARACAN, Serkan ŞEDELE, for their precious suggestions, encouragement and willingness for help in all phases of this study.

Also I would like to thank my friends Özgür ÖZKAN, Barış UZUNLAR, Feza TAŞ, Berkay ÖNSÜ for their encouragement and support during my thesis.

TABLE OF CONTENTS

LIST OF TABLES

TABLE

LIST OF FIGURES

FIGURE

LIST OF SYMBOLS

i_{sa} : Stator a phase current

i_{sb} : Stator b phase current

i_{sc} : Stator c phase current

i_{sd} : d component of stator current

i_{sq} : q component of stator current

i_{rd} : d component of rotor current

i_{rq} : q component of rotor current

$I_{s\alpha}$: α component of stator current

$I_{s\beta}$: β component of stator current

$\vec{I}_s$: Stator current space phasor

$\vec{\Psi}_r$: Rotor flux space phasor

i_{sdref} : reference value of d axis stator current

i_{sdref} : reference value of q axis stator current

V_{sdref} : reference value of d axis stator voltage

V_{sqref} : reference value of q axis stator voltage

P_{core} : Core loss power

R_{eq} : Equivalent resistance

f : Frequency

L_r : Rotor self inductance

L_s : Stator self inductance

$L_{ıs}$: Stator leakage inductance

$L_{ır}$: Rotor leakage inductance

L_s' : Stator transient inductance

R_s : Stator winding resistance

R_r' : Referred rotor resistance

L_m : Mutual inductance

$\vec{i}_{s\Psi r}$: Stator currents space phasor in the rotor flux oriented reference frame

$\vec{i}_{r\Psi r}$: Rotor currents space phasor in the rotor flux oriented reference frame

$\vec{i}_{mr}$: Rotor magnetizing current space phasor in the rotor flux oriented reference frame

$\Psi_{s\alpha}$: α component of the stator flux

$\Psi_{s\beta}$: β component of the stator flux

$\Psi_{r\alpha}$: α component of the rotor flux

$\Psi_{r\beta}$: β component of the rotor flux

σ : Leakage factor

$V_{s\alpha}$: α component of the stator voltage

$V_{s\beta}$: β component of the stator voltage

T_e : Motor torque

w_e : Angular synchronous speed

τ : Digital filter time constant

τ_s, : stator time

G : Gain block

V_{ref} : Magnitude of the reference voltage

UP : U phase upper IGBT switching signal

VP : V phase upper IGBT switching signal

WP : W phase upper IGBT switching signal

UN : U phase lower IGBT switching signal

VN : V phase lower IGBT switching signal

WN : W phase lower IGBT switching signal

θ : Angle of rotor flux space phasor with respect to α axis

P : Number of pole pairs

I_{so} : Initial value of stator phase current in leakage inductance measurement

X_{ls} : Stator leakage reactance

k_p : Proportional coefficient of PI controller

k_i : Integral coefficient of PI controller

V_m : Motor back emf

ψ_{rmin} : Minimum value of rotor flux magnitude

ψ_{rmax} : Maximum value of rotor flux magnitude

ψ_{rmean} : Mean value of rotor flux magnitude

ψ_{ref} : Reference value of rotor flux magnitude

CHAPTER 1

INTRODUCTION

1.1. General

Variable speed drive systems are essential in many industrial applications [5]. In the past, DC motors were used extensively in areas where variable speed operation was required, since their flux and torque could be controlled easily by the field and armature current.

DC motors have certain disadvantages, which are due to the existence of the commutator and the brushes. That is, they require periodic maintenance; they cannot be used in explosive or corrosive environments and they have limited commutator capability under high speed, high voltage operational conditions. These problems can be overcome by the application of alternating current motors, which can have simple and rugged structure, high maintainability and economy; thay are also robust and immune to heavy overloading [1]. These advantages have recently made induction machines widely used in industrial applications. However, the speed or torque control of induction motors is more difficult than DC motors due to their nonlinear and complex structure. The torque of the DC motors can be controlled by two independent orthogonal variables, stator current and rotor flux, where such a decoupling does not exist in induction motors [5].

Recent years have seen the evolution of a new control strategy for AC motors, called “vector control”, which has made a fundamental change in this picture

of AC motor drives in regard to dynamic performance. Vector control makes it possible to control an AC motor in a manner similar to the control of a seperately excited DC motor, and achieve the same quality of dynamic performance [7]. As for DC machines, torque control in AC machines is achieved by controlling the motor currents. However, in contrast to a DC machine, in AC machine, both the phase angle and the modulus of the current has to be controlled, or in other words, the current vector has to be controlled. This is the reason for the terminology "vector control" [1].

The high quality of the dynamic performance of the seperately excited DC motor is a consequence of the fact that its armature circuit and the field circuit are magnetically decoupled. In a DC motor, the mmf produced by the field current and the mmf produced by the armature current are spatially in quadrature. Therefore there is no magnetic coupling between the field circuit and the armature circuit. Because of the repetitive switching action of the commutator on the rotor coils as the rotor rotates, this decoupling continues to exist irrespective of the angular position and speed of the rotor. This makes it possible to effect fast current changes in the armature circuit, without being hampered in this by the large inductance of the field circuit. Since the armature current can change rapidly, the machine can develop torque and accelerate or decelerate very quickly when speed changes are called for, attain the demanded speed in the fastest manner possible. As in the DC motors, in AC motors also, the torque production is the result of the interaction of a current and a flux. But in the AC induction motor, in which the power is fed on the stator side only, the current responsible for the torque and the current responsible for producing flux are not easily seperable. The underlying principle of vector control is to seperate out the component of the motor current responsible for producing the torque and the component responsible for producing the flux in such a way that they are magnetically decoupled, and then control each independently, in the same way as is done in a seperately excited DC motor [7].

One aspect of DC motor control simplicity is that the independent control of torque and flux in a DC drive is due to the basic design of the motor and, in practice,

is not dependent on the parameters of any particular motor. This is not the case with an AC machine in which, torque and flux control is exercised using standard two-axis machine concepts. For decoupling the torque and flux controlling components of current, motor parameters should be known. All inductance parameters are known to be nonlinear functions of the motor flux level and hence may change either intentionally, under field weakening region, or unintentionally, under detuning of the controller. Electrical parameters of the machine should be well known for field orientation. Parameters are also required for the design of the torque, flux and speed controllers and here the problem is common to both AC vector and DC drive systems. Generally, the settling response of the torque and field controllers is dependent on the stator and rotor time constants, respectively (for the DC machine these are dependent on armature and field time constant which are quite easy to measure). The settling response of the speed controller is, of course, load dependent and is thus normally catered for by variable PID controllers which can be adjusted at commissioning. The need to have a good knowledge of the induction motor parameters in addition to online identification of parameters is a significant disadvantage of vector controlled drives in comparison with the DC systems [7].

1.2. Previous Studies on Vector Control and Parameter Estimation in METU

Some studies have been made in METU about vector control and parameter estimation.

In [4] which is a PhD thesis prepared by Erhan AKIN in 1994, principles of vector control and flux calculation methods are given in detail then experimental results of vector control algorithm using indirect field orientation are presented. In application bang-bang control are used in the inverter stage.

In [5] which is a master thesis prepared by Hayrettin CAN in 1999, voltage model with an open integrator is used for flux estimation and hysteresis band current control is used in the inverter stage for vector control of induction machines.

In [6] which is a master thesis prepared by Metin AKIN in 2002, some studies are made to increase speed range of vector controlled induction motor drive and make drive more efficient. Flux estimation methods are discussed and compared. Cascaded filters are used as integrator to overcome the drift problem while taking integral in voltage model. Also space vector pulse with modulation, which gives better solution, is used instead of hysteresis band current control.

In [7] which is also a master thesis prepared by Ertan MURAT in 2002, parameter dependency of motor controllers are introduced. Theory of parameter estimation methods at standstill is explained in detail and also experimental results of these methods are presented. Finally a new online parameter estimation method is introduced and experimental results of online estimation for stator winding resistance is presented.

1.3. Purpose of The Thesis

The aim of this thesis is to combine previous studies in one drive. Induction motor drive system should calculate the parameters automatically prior to starting the control program by using the inverter itself driving the motor. Then vector control should be operated with these parameters. For this purpose, firstly minor mistakes in the design of the hardware cards were located and corrected. Then vector control algorithms are tested. In the application, cascaded filters were used as integrator in flux estimation, space vector pulse width modulation technique was used to calculate duty cycles for required voltages. PI controller was used to obtain reference voltages from reference currents and then parameter estimation methods recommended in [7] are implemented and tested. Finally repeatability of the algorithms and results was proved. The summary of the thesis is as follows:

In Chapter 2, system hardware modules are explained in detail. Vector control software with theory behind it, which includes PI controller used to obtain reference voltages from reference currents, calculation of duty cycles by using

SVPWM technique for required voltages and flux estimation with cascaded filters, are given in detail. Then parameter estimation software modules are presented. In Chapter 3, improvements made on the hardware are given and the necessity for improvements is explained. In Chapter 4, calibration and testing of the system is presented. In Chapter 5, implementation of self commissioning algorithms are given and Chapter 6 is devoted to discussion and further studies.

CHAPTER 2

SYSTEM DESCRIPTION

2.1. Hardware

This section explains the hardware system in detail. The performance of the system and its calibration is presented in Chapter 4. The block diagram of set-up is shown in Figure 2.1.

.

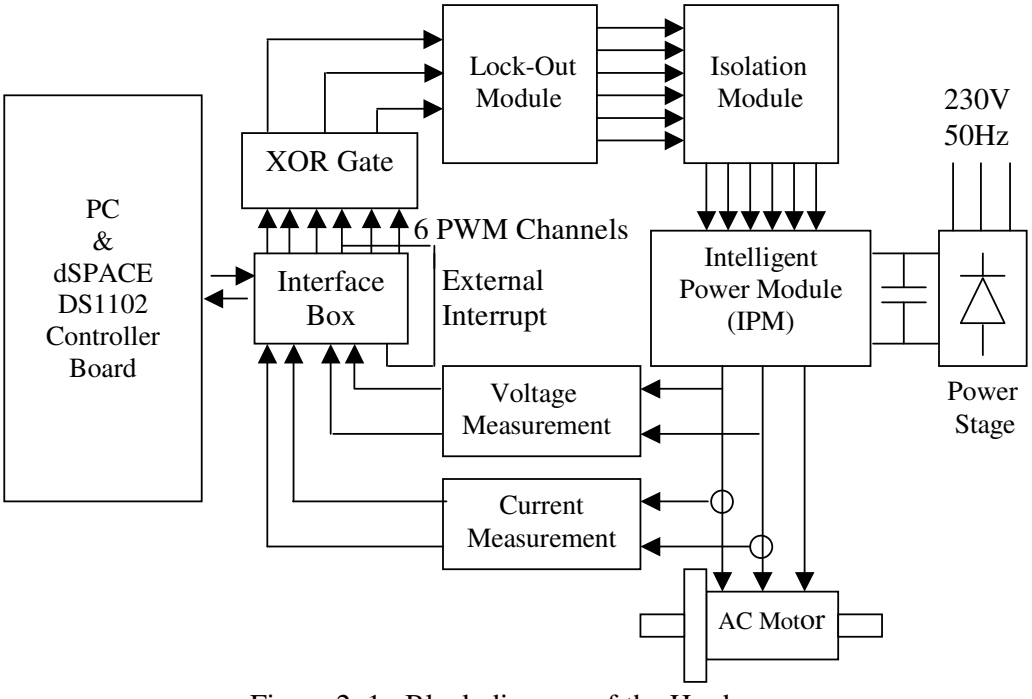

Figure 2. 1. Block diagram of the Hardware

The Hardware set-up used for field orientation control consists of Lock-out module, isolation module, intelligent power module, current and voltage measurement module, power stage module, XOR gate and an interface box to supply communication with DSP. An AC motor is driven with this hardware. The description of each block is given in the following sections.

2.1.1. Power Stage of Inverter

The power stage of the system is shown in Figure 2.2. In order to obtain DC link voltage level, three phase line voltage (V_{rms} = 380V) is converted to DC by using a standard 3-phase uncontrolled bridge rectifier and a filter capacitor is used to eliminate voltage ripples. Stray inductance of DC link connections may cause huge peak on the output current. To reduce the stray inductance, connections between DC link and inverter should be kept as close as possible. To absorb the surge voltage on the DC link, a snubber capacitance is used.

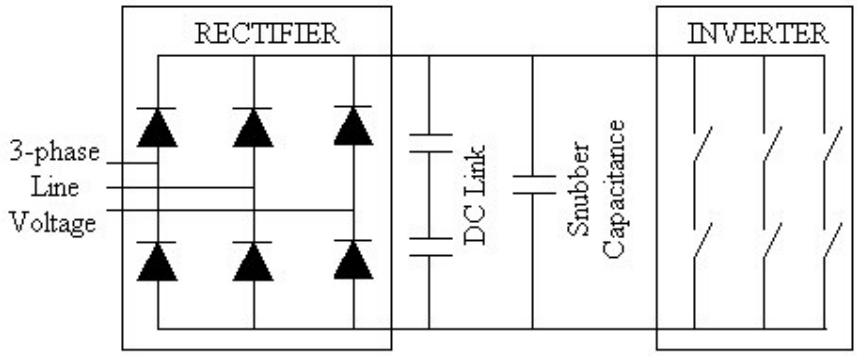

Figure 2. 2. Power stage of the hardware

Uncontrolled bridge rectifier used in power stage of the hardware has a rating of 1600V, 35A. Two capacitors with a rating of 2200μF, 400V each are used in series to eliminate voltage ripples in DC link. Also in power stage, PM25RSB120 intelligent power module (IPM) is used as an inverter.

The technical specifications of IPM is given below:

- 1200 V, 25 A current-sense, 15 kHz IGBT type inverter
- Monolithic gate drive and protection logic
- Detection, protection and status indication circuits for over current, short circuit, over temperature and under voltage.
- Dead time guarantee 2.5 μs.

2.1.2. Isolation Module

The isolation module was developed in [5]. The aim of this circuit is to provide isolation between the intelligent power module (IPM) and the lock-out module. The isolation is realized by using optocoupler ICs. This module isolates the lock-out module signal outputs (UN, UP, VN, VP, WN, WP signals) from the inputs of the IPM. Moreover, the isolation module also isolates fault output signals (FO, UFO, VFO, WFO signals) of the IPM from the lock-out module. Configuration of the isolation module is given in Figure 2.3 and the schematic and PCB circuit of the isolation module are given in Appendix. These circuits and boards are similar to those developed in Reference [5].

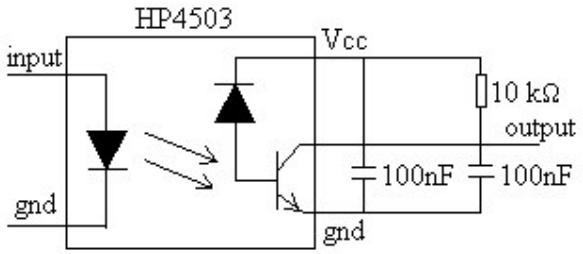

Figure 2. 3. Configuration of the isolation module

The power supply, input and outputs of the isolation module are described in the following sections.

2.1.2.1. Power Supply of The Isolation Module

Power supply of the isolation module is placed on the same board. The isolation module requires 4 isolated 15V DC supplies (on CONN4-CONN7). Digital ground of the 5V supply is also required (on CONN1-CONN3). M57120L and M57140 hybrid ICs are used to provide isolated 15V DC supplies.

2.1.2.2. Input Signals of The Isolation Module

Gets 6 inputs from the lock-out module: UP, UN, VP, VN, WP, WN.

UP = Pulse stream for upper IGBT in U-phase (with dead-time delays)
UN = Pulse stream for lower IGBT in U-phase (with dead-time delays)
VP = Pulse stream for upper IGBT in V-phase (with dead-time delays)
VN = Pulse stream for lower IGBT in V-phase (with dead-time delays)
WP = Pulse stream for upper IGBT in W-phase (with dead-time delays)
WN = Pulse stream for lower IGBT in W-phase (with dead-time delays)

2.1.2.3. Output Signals of The Isolation Module

Generates 4 output signals to lock-out module: FO, UFO, VFO, WFO.

FO = Fault output from all lower IGBT's and thermal protection of the IPM. (Optically isolated)
UFO (or F1) = Fault output from upper IGBT in U phase of IPM (Optically isolated)
VFO (or F2) = Fault output from upper IGBT in V phase of IPM (Optically isolated)
WFO (or F3) = Fault output from upper IGBT in W phase of IPM(Optically isolated)

2.1.3. Lock-Out Module

The lock-out module was developed in [5]. This board provides the dead time delay between the upper and lower IGBT signals of the inverter. Moreover, it also indicates the fault messages, which are generated by the IPM module using LEDs on

the board. The dead time delay between the upper and lower IGBT of the inverter is adjusted to 3 μsec by using calibration potentiometers, which are on the board and can be seen in Figure 2.4. Measurements of dead time durations after the adjustment were performed and presented in section 4.1.4.

P1, P2, P3 output signals of the DSP board, which convey the phase information, are entered to the lock-out module. P1, P2, P3 output signals of the DSP board are first inverted and delayed to trigger the lower and upper IGBTs of the inverter. These phase signals are used to obtain UP, UN, VP, VN, WP, WN signals which are isolated from the IPM by the isolation module. The waveforms of input signals P1, P2, P3 and the output signals UV, UN, VP, VN, WP, WN of the lock-out module are given in Figure 2.5.

The correspondence between the I/O signals and the calibration potentiometers are given as follows:

I/O Relation Logic	Delay Adjustment Potentiometers
WP = P1	POT1
WN = NOT(P1)	POT2
VN = NOT(P2)	POT3
VP = P2	POT4
UP = P3	POT5
UN = NOT(P3)	POT6

Lock-out module has 7 LEDs as shown in Figure 2.4 for indicating the present state of the fault signals, which are created by IPM. The functions of these LEDs are shown as follows:

LED1(red) = IPM disabled due to fault on lower IGBTs (U, V or W) or over-temperature of IPM.

LED2(red) = IPM disabled due to fault on upper IGBT of U-phase of IPM.

LED3(red) = IPM disabled due to fault on upper IGBT of V-phase of IPM.

LED4(red)= IPM disabled due to fault on upper IGBT of W-phase of IPM.

LED5(yellow) = IPM disabled due to user pressing the STOP button.

LED6(yellow) = IPM disabled by the DSP.

LED7(red) = IPM disabled due to over-temperature of IPM.

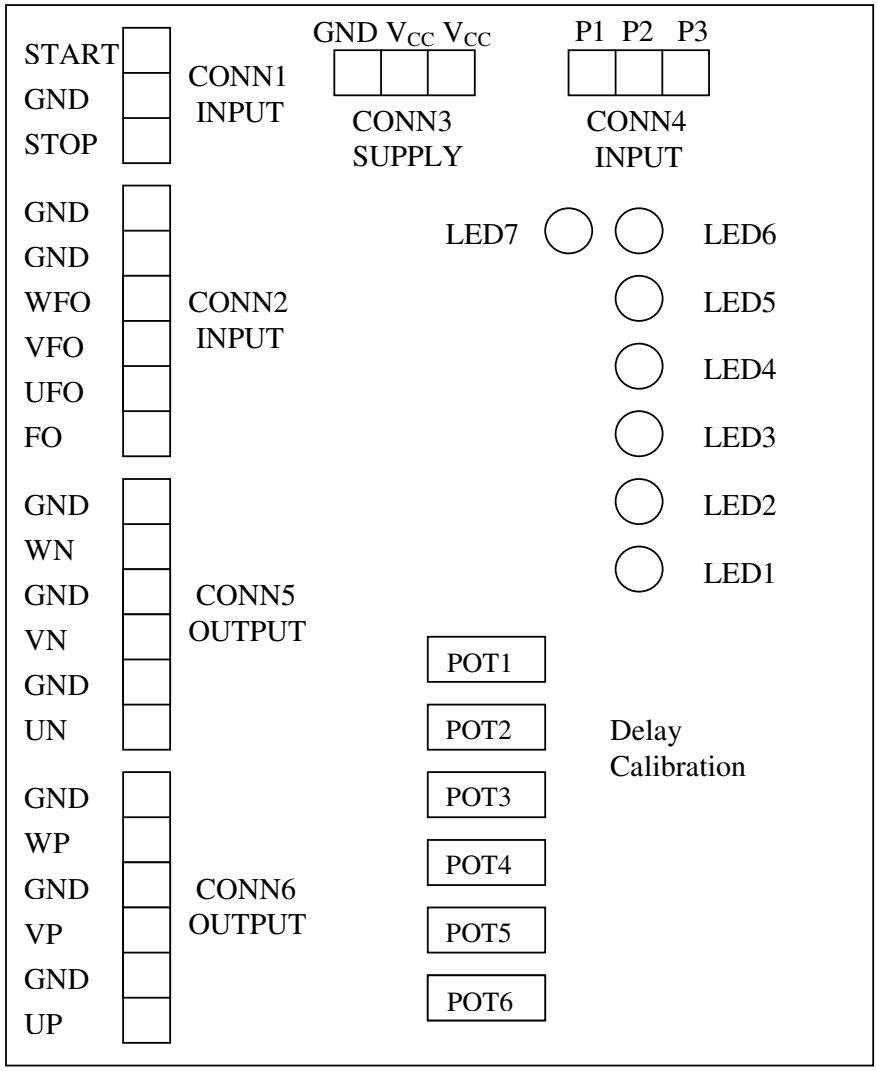

Figure 2. 4. General component layout of the lock-out module

Whenever a fault signal occurs, module becomes disabled automatically. Start button is used to enable the module again.

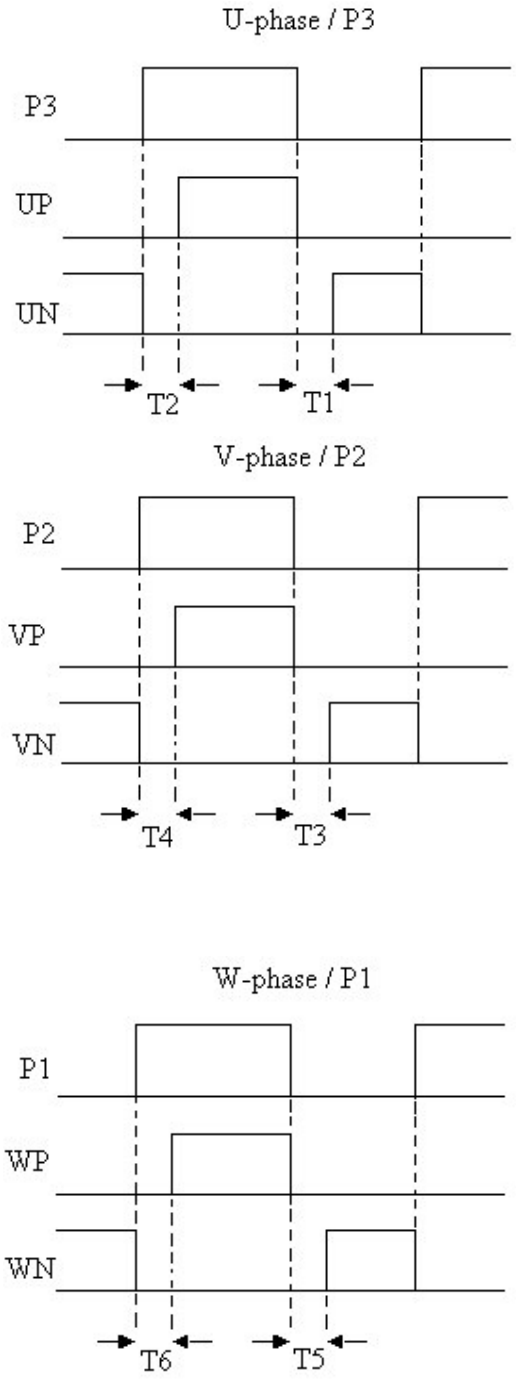

Figure 2. 5. Waveforms of the input signals P1, P2, P3 and the output signals UP, UN, VP, VN, WP, WN of the lock-out module

2.1.4. Current and Voltage Measurement Circuit

Two of the stator currents and voltages are sensed with current and voltage sensors. The measured signals are amplified with an OP-AMP amplifier. The output of the amplifier is filtered with an RC filter. The cut-off frequency of the filter is selected to be as 0.5 kHz. Then filter output is sent to ADC of the DSP. The hardware circuit used for current and voltage measurement is shown in Figure 2.6.

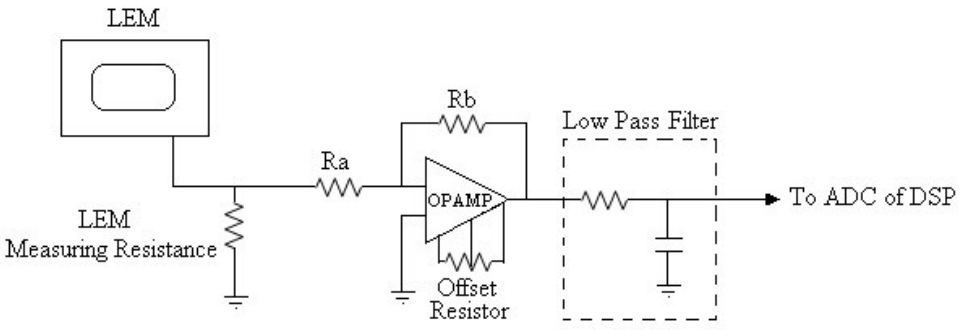

Figure 2. 6. Circuit used for current and voltage sensing including low pass filter

All ADCs have single ended bipolar inputs with $\pm$ 10V input span [13]. Ra and Rb are gain resistors and used to adjust the output of filter so that it cannot exceed the maximum input level of ADCs. Offset resistor is a potentiometer, which is used to minimize the offset in the signal. Calibration of the voltage and current measurement modules are given in section 4.2 and 4.3 respectively.

2.1.5. XOR Gate

In this thesis symmetric PWM was used to drive inverter. The DSP card, which is used to obtain PWM cycles, can only generate PWM cycles with high side at the beginning and low side at the end. In order to generate a symmetric duty cycle, two channels were used with the aid of an EXOR gate for which the truth table is given in Table 2.1.

Table2. 1. XOR Truth Table

A1	A2	Output
0	0	0
0	1	1
1	0	1
1	1	0

As an example, to obtain the output in Figure 2.7. A1 and A2 are used. From the truth table when A1 and A2 is the same, the output is zero and when the A1 and A2 are different, output is high. So symmetric PWM is obtained at the end of XOR Gate. In the system six PWM outputs were generated and three inverter input signals were obtained.

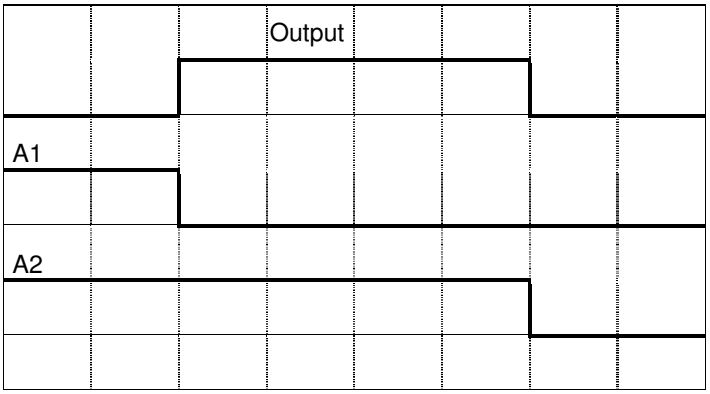

Figure 2.7. Symmetric PWM output and two PWM channels of DSP used to obtain the output

2.2. Software

In this section, the software used for parameter estimation and vector control is explained. Flowcharts of the software are given and modules used in these softwares are explained with theory background. Also programming language and other programs used in this thesis are described.

First of all the aim of the software is given as; To drive the motor with vector control at a desired torque or speed, motor currents and voltages are sampled simultaneously by the software and required PWM switching signals are generated. Software is written in C programming language, then compiled and downloaded to the DSP with a program called down31. A program LD31 is used to disable the program, which is downloaded and working in controller card, or to restart the disabled program. Both programs, down31 and LD31, came with controller board and work in MsDOS environment. TRACE program is used to observe the variables such as voltage, current, flux etc. in the program. To be able to observe variables in TRACE, a trc file must be formed and put into the same directory with software written in C language. Trc file, which consists of variable names and their types, can be written in notepad or in another editor program. TRACE works in windows environment. While the TRACE program is active, the software cannot be stopped via LD31 program. First TRACE program must be deactivated.

2.2.1. Flowchart of The Software

One of the objectives while implementing the software was the modularity. When a change is made in a module, other modules are not affected from the change. Also special care was taken to make correct processes at the correct times. Flowchart of the software used in vector controlled drive is given in Figure 2.8 and details of the modules used in this software are explained in section 2.2.2. Flowchart of the software used for parameter estimation is given in Figure 2.9 and details of the modules used in this software are explained in section 2.2.3.

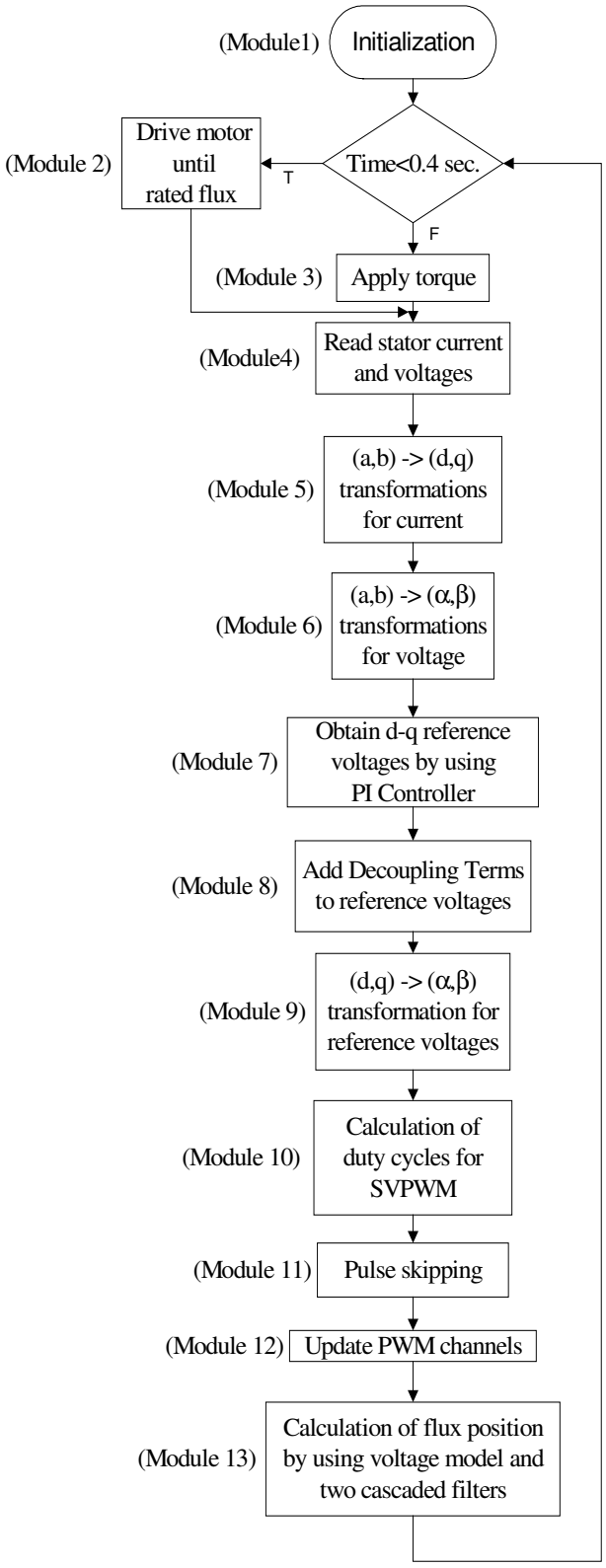

Figure 2.8. Flowchart of vector controlled induction machine drive software

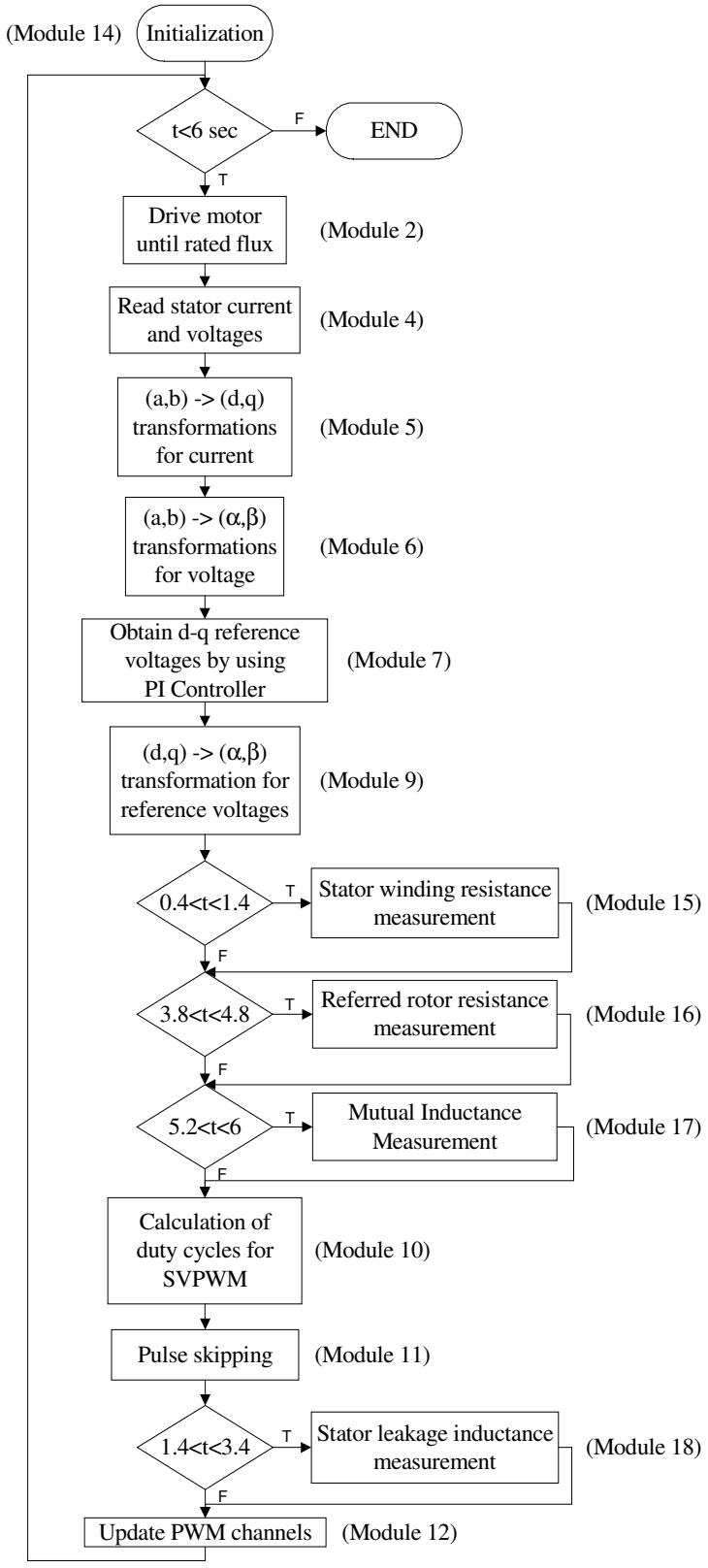

Figure 2. 9. Flowchart of the software used for parameter estimation

2.2.2. Modules Used in Vector Control Software

2.2.2.1. Initialization module (Module 1)

In this module the variables used in vector control software are defined.

Initialization

TS	: Switching period, control cycle
isa, isb, isc	: a, b, c phase currents of motor
isalfa, isbeta	: α,β components of motor current
isd, isq	: d, q components of motor current
isalfaref, isbetaref	: α,β components of reference current
isdref	: d component of reference current creating rated flux
isqref	: q component of reference current creating desired torque
vsa, vsb	: Motor phase voltages
vsalfa, vsbeta	: α,β components of motor voltage
vsrefalfa, vsrefbeta	: α,β components of reference voltage
vsdref, vsqref	: d, q component of reference voltage
t	: time (second)
fir	: rotor flux
firalfa, firbeta	: α,β components of rotor flux
fisalfa, fisbeta	: α,β components of stator flux
firalfapre, firbetapre	: previous values of α,β components of rotor flux
costeta, sinteta	: sine and cosine of rotor flux position
errorisdref	: error between d component of reference current and d component of motor current
errorisqref	: error between q component of reference current and q component of motor current
errorisdrefint	: integral of error between d component of reference current and d component of motor current
errorisqrefint	: integral of error between q component of reference current and q component of motor current

kiisd, kiisq	: integrator coefficient of PI controller
kpisd, kpisq	: proportional coefficient of PI controller
decoupleD	: decoupling term of reference voltage d component
decoupleQ	: decoupling term of reference voltage q component
ws	: synchronous speed
kd	: filter constant
sig	: leakage factor
ls	: stator self inductance
rs	: stator winding resistance
Tz	: half of the zero voltage application period in SVPWM
Tk	: half of the application period of voltage Vk in sector k
Tkk	: half of the application period of voltage V_{k+1} in sector k
ta1on, tb1on, tc1on	: on time duration of PWM channels 1,3,5
dutya1, dutya2	: duty cycles of desired PWM signals of inverter leg a
dutyb1, dutyb2	: duty cycles of desired PWM signals of inverter leg b
dutyc1, dutyc2	: duty cycles of desired PWM signals of inverter leg c

Figure 2.10. Initialization module

2.2.2.2. The module for driving the motor until rated flux (Module 2)

Motor must be driven until rated flux for normal operation. The required time for the motor to reach rated flux can be calculated by using equation 2.4.

$$V = N\frac{d\psi}{dt} \tag{2.1}$$

$$N\psi = \int V dt \tag{2.2}$$

When DC voltage is applied to motor Equation 2.2 becomes Equation 2.3.

$$N\psi = V\Delta t \tag{2.3}$$

$$V\Delta t = L_r i_r \Rightarrow \Delta t = \frac{L_r i_r}{V} \Rightarrow \Delta t = \frac{L_r}{r_r} \tag{2.4}$$

In equations r_r, V, L_r and i_r represents rotor resistance, rotor voltage, rotor self inductance and rotor current respectively. When DC voltage is applied to motor, required time for the flux to reach its steady state is depend on the rotor time constant as seen from Equation 2.4. In the experiment, this time is chosen as approximately seven times the rotor time constant.

In the software, DC voltage is applied to motor for the first 0.4 second of the program after the initialization. i_{sdref} is set to its rated value and i_{sqref} is set to zero. i_{sdref} is calculated and used as 2.4 for the motor used in this thesis. Also the angle theta is set to zero to maintain the rotor stationary. In each control cycle, reference currents are compared with measured currents and PI controller is used to obtain reference voltages. Since current control is performed, motor phase currents cannot reach to a level, which damages the motor itself. During this period dc current flows in the machine and flux is set to its rated value. The content of the module is shown below.

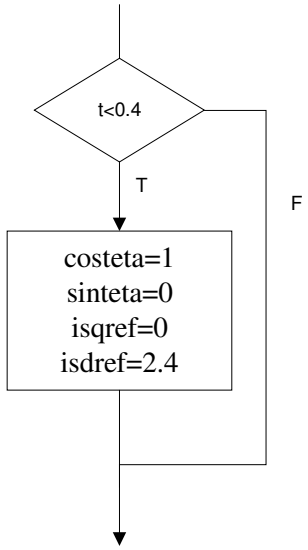

Figure 2.11. Module to drive motor until rated flux

2.2.2.3. Module used to apply Torque

When the flux is set to its rated value, torque producing component of stator current is set to its reference value(isqref=...;) and motor starts to produce torque.

2.2.2.4. Module for reading the motor voltages and currents (Module 4)

In this module motor currents and voltages are read by the software with the help of DSP macros. First Analog to Digital Converters (ADC) are started and then four variables, two phase currents and two phase voltages, are read. The conversion of the ADCs must be started by a preceding call to the function ds1102_ad_start() [13]. Then ADC channels are read with DSP macro ds1102_ad (long channel). The content of the module is given in the following figure.

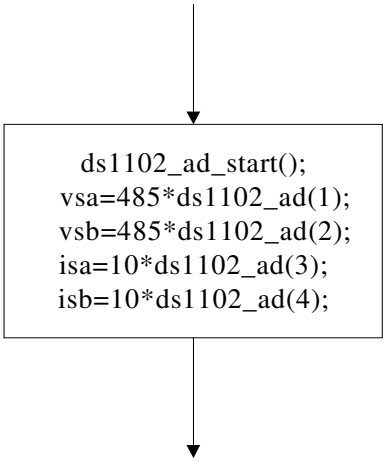

Figure 2.12. Module for reading motor voltages and currents

2.2.2.5. Module for (a,b) -> (d,q) transformation of currents (Module 5)

The aim of the module is to obtain time invariant flux and torque components of the stator currents. In order to obtain these time invariant components, first a projection is required that modifies the three phase system into the (α,β) two dimension orthogonal system

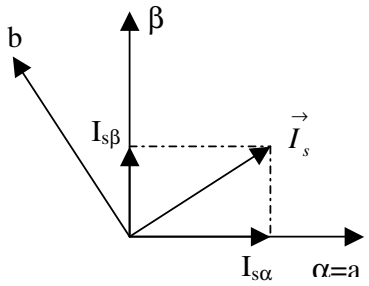

Figure 2.13. Projection of stator current vector to α,β components

Clarke Transformation:

$$I_{s\alpha} = i_{sa} \tag{2.5}$$

$$I_{s\beta} = \frac{1}{\sqrt{3}} i_{sa} + \frac{2}{\sqrt{3}} i_{sb} \tag{2.6}$$

After the projection of stator current vector to two orthogonal (α,β) axis, time variant components of current vector are obtained whose α axis is aligned with the phase a axis rotating with the same synchronous speed. Then, another transformation is required which modifies two phase time variant orthogonal system (α,β) into the d, q time invariant rotating reference frame. The projection of α,β system to d, q system for rotor flux orientation is shown below. [9]

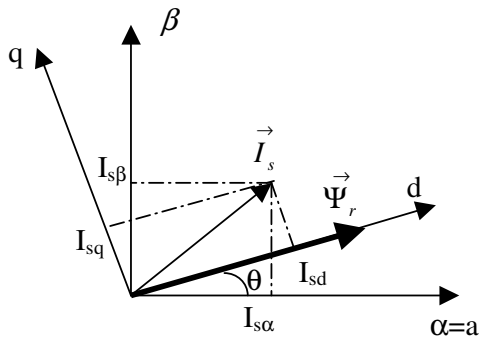

Figure 2.14. Projection of stator current vector from a,b co-ordinates to d,q co-ordinates for rotor flux oriented control

Rotor flux orientation, the most popular vector control algorithm in which d axis is aligned with rotor flux linkage vector as shown in Figure 2.13, where θ is the rotor flux position with respect to α axis. The flux and torque components of the current vector are determined by the following equations:

Park Transformation:

$$I_{sd} = I_{s\alpha} \cos\theta + I_{s\beta} \sin\theta \tag{2.7}$$

$$I_{sq} = -I_{s\alpha} \sin\theta + I_{s\beta} \cos\theta \tag{2.8}$$

By projection of a,b co-ordinates to d,q co-ordinates, a co-ordinate system is obtained with the following characteristics:

- Two co-ordinate time invariant system
- Torque control is achieved by controlling I_{sd} (flux component) and I_{sq} (torque component) [9]

Measured currents i_{sa} and i_{sb} are firstly transformed to two co-ordinate time variant system. Then i_{salfa}, i_{sbeta} and angle(θ) between α axis and rotor flux, which is calculated in section 2.2.2.12, are used to obtain two co-ordinate time invariant system. The content of the module is given below.

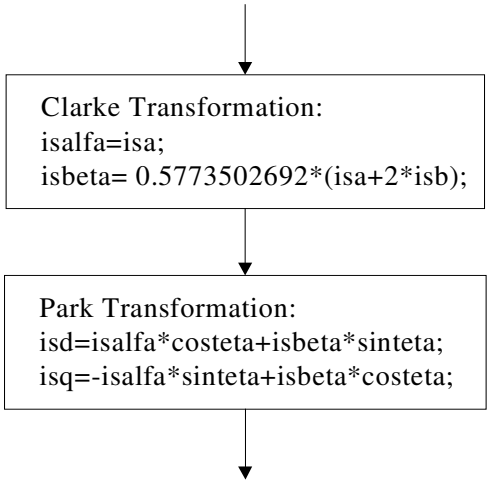

Figure 2.15. Module for (a,b) -> (d,q) transformation of currents

2.2.2.6. Module for (a,b) -> (α,β) transformation of voltages (Module 6)

In order to obtain α,β components of voltage, Clarke Transformation is used. These components are used in flux calculations, which are given later in detail.

The content of the module is given below:

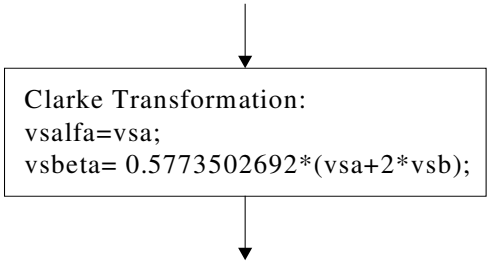

Figure 2. 16. Module for (a,b) -> (α,β) transformation of voltages

2.2.2.7. PI Controller Module (Module 7)

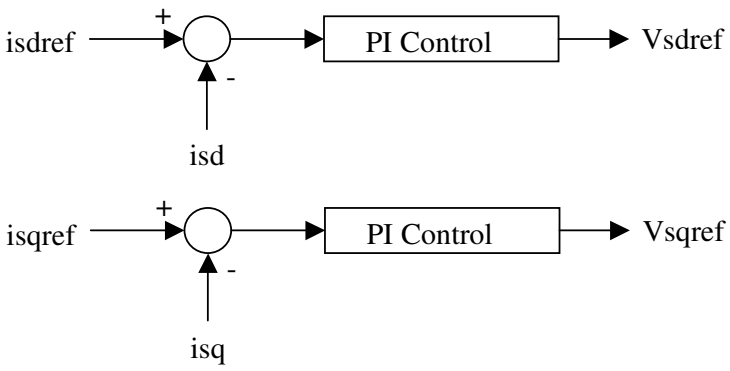

Figure 2.17. Block Diagram of PI controller

Reference voltages required in Space Vector Pulse Width Modulation (SVPWM) technique is calculated using d,q components of measured currents. Measured currents are compared with reference values and error signals are obtained. Then PI controller is used to calculate reference voltage values from error signals. Calculation of PI controller parameters is given in Appendix C.

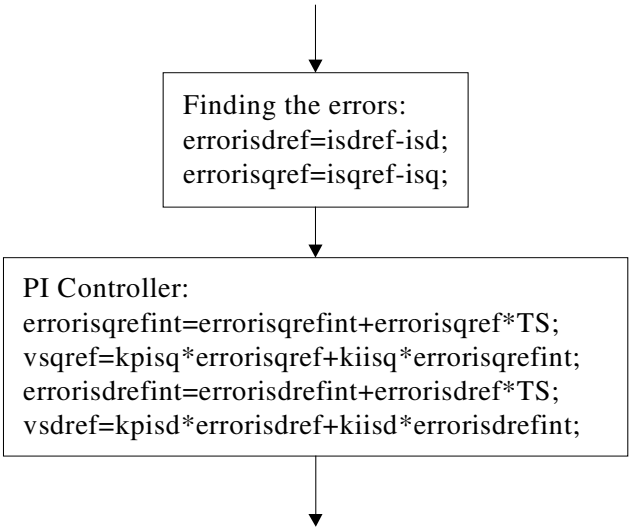

Figure 2.18. Module to obtain reference voltages from d,q components of current by using PI controller

2.2.2.8. Module used to find decoupling terms (Module 8)

In this module decoupling terms are found. Before giving the codes the theory behind this module is explained briefly.

Motor d-q model is given in detail in appendix. Here stator voltage in the reference frame fixed to the rotor flux is given in the following equation:

$$\vec{U}_{s\psi r} = R_s \vec{i}_{s\psi r} + L_s \frac{d\vec{i}_{s\psi r}}{dt} + L_m \frac{d\vec{i}_{r\psi r}}{dt} + jwL_s \vec{i}_{s\psi r} + jwL_m \vec{i}_{r\psi r} \tag{2.9}$$

where $\vec{i}_{s\psi r}$ is the space phasor of the stator currents in the reference frame fixed to the rotor flux (x,y) and can be expressed as follows:

$$\vec{i}_{s\psi r} = i_{sx} + ji_{sy} \tag{2.10}$$

Rotor magnetizing current space phasor in the rotor flux oriented reference frame ($\vec{i}_{mr}$) is obtained by dividing the rotor flux linkage space phasor established in this reference frame ($\vec{\psi}_{r\psi r}$) by the magnetizing inductance (L_m).

$$\vec{i}_{mr} = \frac{\vec{\psi}_{r\psi r}}{L_m} = \vec{i}_{s\psi r} + \frac{L_r}{L_m}\vec{i}_{r\psi r} \tag{2.11}$$

As a result of the special selection of the reference frame the rotor magnetizing current space phasor is coaxial with the direct axis and thus $\vec{i}_{mr} = \left|\vec{i}_{mr}\right|$ the rotor current space phasor in the special reference frame is obtained in terms of the stator current and rotor magnetizing space phasors as

$$\vec{i}_{r\psi r} = \frac{L_m(\left|\vec{i}_{mr}\right| - \vec{i}_{s\psi r})}{L_r} \tag{2.12}$$

Substitution of equation (2.12) into equation (2.9) yields the following differential equation for the stator currents, if both sides of the equation are divided by the stator resistance R_s and if it is expressed in the form required by a time-delay element:

$$T_s^{'}\frac{d\vec{i}_{s\psi}}{dt} + \vec{i}_{s\psi r} = \frac{\vec{U}_{s\psi r}}{R_s} - jwT_s^{'}\vec{i}_{s\psi r} - (T_s - T_s^{'})\left(jw\left|\vec{i}_{mr}\right| + \frac{d\left|\vec{i}_{mr}\right|}{dt}\right) \tag{2.13}$$

$T_s^{'}$ is the stator transient time constant of the machine, $T_s^{'} = L_s^{'}/R_s$, where $L_s^{'}$ is the stator transient inductance $L_s^{'} = (L_s - L_m^2/L_r)$, and can be expressed in terms of the total leakage factor σ and the the stator inductance as $L_s^{'} = \sigma L_s$. T_s is the stator time constant $T_s = L_s/R_s$, thus it is also possible to express $T_s^{'}$ as σT_s.

By resolving equation (2.13) into its real (x) and imaginary axis (y) components, the following two-axis differential equations are obtained for the stator currents:

$$T_s^{'}\frac{di_{sx}}{dt}+i_{sx}=\frac{U_{sx}}{R_s}+wT_s^{'}i_{sy}-(T_s-T_s^{'})\frac{d\left|\vec{i}_{mr}\right|}{dt} \tag{2.14}$$

$$T_s^{'}\frac{di_{sy}}{dt}+i_{sy}=\frac{U_{sy}}{R_s}-wT_s^{'}i_{sx}-(T_s-T_s^{'})w\left|\vec{i}_{mr}\right| \tag{2.15}$$

It can be seen from the equations (2.14) and (2.15) there is an unwanted coupling between the stator circuits on the two axes. For the purposes of rotor flux oriented control, it is the direct axis stator current i_{sx} (rotor flux producing component) and the quadrature axis stator current i_{sy} (torque producing component), which must be independently controlled. However, since the voltage equations are coupled, and the coupling term in u_{sx} also depends on i_{sy} and the coupling term in u_{sy} also depends on i_{sx}, u_{sx} and u_{sy} cannot be considered as decoupled control variables for the rotor flux and electromagnetic torque. The stator currents i_{sx} and i_{sy} can only be independently controlled (decoupled control) if the stator voltage equations are decoupled and the stator current components i_{sx} and i_{sy} are indirectly controlled by controlling the terminal voltages of the induction machine.

From equations (2.14) and (2.15) there is in the direct axis voltage equations a rotational voltage coupling term $wL_s^{'}i_{sy}$, and thus the quadrature axis stator current i_{sy} affects the direct axis stator voltage u_{sx}. Similarly, in the quadrature axis voltage equation there is a rotational voltage coupling term $-wL_s^{'}i_{sx}-(L_s-L_s^{'})w\left|\vec{i}_{mr}\right|$ and thus the direct axis stator current i_{sx} affects quadrature axis voltage u_{sy}. By assuming $\left|\vec{i}_{mr}\right|$=constant it follows from equations (2.14) and (2.15) that the stator current components can be independently controlled if the decoupling rotational voltage components,

$$U_{dx} = -wL_s^{'} i_{sy} \tag{2.16}$$

$$U_{dy} = wL_s^{'} i_{sx} + (L_s - L_s^{'}) w \left| \vec{i}_{mr} \right| \tag{2.17}$$

are added to the outputs (u_{sx},u_{sy}) of the current controllers which control i_{sx} and i_{sy} respectively. This can be proved by considering that u_{sx}+u_{dx} yields the direct axis terminal voltage component, and the voltage on the output of the direct axis current controller is

$$u_{sx} = R_s i_{sx} + L_s^{'} \frac{di_{sx}}{dt} \tag{2.18}$$

Similarly u_{sy}+u_{dy} gives the quadrature axis stator voltage component and the voltage on the output of the quadrature axis current controller is

$$u_{sy} = R_s i_{sy} + L_s^{'} \frac{di_{sy}}{dt} \tag{2.19}$$

In field oriented control $\left| \vec{i}_{mr} \right| = i_{sx} = cons\tan t$ so that u_{dy} becomes:

$$U_{dy} = wL_s i_{sx} \tag{2.20}$$

In this module firstly decoupling terms are found and then these terms are added to the reference voltages, which were obtained by using PI controller. The content of the module is given below:

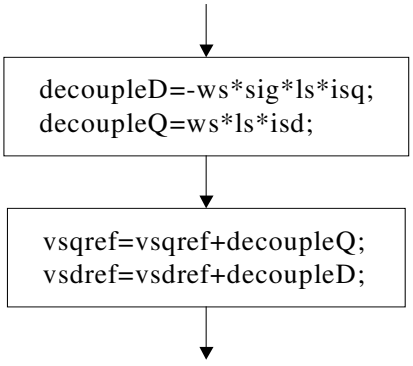

Figure 2. 19 . Module used to find decoupling terms

2.2.2.9. Module to obtain (α,β) components of reference voltage (Module 9)

To obtain alpha, beta components of reference voltage inverse park transformation is used. The content of the module is given in the following figure.

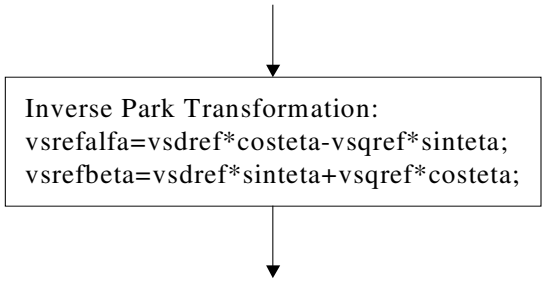

Figure 2. 20. Module to find (α,β) components of reference voltage

2.2.2.10. Module used to calculate duty cycles for SVPWM (Module 10)

In the software, Space Vector Pulse Width Modulation (SVPWM) technique is used to calculate duty cycles of inverter legs for the required voltages. SVPWM technique is explained in previous thesis [6], [7] in detail. Here the theory of this modulation technique will not be explained again.

In the module firstly, the sector is calculated according to α,β components of the reference voltage, then on times of zero voltage and non-zero voltages according to sector are calculated and finally duty cycles for each inverter leg is obtained. Symmetric PWM is used in the application. To obtain symmetric cycles two PWM channels are used to create one output with an EXOR gate as explained in section 2.1.5. Symmetric PWM is taken into account while making duty cycle calculations. The flowchart of the module is given in the following figure.

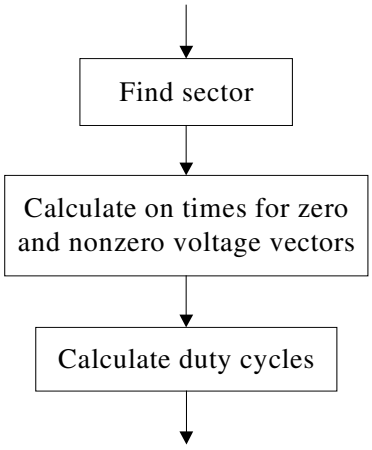

Figure 2. 21. Flowchart of the module used to calculate duty cycles

For the simplicity calculations for only one sector is given here, calculations for the other sectors are similar to the sample. In Figure 2.22, calculation of sector number and on times of zero and non-zero voltages are shown as c coded software. Where K is a constant and calculated from TS and DC link voltage ($K = \frac{\sqrt{3}TS}{2U_{dc}}$).

```
Calculation of sector from reference voltage:

if (vsrefbeta>=0)          //Either Sector1, 2 or 3; V1=(100);V2=(110)
                             V3=(010)V4=(011) V0=(000) V7=(111)
 {
   if (vsrefbeta<=kok3*vsrefalfa)            //Now we are in sector1
   {
        Tk=K/2*(kok3*vsrefalfa-vsrefbeta);//T1
        Tkk=K*vsrefbeta;                        //T2
        Tz=TS/2-(Tk+Tkk);             //Half of the the period of time when zero
                                        vector (both kinds) will be applied.
        ta1on=Tz/2;
        tb1on=Tz/2+Tk;
        tc1on=Tz/2+Tk+Tkk;

   }
```

Figure 2. 22. Calculation of sector from reference voltages

Calculation of duty cycles is given in Figure 2.23. dutya1 and dutya2 outputs of this module are sent to XOR Gate to create inverter phase a leg switching cycles while dutyb1 and dutyb2 creates phase b leg, dutyc1 and dutyc2 creates phase c leg switching cycles.

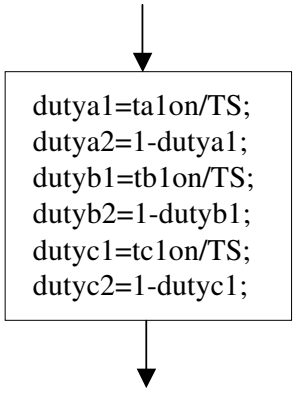

Figure 2. 23. Calculation of duty cycles

2.2.2.11. Module used for pulse-skipping (Module 11)

In the Lock-out circuit explained in section 2.1.3, dead time is added to signals not to cause short circuit in inverter legs. In application, dead time is adjusted to 3 μs. This means that signals smaller than 3 μs will be lost in lock-out circuit. In experiments these signals are not applied to circuit not to create any problem unintentionally. For this purpose instead of these signals, minimum duty cycle as shown in the following figure is applied in this thesis.

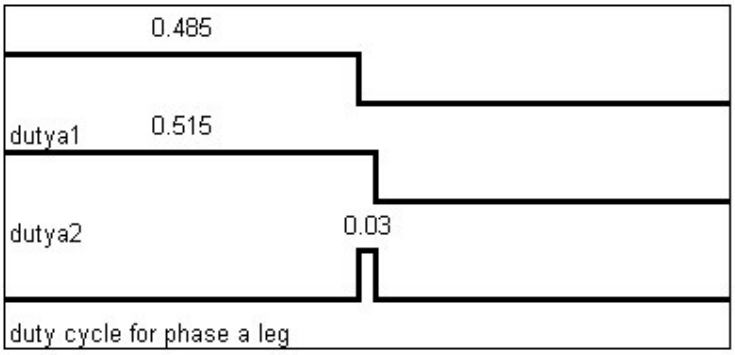

Figure 2. 24. Minimum applicable duty cycle in SVPWM

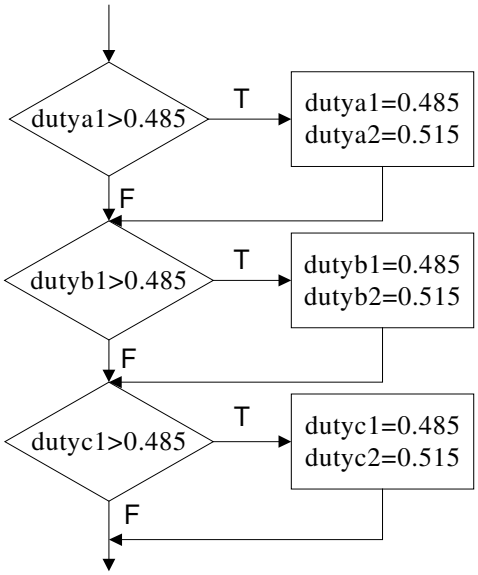

Figure 2. 25.Module used for pulse skipping

2.2.2.12. Module used to update PWM outputs (Module 12)

Firstly the necessity for update must be explained. The Space Vector Pulse Width Modulation technique is based on the fact that, as explained in [6] and [7] in detail, every reference voltage vector inside the dashed hexagon, shown in Figure 2.26, can be expressed as a weighted average combination of the two adjacent active space vectors and the zero-state vectors 0 and 7. Therefore, in each cycle imposing the desired reference vector may be achieved by switching between these four inverter states [10].

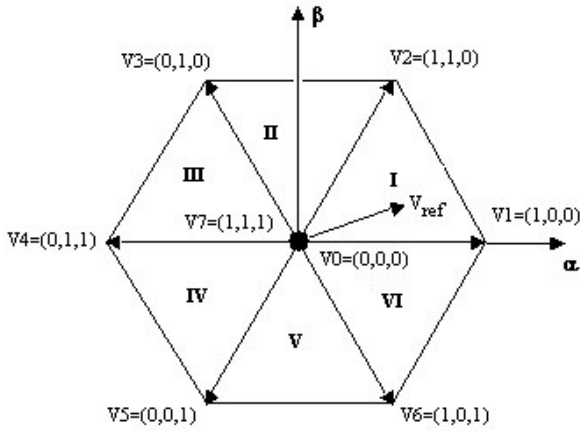

Figure 2. 26.Representation of the inverter states in the stationary reference frame

In section 2.2.2.9 on times of zero and non-zero vectors with respect to sector is calculated by using reference voltage and then duty cycles for inverter legs are calculated. These duty cycles must be updated and sent to inverter legs to constitute reference voltage. Calculated duty cycles are updated in every 100 μs, which is the control cycle of the program. To update the duty cycles DSP macro ds1102_p14_pwmvar(long channel, float duty) is used. With this macro, the PWM duty-cycle of the selected channel is updated to the new value specified by the parameter duty, which must be in the range 0.0 ... 1.0. The parameter channel must be in the range 1...6.

The content of the module is given in the following figure.

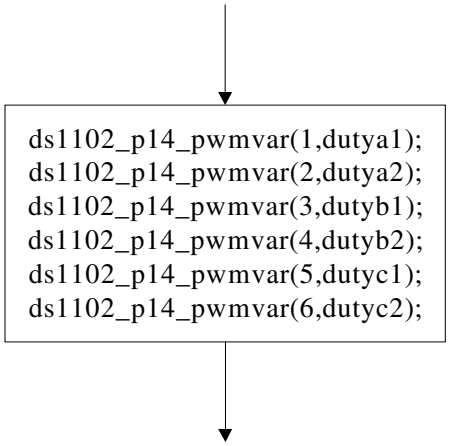

Figure 2. 27. Module used to update duty cycles

2.2.2.13. Module used to calculate rotor flux position by using voltage model and two cascaded filters (Module 13)

The aim of this module is to obtain position of the rotor flux needed in field oriented control. For this purpose firstly α,β components of stator flux are obtained by using voltage model. Then α,β components of rotor flux are obtained from stator flux components and finally rotor flux magnitude and position are calculated.

Voltage model:

$$\psi_{s\alpha} = \int (V_{s\alpha} - R_s I_{s\alpha})dt \tag{2.21}$$

$$\psi_{s\beta} = \int (V_{s\beta} - R_s I_{s\beta})dt \tag{2.22}$$

Rotor flux:

$$\Psi_{r\alpha} = \frac{L_r}{L_m}\left(\psi_{s\alpha} - \sigma L_s i_{s\alpha}\right) \tag{2.23}$$

$$\Psi_{r\beta} = \frac{L_r}{L_m}\left(\psi_{s\beta} - \sigma L_s i_{s\beta}\right) \tag{2.24}$$

Rotor flux position is simply calculated by using α,β components of rotor flux as follows

$$\psi_r = \sqrt{\left(\psi_{r\alpha}{}^2 + \psi_{r\beta}{}^2\right)} \tag{2.25}$$

$$\cos\theta = \frac{\psi_{r\alpha}}{\psi_r} \tag{2.26}$$

$$\sin\theta = \frac{\psi_{r\beta}}{\psi_r} \tag{2.27}$$

As seen in equations (2.21) and (2.22) to calculate stator fluxes integral process must be performed. In the experiments, two cascaded filters are used as an integrator. This process can be expressed as follows

Digital Filter:

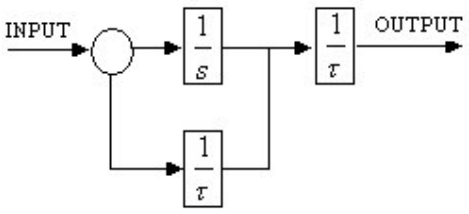

Figure 2. 28. Schematic representation of digital filter

$$\left|F(jw)\right| = \frac{1}{\sqrt{(1+(w\tau)^2)}} \tag{2.28}$$

$$\angle F(jw) = -\tan^{-1}(w\tau) \tag{2.29}$$

Gain and phase shift of the filter are given in equations (2.28) and (2.29). When two filters are cascaded equation (2.28) becomes (2.30) and (2.29) becomes (2.31).

$$\left|F(jw)\right| = \frac{1}{1+(w\tau)^2} \tag{2.30}$$

$$\angle F(jw) = -2\tan^{-1}(w\tau) \tag{2.31}$$

Integrator:

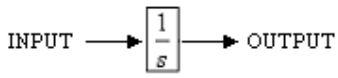

Figure 2. 29. Schematic representation of integrator

$$\left|F(jw)\right| = \frac{1}{w} \tag{2.32}$$

$$\angle F(jw) = -90^{o} \tag{2.33}$$

To be able to use two cascaded filters as an integrator gain and phase shift must be equal. So equation (2.31) and (2.33) must be equal;

$$-2\tan^{-1}(w\tau) = 90 \Rightarrow \tau = \frac{1}{w} \tag{2.34}$$

Also gain of two cascaded filters must be equal to integrators gain. To make this possible a gain block (G=2/w) is added to the system.

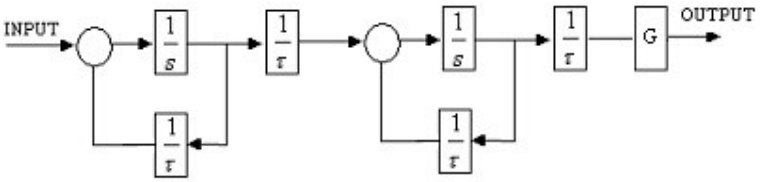

Figure 2. 30.Two cascaded filters as an integrator

$\frac{1}{\tau}$ and G are functions of frequency. $\frac{1}{\tau}$ is the filter coefficient, which is represented as kd in the software and equals to w. kd and Gain block (G) are strictly depend on the value of synchronous speed(w). Synchronous speed is estimated from rotor flux components as follows.

Rotor flux angle can be calculated from α,β components of rotor flux as shown below:

$$\theta = \tan^{-1}\left(\frac{\psi_{r\beta}}{\psi_{r\alpha}}\right) \tag{2.35}$$

Stator angular velocity can be obtained by taking the differential of rotor flux angle:

$$w = \dot{\theta} = \frac{\left(\psi_{r\alpha}\dot{\psi}_{r\beta} - \psi_{r\beta}\dot{\psi}_{r\alpha}\right)}{\psi_{r\alpha}^{\ 2} + \psi_{r\beta}^{\ 2}} \tag{2.36}$$

If this equation is rewritten in terms of sampled data. Following equation is obtained.

$$w(k) = \frac{\left(\psi_{r\alpha}(k)\left(\psi_{r\beta}(k) - \psi_{r\beta}(k-1)\right) - \psi_{r\beta}(k)\left(\psi_{r\alpha}(k) - \psi_{r\alpha}(k-1)\right)\right)}{\left(\psi_{r\alpha}(k)^2 + \psi_{r\beta}(k)^2\right)T} \tag{2.37}$$

$$\Rightarrow w(k) = \frac{\psi_{r\alpha}(k-1)\psi_{r\beta}(k) - \psi_{r\alpha}(k)\psi_{r\beta}(k-1)}{\left(\psi_{r\alpha}(k)^2 + \psi_{r\beta}(k)^2\right)T} \tag{2.38}$$

As may be seen from the equation (2.38) w depends on the α, β components of rotor flux. Also estimation of rotor flux depends on stator voltage and currents.

Stator voltage and voltage drop on stator resistance becomes comparable at low speeds and as a result error in flux estimation may increase. This causes fluctuations in flux. Estimated rotor flux for different speeds is given in section 4.1.5.

The content of the module is given in the following figure:

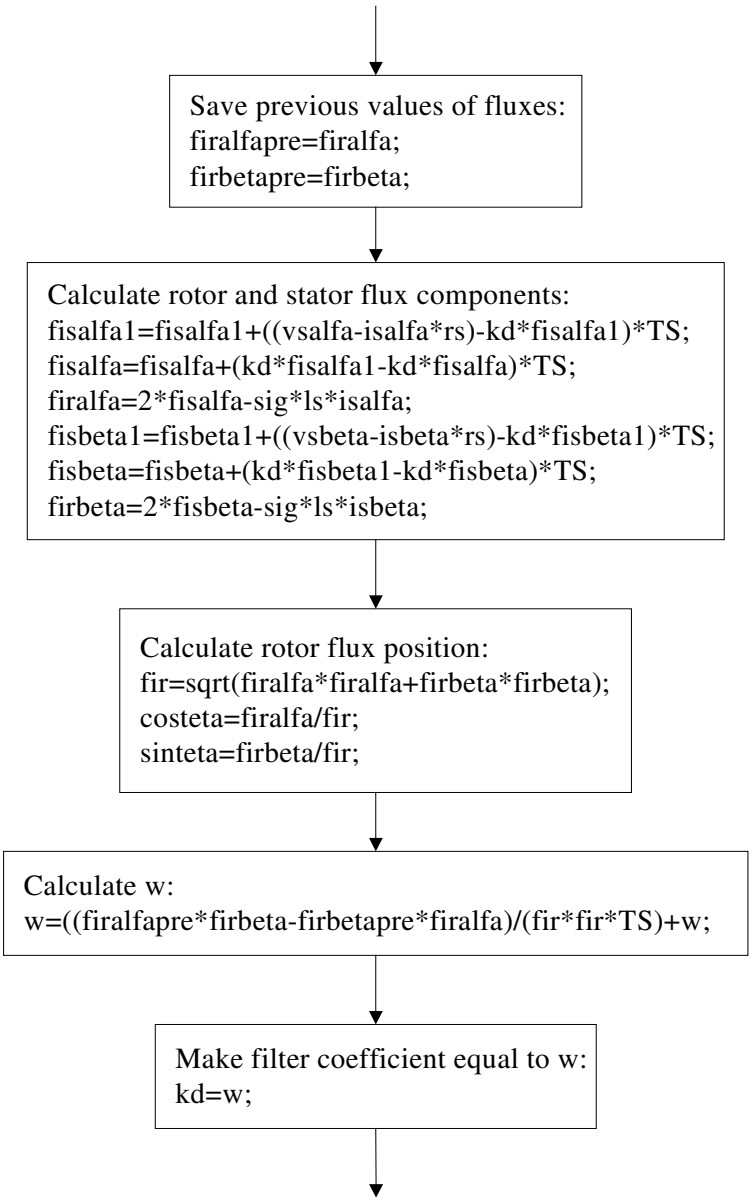

Figure 2. 31. Module used for calculation of rotor flux position by using voltage model and two cascaded filters as an integrator

2.2.3. Modules Used in Parameter Estimation Software

Modules from (1) to (12) are given in section 2.2.2 and some of them are used in this software without any change. So they will not be explained again except module (1). Because module (1) describes variables used in software and in parameter estimation software new variables are added. In this section, new modules that are used to calculate stator winding resistance, stator transient inductance, referred rotor resistance and mutual inductance are given. Theory and experimental results of these modules are explained in Chapter 5.

2.2.3.1. Initialization module (Module 14)

In this module the variables used in parameter estimation software are defined.

Initialization	
TS	: Switching period, control cycle
is	: peak value of stator current vector
isa, isb, isc	: a, b, c phase currents of motor
isave	: average value of stator phase a current during stator winding resistance measurement test
issum	: total value of stator phase a current during stator winding resistance measurement test
isalfa, isbeta	: α,β components of motor current
isd, isq	: d, q components of motor current
isalfaref, isbetaref	: α,β components of reference current
isdref	: d component of reference current creating rated flux
isqref	: q component of reference current creating desired torque
Irms	: rms value of stator phase current
vsa, vsb	: Motor phase voltages
vsalfa, vsbeta	: α,β components of motor voltage

vsrefalfa, vsrefbeta	: α,β components of reference voltage
vsdref, vsqref	: d,q component of reference voltage
vssum	: total value of stator phase a voltage during stator winding resistance measurement test
vref	: reference voltage value for V/f control
power	: instantaneous power injected to the machine
t	: time (second)
t1	: time used in V/f control
f	: frequency
costeta, sinteta	: sine and cosine of rotor flux position
errorisdref	: error between d component of reference current and d component of motor current
errorisqref	: error between q component of reference current and q component of motor current
errorisdrefint	: integral of error between d component of reference current and d component of motor current
errorisqrefint	: integral of error between q component of reference current and q component of motor current
kiisd, kiisq	: integrator coefficient of PI controller
kpisd, kpisq	: proportional coefficient of PI controller
sigls	: stator transient inductance
leakage	: stator and rotor leakage inductance
rses	: estimated stator winding resistance
requ	: total of stator winding resistance and referred rotor resistance
requsum	: total value of requ over a time duration
requave	: average value of requ over a time duration
rrotor	: referred rotor resistance
Vm	: motor back emf
im	: magnetizing current
ic	: core loss branch current
Lm	: Mutual inductance

powertotal	: total of power over a time duration
Irmstotal	: total of rms current over a time duration
Vrmstotal	: total of rms voltage over a time duration
p	: average value of power over one period
i	: average value of rms current
v	: average value of rms voltage
Rc	: core loss resistance
pcore	: core loss power
u1, u2, u3, u4	: variables used for different purposes
Tz	: half of the zero voltage application period in SVPWM
Tk	: half of the application period of voltage Vk in sector k
Tkk	: half of the application period of voltage V_{k+1} in sector k
ta1on, tb1on, tc1on	: on time duration of PWM channels 1,3,5
dutya1, dutya2	: duty cycles of desired PWM signals of inverter leg a
dutyb1, dutyb2	: duty cycles of desired PWM signals of inverter leg b
dutyc1, dutyc2	: duty cycles of desired PWM signals of inverter leg c

Figure 2. 32. Initialization module for parameter estimation software

2.2.3.2. Module used to calculate stator winding resistance (Module 15)

Theory of the module is given in section 5.2. In this module, phase A currents and voltages are read and added to the previous sums during one second duration and at the end of the measurement time, total value of voltage is divided by total value of current to find stator winding resistance. Also in this module average value of current is calculated which is used in stator transient inductance measurement. The content of the module is given below.

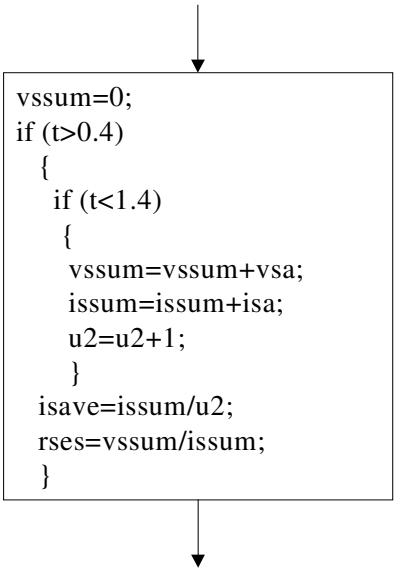

Figure 2. 33. Module used to calculate stator winding resistance

2.2.3.3. Referred rotor resistance measurement (Module 16)

The theory of the module is given in section 5.4. In this module, motor is driven at V/f ratio control. Reference voltage and frequency was given as 20V and 50 Hz respectively. Input power and rms value of stator currents are calculated for 1.4 second duration by using equation (5.9). For a time of 0.3 seconds, average values of input power and rms current are calculated. Rs was measured in dc test. Referred rotor resistance is calculated by using equations (5.11)-(5.13). The place of this module is important in parameter estimation software. In this module SVPWM technique is used to obtain duty cycles for inverter and PI controller is not used. For this reason module is inserted in front of Module 10. And at the end of module PI controller error variables are reset.

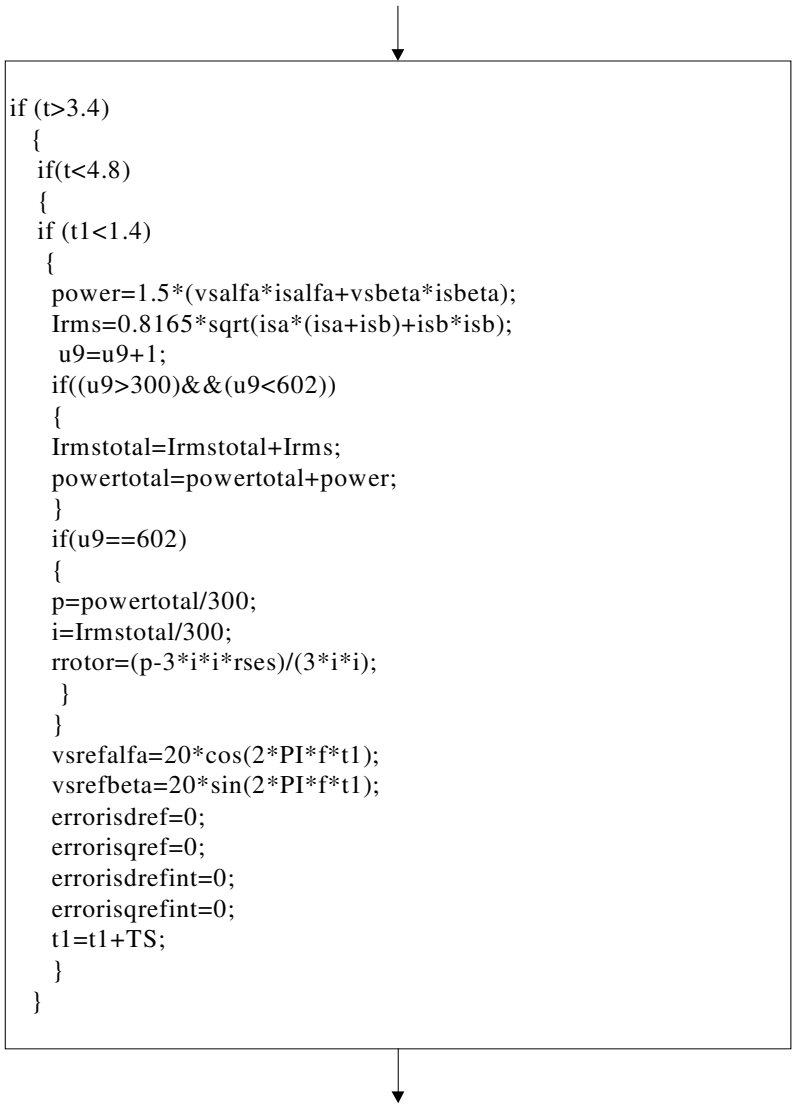

Figure 2. 34.Module used to measure referred rotor resistance

2.2.3.4. Mutual inductance measurement module (Module 17)

The theory of this module is explained in section 5.4. In this module motor is driven in V/f control with 310V reference at 50 Hz. First 0.6 seconds no process is made. System is waited to reach its steady state. Then power, rms value of current and voltage are calculated and added to the previous sum during one period which is 20 msec for 50 Hz and averages of these values are obtained.

In this thesis two phase currents and two phase voltages are measured so rms values must be calculated. Assuming a set of sinusoidal currents, the rms value, in terms of instantaneous quantities can be written as [11]

$$I_{rms} = \sqrt{\frac{2}{3}}\sqrt{\left(isa(isa + isb) + isb^2\right)} \tag{2.39}$$

Similarly rms of the voltage can be written as

$$V_{rms} = \sqrt{\frac{2}{3}}\sqrt{\left(vsa(vsa + vsb) + vsb^2\right)} \tag{2.40}$$

where isa, isb and vsa, vsb are the instantaneous values of stator currents and stator voltages respectively.

At the end of the module, calculation for mutual inductance is performed by using equations (5.13)-(5.19). The content of the module is given in Figure 2.35. This module is inserted in front of Module 10. Since PI controller is not used in this module the error variables of PI controller are reset at the end of this module.

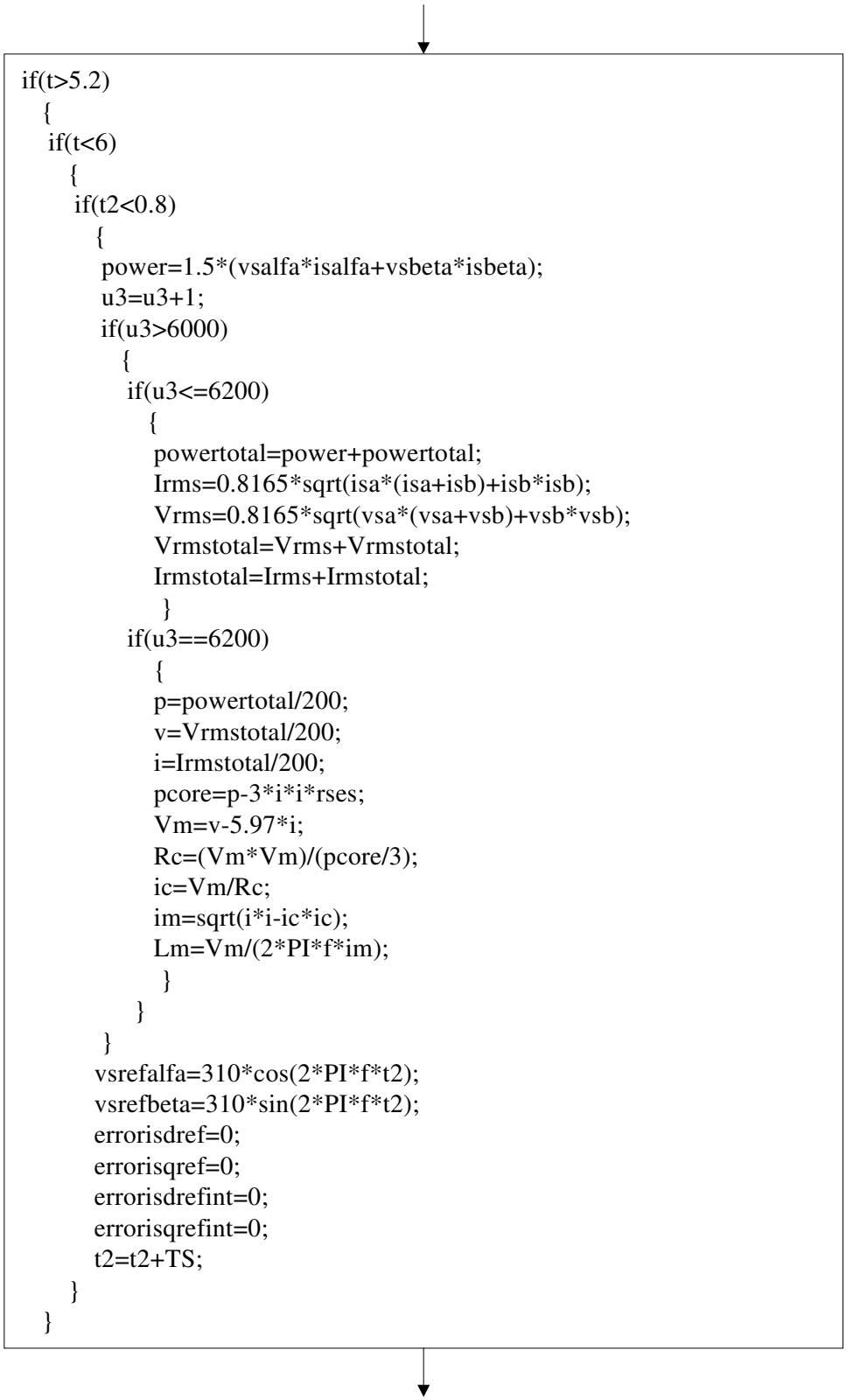

Figure 2. 35. Mutual inductance measurement module

2.2.3.5. Stator leakage inductance measurement module (Module 18)

The theory of the module is given in section 5.3. In the software first three measurements are taken and averaged. Then measured leakage inductances are compared with the average value of first three measurements. When the error reaches to a level of 5% calculation is finished and calculated leakage inductance values are averaged to find out leakage inductance.

The place of this module in the software is very critical since the duty cycles are given in the module externally. This module is inserted after module 10 in the software. Since the PI parameters is not used in the module PI controller error variables are reset at the end of the module.

The content of the module is given as follows

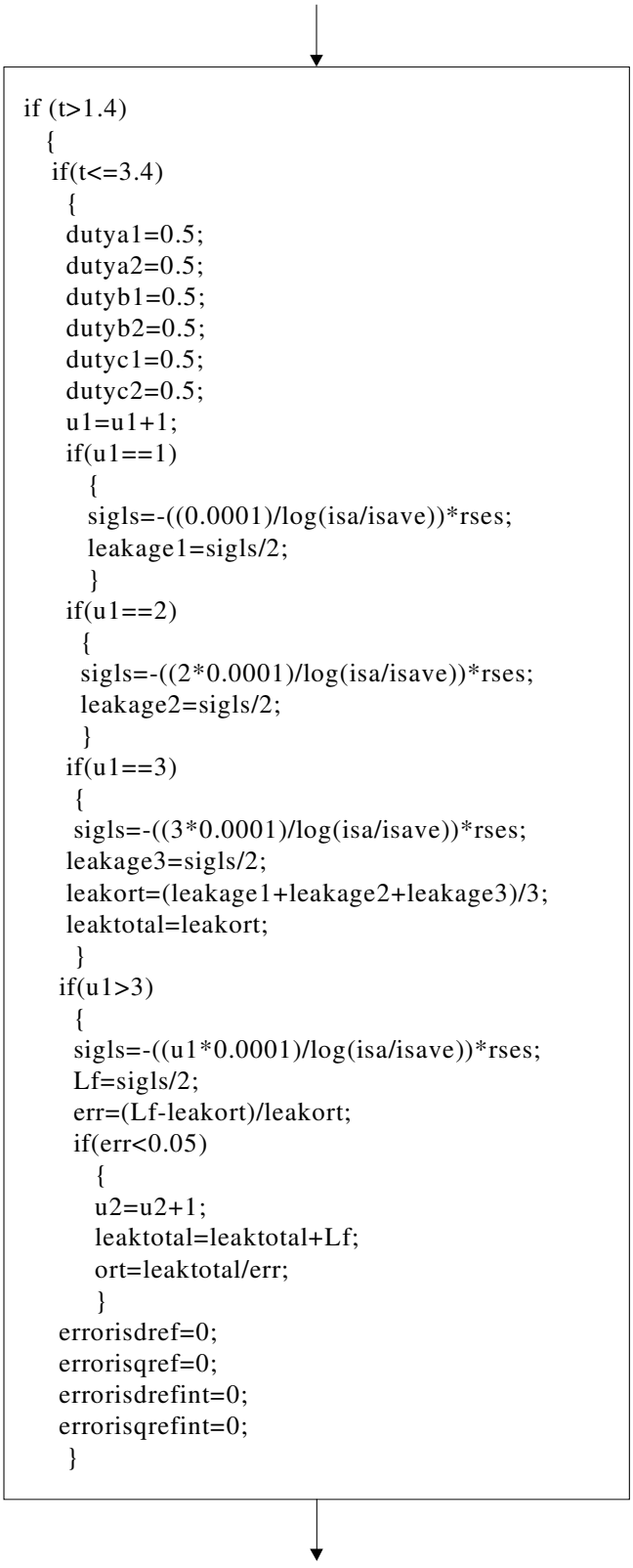

Figure 2. 36. Stator transient inductance measurement module

2.3 Time Diagrams of The Software

2.3.1. Time Diagram of Vector Control Software

Time diagram of the vector control software is given in the following figure.

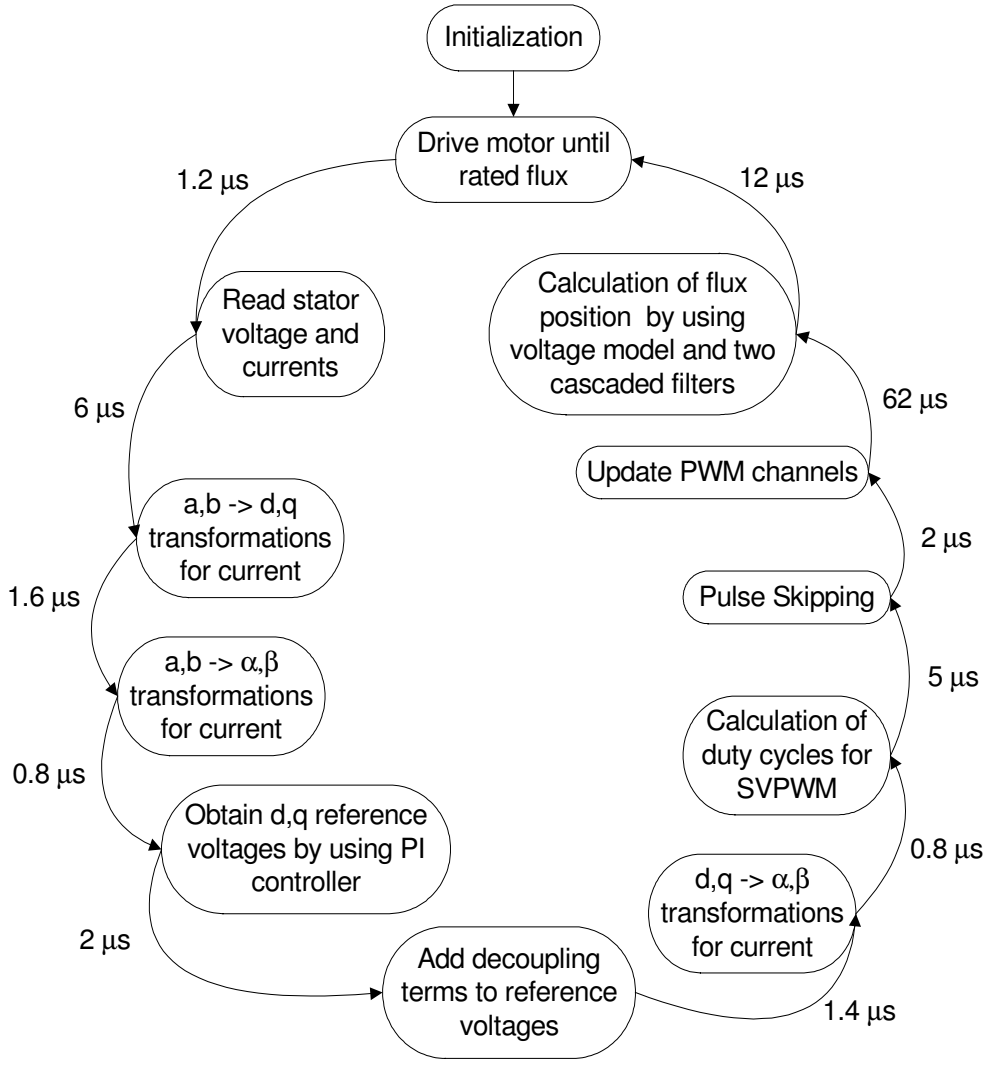

Figure 2. 37. Time diagram of vector control software

In this real time application, all calculations and processes in the software must be performed in one control cycle, which is adjusted to 100 µsec in this thesis.

As seen from the figure, execution time of the software is 94.8 μsec. From this point of view, there is no problem with execution time. But in this thesis, variables like flux, current etc. are observed with a program called TRACE. This program create some problems when the execution time is very close to control cycle, so reduce in execution time was required. To overcome this problem all the codes are overviewed and following solution is reached.

As seen from Figure 2.37, updating of the PWM channels take 62 μsec. In the datasheets of DSP card, the execution time of PWM channel update is given as follows

Table2. 2. Execution time of PWM channel update

Function	Execution time in μsec	
	Single	Sequential
ds1102_p14_pwmvar()	2,1	10,2

In the software this macro is used 6 times sequentially, so execution time is 62 μsec as shown in Figure 2.37. This time is reduced by inserting two of six channel updates between other modules. New calculation and process time of the software is 79 μsec.

2.3.2. Time diagram of parameter estimation software

Execution time of the new modules used in parameter estimation software are calculated as follows

Execution time of Module 14 (Stator winding resistance measurement) : 5.3 μsec
Execution time of Module 15 (Referred rotor resistance measurement) : 11 μsec
Execution time of Module 16 (Mutual inductance measurement) : 10 μsec
Execution time of Module 17 (Stator leakage inductance measurement) : 3 μsec

These modules may not be active at the same time as seen from flowchart of the software. Module 15 has the maximum execution time as seen above. So maximum execution time of the software can be calculated when module 15 is active. In the following figure this case is shown.

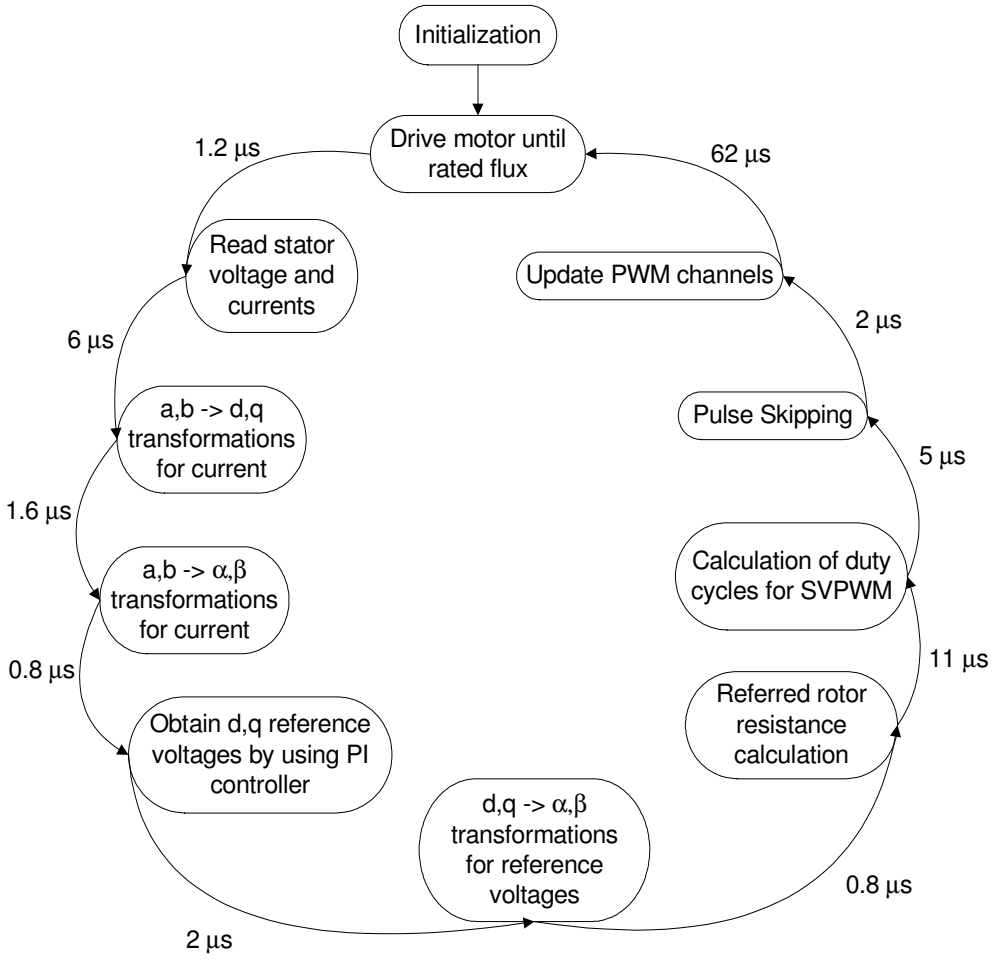

Figure 2. 38. Time diagram of parameter estimation software

As seen from the figure, total execution time of the software is 92.4 µsec. The same change to reduce execution time is performed as in section 2.3.1. New execution time of the software is 76 µsec.

CHAPTER 3

IMPROVEMENTS ON HARDWARE AND SOFTWARE

3.1. Introduction

There were some problems dealing with the hardware prior to starting this thesis. These problems had to be overcome first. Then some improvements were made on both hardware and software to make the drive more efficient and reliable. In this chapter, these improvements are explained.

3.2. Improvements on Dead Time circuit of Lock-Out Module

Lock-out module provides the dead time delay between the upper and lower IGBT signals of the inverter. The circuits, which were used at the beginning of this research, are described below.

P1, P2, P3 output signals of the DSP board, which are introduced in section 2.1.3, are entered to the lock-out module. Then these signals are first inverted and delayed to trigger the lower and upper IGBTs of the inverter. For simplicity only one of three delay circuits is given in Figure 3.1.

As may be seen from Figure 3.1, P1 output of the DSP board is entered to the Lock-out module. It is first inverted with a NOT gate and delayed with an RC circuit. Then UP and UN are obtained which are the upper and lower IGBT switching signals respectively for one inverter leg.

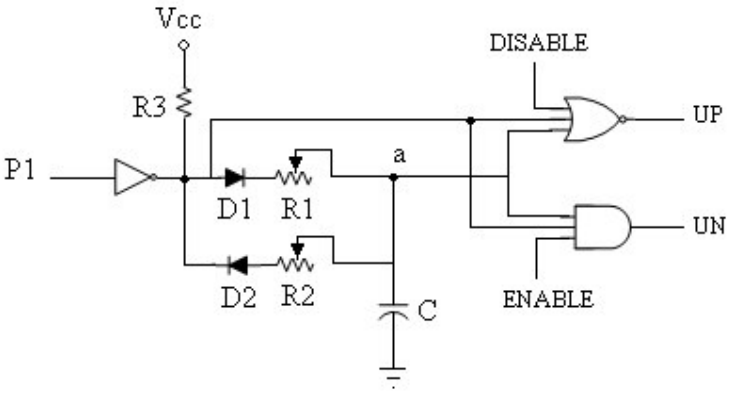

Figure 3. 1.Dead time delay circuit for one leg of the inverter

When the set-up is energized, capacitor is charged automatically through the path Vcc, R3, D1 and R1 because at start-up P1, P2 and P3 are zero. ENABLE signal is 1 while there is no fault due to IPM. DISABLE signal is obtained by inverting the ENABLE signal so DISABLE signal is 0 whenever the ENABLE signal is 1.

When P1 is logic 1, the output of the NOT gate is logic 0. Capacitor is initially charged, so voltage at point a is logic 1. Capacitor starts to discharge through the path R2 and D2. During discharge period, the outputs UP and UN are both zero. The truth tables of NOR and AND gates are given in Table 3.1. Dead time delay circuit becomes as follows during P1=1 and capacitor is charged.

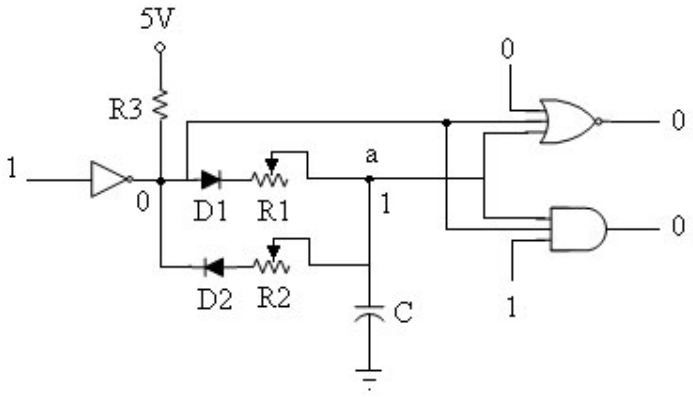

Figure 3. 2.Dead time circuit with P1=1 and capacitor is charged

Table 3. 1.Truth table of AND Gate and NOR Gate

INPUTS			OUTPUT
0	0	0	0
0	0	1	0
0	1	0	0
0	1	1	0
1	0	0	0
1	0	1	0
1	1	0	0
1	1	1	1

AND GATE

INPUTS			OUTPUT
0	0	0	1
0	0	1	0
0	1	0	0
0	1	1	0
1	0	0	0
1	0	1	0
1	1	0	0
1	1	1	0

NOR GATE

When the capacitor is discharged to a level which is logic zero, all of the inputs of NOR gate becomes 0 and its output goes to logic 1. The output of AND gate is still logic 0 because two of its three inputs are zero. D1 and D2 don't conduct in this period. Circuit is shown below while P1=1 and capacitor is discharged.

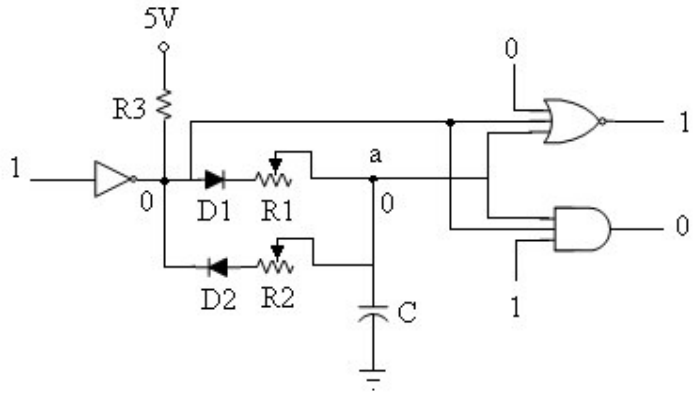

Figure 3. 3 . Dead time delay circuit with P1=1 and capacitor is discharged

When P1 falls to logic 0, the output of the NOT gate becomes logic 1. Voltage at point a is still logic 0 because the capacitor is discharged. Capacitor starts to charge through the path Vcc, R3, D1 and R1. During charging period UP and UN are both zero. Circuit is shown below during this period.

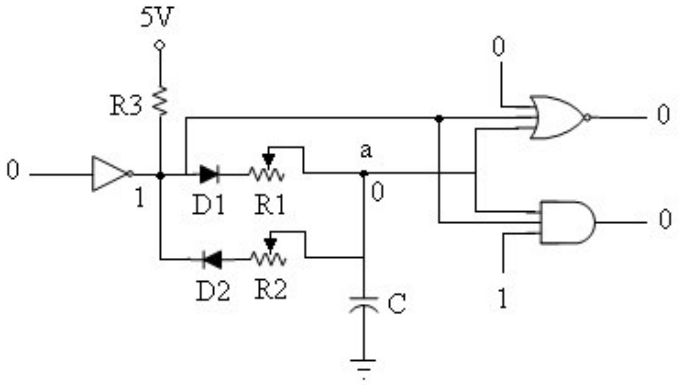

Figure 3. 4.Dead time delay circuit with P1=0 and capacitor is discharged

When the capacitor is charged to a level which is logic 1, all of the inputs of AND gate becomes logic 1 and its output also goes to logic 1. The output of NOR gate is still logic 0, because two of its three inputs are logic 1. Circuit is shown below while P1=0 and capacitor is charged.

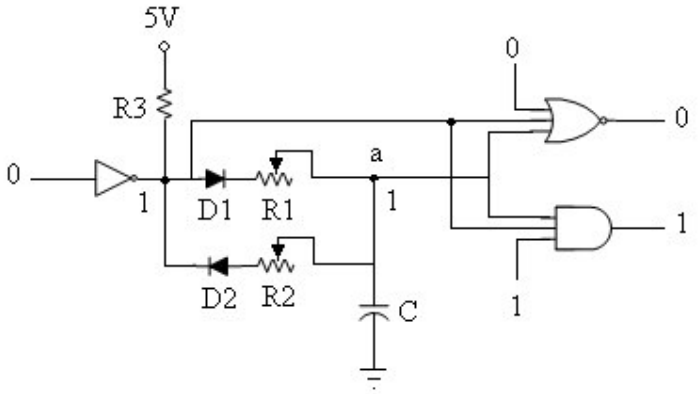

Figure 3. 5.Dead time delay circuit with P1=0 and capacitor is charged

Then P1 goes to logic 1 again while capacitor is charged and sequence is repeated. Whenever a fault occurs due to IPM, ENABLE signal falls to logic 0 and DISABLE signal goes to logic 1 both output UP and UN are zero. Module is disabled. Input signal P1 and corresponding output signals UP and UN are shown in the following figure.

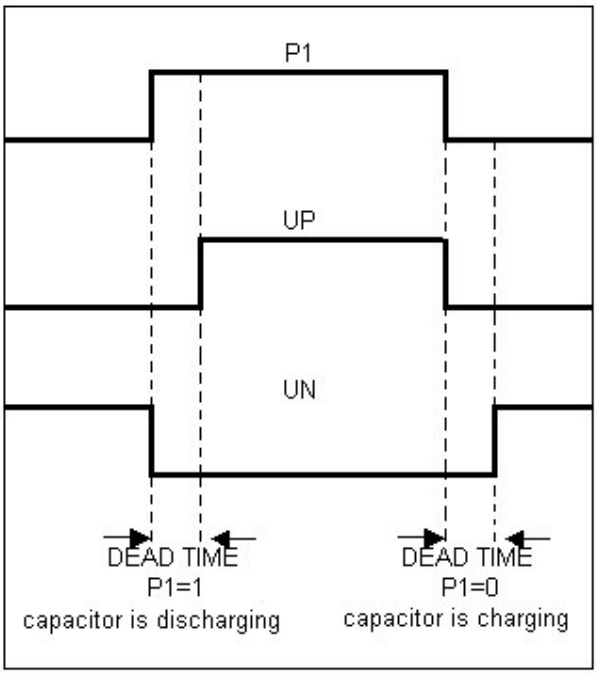

Figure 3. 6.Input signal P1 and corresponding output signals UP and UN

Dead time delay is adjusted by setting the values of R1, R2, R3 and C. To be able to give different dead time delays R1 and R2 are chosen as adjustable pots. In this thesis dead time is adjusted to 3 μsec. PWM frequency is set to 100 μsec. Dead time delay circuit works properly when an input signal is wider than dead time duration.

3.2.1. The Analysis of the Problem

3.2.1.1. Expected Operation

Input signal P1, corresponding output signals UP, UN and capacitor voltage are shown in the following figure for P1=0.5 duty cycle. Capacitor voltage is initially charged as seen from the figure. When P1 goes logic 1, capacitor voltage starts to decrease. When capacitor voltage falls to a level which is logic 0 (2V in this circuit), UP becomes high. So dead time is added to P1 and as a result UP is obtained.

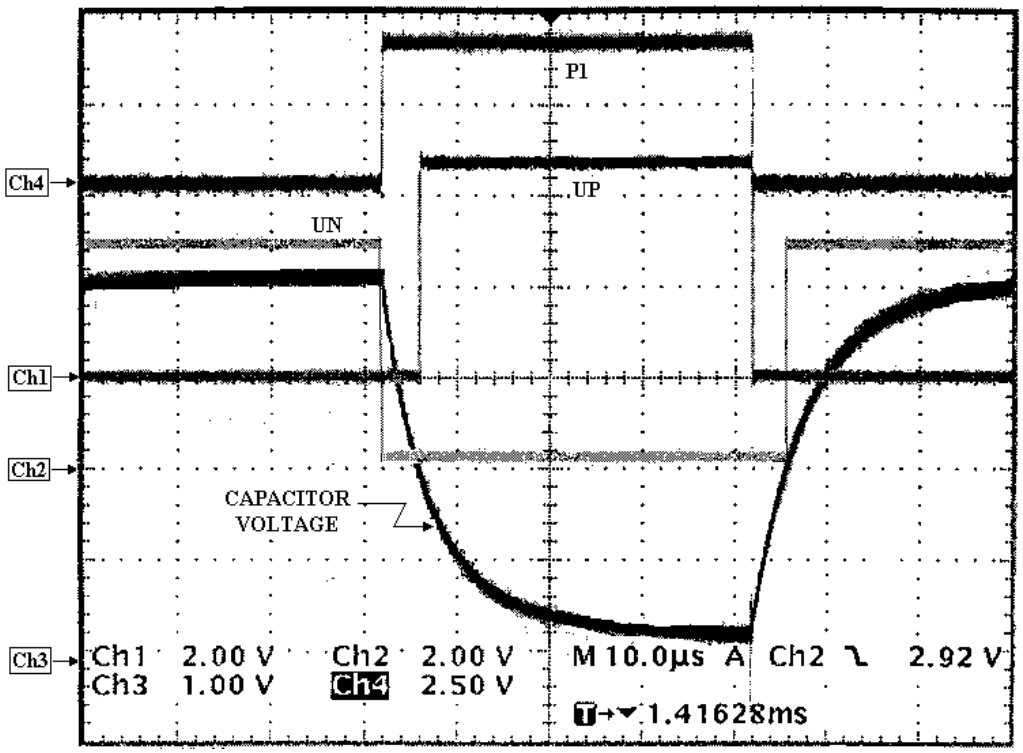

Figure 3. 7.P1, UP, UN and Capacitor voltages during normal operation

When P1 goes logic 0, capacitor voltage starts to increase. When capacitor voltage reaches to a level, which is logic 1 (2V in this circuit), UN becomes high. So dead time is added to P1 and as a result UN is obtained.

3.2.1.2. Problem of The Circuit When a Narrow PWM Pulse is Required

Some problems occur when the input signal gets narrower. As an example, following figure is obtained when P1=0.05 duty cycle is applied to the circuit. As shown from the figure, capacitor cannot be discharged completely due to narrow input signal. Dead time duration between P1 and UP is correct but capacitor voltage could not fall to the value zero. When P1 is zero, in normal conditions capacitor starts to charge from zero voltage level but in this case it started to charge from a value of 1.6V. So dead time between falling edge of P1 and UN could not be set to the adjusted value(3 µsec). At this time it is nearly 500 nanosec. This makes the inverter leg short circuited and damages IPM.

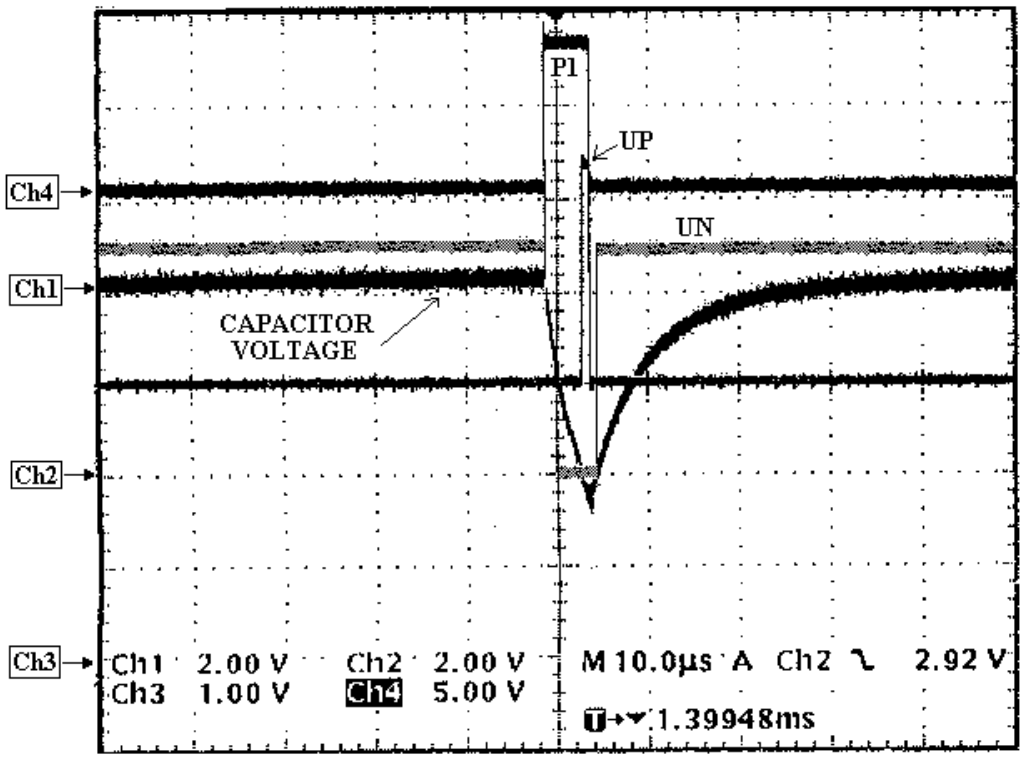

Figure 3. 8.P1, UP, UN and Capacitor voltages during P1=0.05

As seen from Figure 3.8 dead time is added to P1 input signal and UP output signal is obtained while the capacitor is discharging. Also dead time is inserted between P1 and UN while the capacitor is charging. When narrow PWM pulses are applied to the circuit, capacitor cannot be discharged completely and dead time durations become shorter than the adjusted value. As a result IPM is damaged. This problem occurs due to using only one capacitor while adding dead times between signals.

3.2.2. Modified Dead Time Circuit

In this thesis to correct the problem following circuit is implemented on the same board by making some modifications.

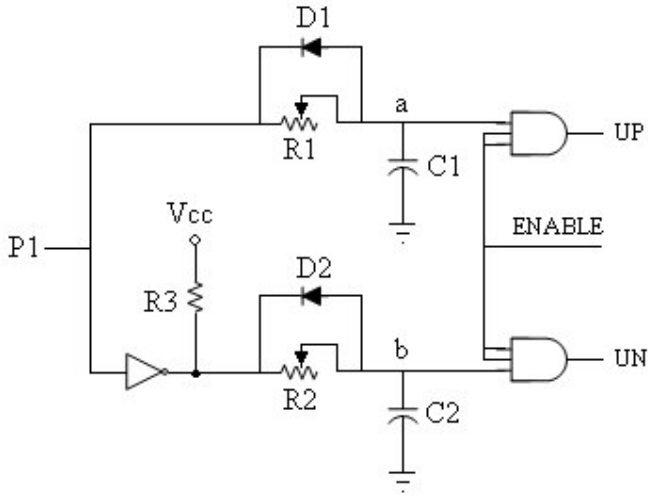

Figure 3. 9. Dead time circuit after modifications

In this new circuit, when the set-up is energized capacitor C1 remains discharged and capacitor C2 charges to its rated value through the path Vcc, R3 and R2. As soon as ENABLE signal is logic 1, the circuit is active and UP is 0 UN is 1 with P1=0.

When P1 is logic 1, capacitor C1 starts to charge. The voltage at point a and consequently UP is logic 0. Capacitor C2 was initially charged but as soon as P1 is logic 1, output of the NOT gate becomes logic 0 and capacitor C2 is discharged quickly through the path C2 and D2. As a result the voltage at point b and UN is logic 0.

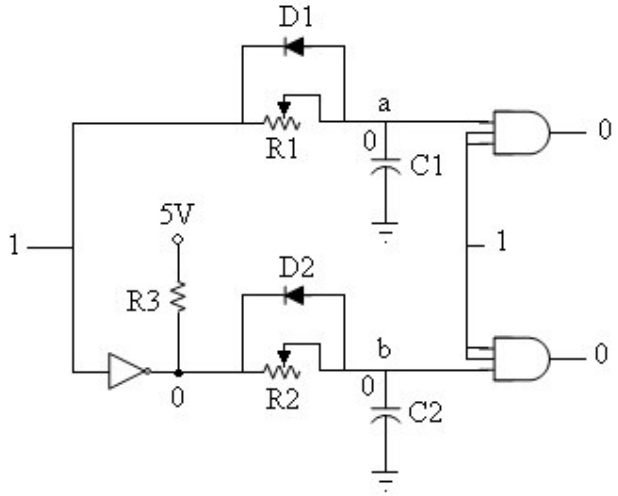

Figure 3. 10.New dead time delay circuit with as soon as P1=1

UP becomes 1 whenever C1 capacitor voltage reaches to a level of logic 1. UN is still 0. The circuit becomes as follows

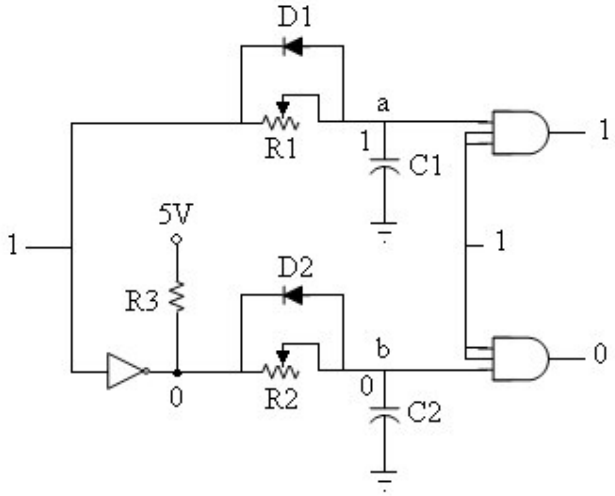

Figure 3. 11.New dead time delay circuit with P1=1

When P1 is logic 0, output of the NOT gate becomes logic 1 and capacitor C2 starts to charge through the path Vcc, R3 and R2. The voltage at point b and consequently UN is logic 0 during this period. Capacitor C1 was initially charged but as soon as P1 is logic 0, capacitor C1 is discharged quickly through the path C1 and D1. As a result the voltage at point a and UP is logic 0.

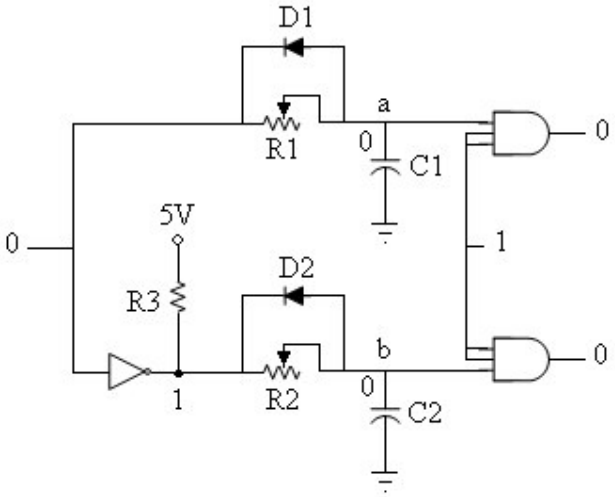

Figure 3. 12.New dead time delay circuit with as soon as P1=0

UN becomes 1 whenever C2 capacitor voltage reaches to a level of logic 1. UP is still 0. The circuit becomes as follows

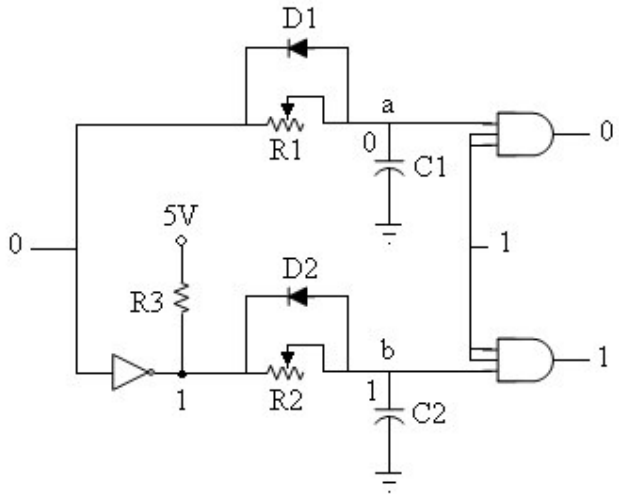

Figure 3. 13. New dead time delay circuit with P1=0

Then Up goes to high again and sequence is repeated. Modified dead time circuit is tested with P1=0.05 duty cycle and performance of the modified dead time circuit is presented in Figures 3.14 and 3.15. Upper IGBT switching signal (UP), P1 input signal and C1 capacitor voltage are shown in Figure 3.14.

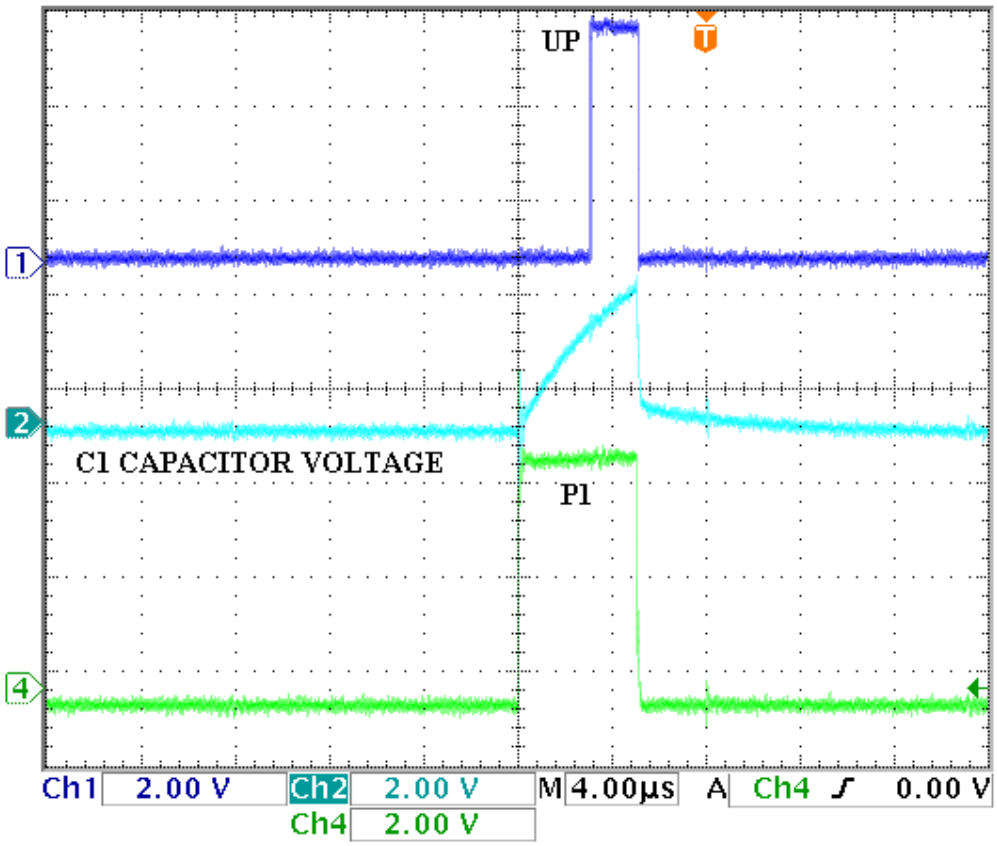

Figure 3. 14. UP and C1 Capacitor voltage during P1=0.05 duty cycle is applied to the modified dead time circuit

As seen from the figure, C1 capacitor starts to charge when P1 is logic 1 and UP becomes high when capacitor voltage reaches to a level of logic 1 (2V in this application). Normally charging process of capacitor continues until rated value but in this case capacitor voltage cannot reach to the rated value due to narrow PWM signal. Incomplete charging does not create any problems in this circuit.

When P1 signal goes to logic 0, capacitor is discharged quickly and circuit is ready for the following PWM pulse. As seen from the figure dead time duration (3 µsec) is correctly added between P1 input signal and switching signal of upper IGBT (UP). Lower IGBT switching signal (UN), P1 input signal and C2 capacitor voltage are shown in Figure 3.15.

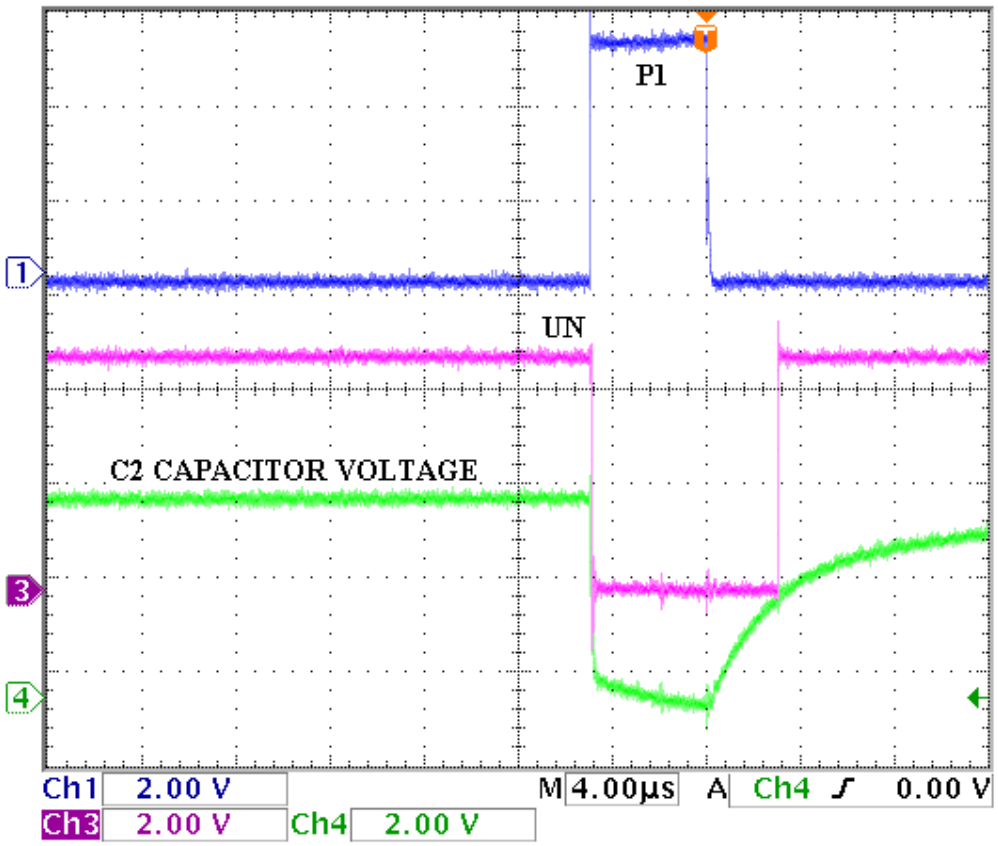

Figure 3. 15. UN and C2 Capacitor voltage during P1=0.05 duty cycle is applied to the modified dead time circuit

As seen from the figure, C2 capacitor starts to charge when P1 is logic 0 and UN becomes high when capacitor voltage reaches to a level of logic 1 (2V in this application). Charging process of capacitor continues until rated value.

When P1 signal goes to logic 1, capacitor is discharged quickly. As seen from the figure dead time duration (3 µsec) is correctly added between P1 input signal and switching signal of lower IGBT (UN).

This circuit gives the correct dead time delays whatever the duty cycle is applied. Input signal P1 and corresponding output signals UP and UN are shown in the following figure. Also capacitors producing dead time durations are defined in the figure.

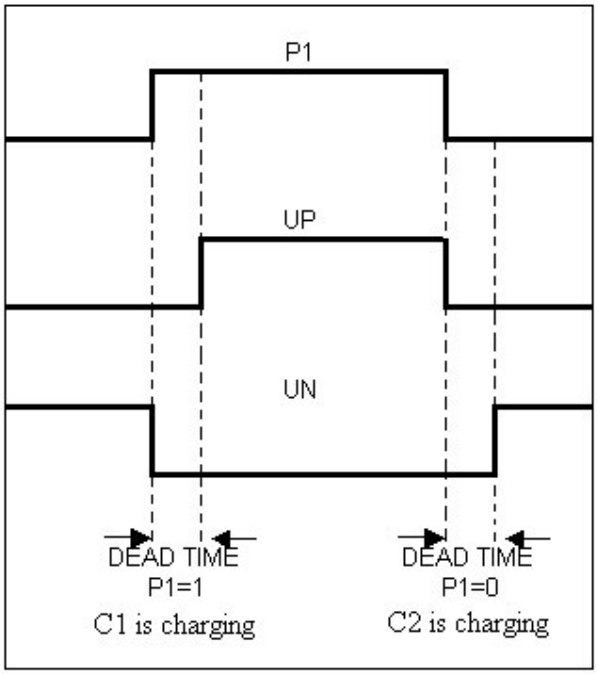

Figure 3. 16.Input signal P1 and corresponding output signals UP and UN

3.3. Improvements on protection circuit of Lock-out module

Protection circuit of the hardware is on the lock-out module. Whenever a fault occurs, IPM creates a fault signal, which is active low. This fault signal comes to the Lock-out module and PWM pulses to IPM are inhibited with this signal, so module is disabled and IPM is protected. The protection circuit at the beginning of the project was as follows

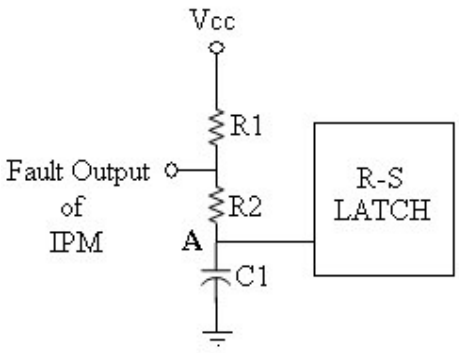

Figure 3. 17. Protection circuit

Fault output of the IPM is filtered with an RC filter, which eliminates switching noises and then this signal is given to the RS latch as an input. RC filter was set to 10 msec initially by setting R2=40kΩ and C1=10nF. R3 is taken as 10kΩ. 74LS279 is used as an RS latch whose input high current is nearly 0.1mA.

It was observed that sometimes a fault signal is produced although IPM actually was operating properly and fault free. This was due to using very high resistance values with an LS279, which has a very high input high current level. Since input high current level is nearly 0.1 mA, voltage drop on R1 is 1V and voltage drop on R2 is 4V so that voltage at point A is nearly 0V although fault output of IPM is 5V. This causes the protection circuit to trip. This problem is overcome by using an HC279, which has a very low input high current (nearly 20 μA) with respect to LS279.

Also at the beginning of this project, time constant of the filter was adjusted to 10 msec due to mistake in the datasheets. The protection circuit cannot protect the IPM with this filter because IPM is defected completely in 10msec. Filter time constant is adjusted to 10 μsec in this thesis. For this reason, filter resistance component is changed. New value of R2 is 1 kΩ.

3.4. Improvements on decoupling module of vector control software

In the previous studies, reference values of direct axis stator current (I_{sdref}) and quadrature axis stator current (I_{sqref}) components were used while obtaining decoupling terms as shown in the following equations. Theory of this module and used variables are given in section 2.2.2.7. Reference values of direct axis stator current (I_{sdref}) and quadrature axis stator current (I_{sqref}) are given as 2.4 and 1.53 respectively and measured as in the following figure.

decoupleD=-ws*sig*ls*isqref (3.1)

decoupleQ=ws*ls*isdref (3.2)

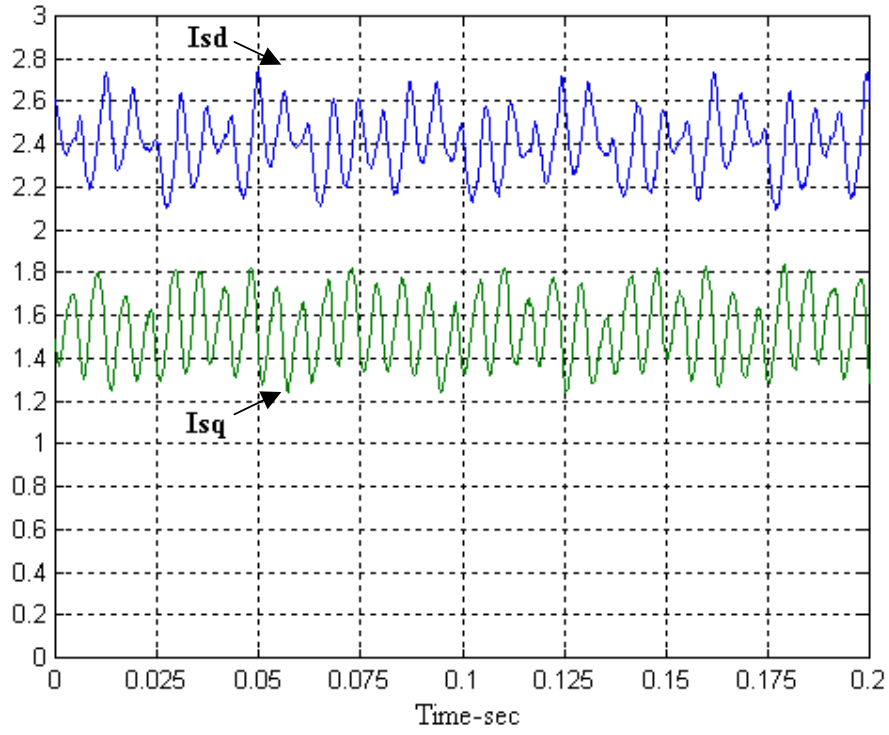

Figure 3. 18. d and q components of stator current before modification

Real values of the stator currents should be used in the decoupling equations to achieve decoupling properly. Real values of Isd and Isq are used in the equations as follows

decoupleD=-ws*sig*ls*isq (3.1)

decoupleQ=ws*ls*isd (3.2)

When the real values of direct axis and quadrature axis stator current components are used in the decoupling calculations, current values close to their reference values and fewer ripples occur as shown in the following figure

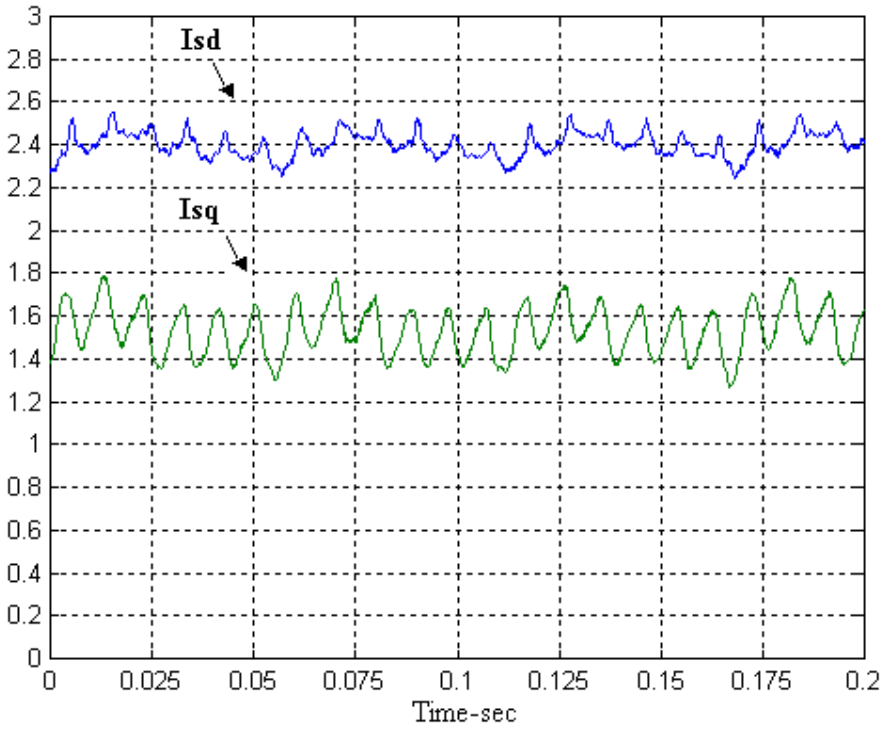

Figure 3. 19. d and q components of stator current after modification

After the modifications made on both hardware and software;

- protection circuit is working properly
- dead time delay circuit inserts dead times between signals correctly even if the input signal is very narrow
- and finally voltage decoupling process is performed more accurately.

CHAPTER 4

CALIBRATION AND TESTING OF THE SYSTEM

4.1. Introduction

In this chapter, calibration of voltage and current measurement modules, which are explained in section 2.1.4, are given first. Then dead time adjustment, inverter turn-on and turn-off times are verified. Also calculation of flux and experimental results in different speeds are presented with figures obtained from TRACE program.

4.2. Calibration of the voltage measurement module

For the calibration purpose, single phase line voltage is connected to the variac, and the output of the variac is connected to the input of the LEM as shown in the following figure.

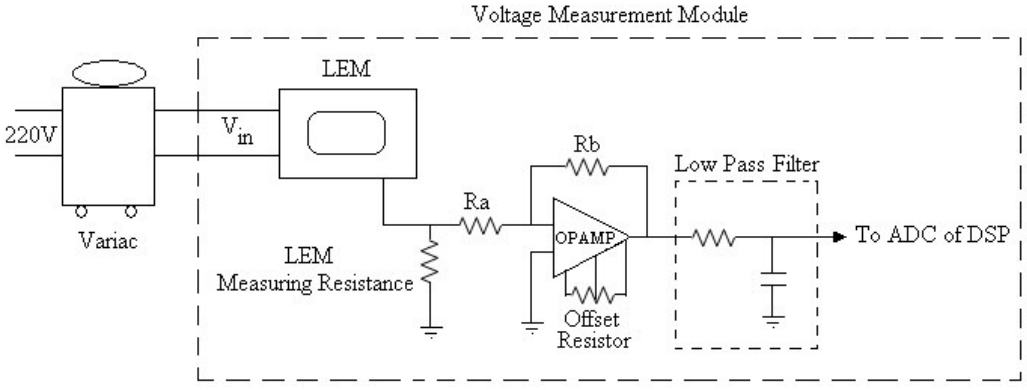

Figure 4. 1. Set-up used in the calibration of voltage measurement module

Calibration of the module is performed for different voltage levels by comparing the data obtained from TRACE program with oscilloscope output at 50 Hz.

Cut-off frequency of the filter at the output of the module is 500Hz. Characteristic of the filter can be explained as follows

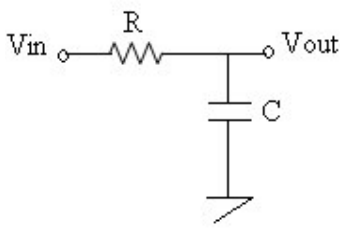

Figure 4. 2. Analog Filter

$$V_{out} = \frac{\frac{1}{jwC}}{R + \frac{1}{jwC}} V_{in} \tag{4.1}$$

$$\frac{V_{out}}{V_{in}} = \frac{1}{1 + jwC} \tag{4.2}$$

If equation (4.2) is written in terms of phasors, gain and phase shift of filter can be obtained.

$$Gain = \left| \frac{V_{out}}{V_{in}} \right| = \frac{1}{\sqrt{1 + (wRC)^2}} \tag{4.3}$$

$$PhaseShift = \angle(-\tan^{-1} wRC) \tag{4.4}$$

Since the filter used in this circuit has a cut-off frequency of 500Hz, multiplication of R and C can be found as follows

$$\frac{1}{\sqrt{1 + (wRC)^2}} = \frac{1}{\sqrt{2}} \Rightarrow RC = \frac{1}{w} = \frac{1}{2\pi f} = \frac{1}{2\pi 500} = 3.18 \cdot 10^{-4} \tag{4.5}$$

Characteristic of the filter can be written as

$$\frac{1}{\sqrt{1+(1.011\cdot 10^{-7} w^2)}} \angle(-\tan^{-1}(3.18\cdot 10^{-4} w)) \tag{4.6}$$

Phase difference and gain of the filter can be calculated at different frequencies.

Table 4. 1. Filter gain and phase difference at different frequencies

Frequency (Hz)	Gain	Phase Shift (Degrees)
10	0,999	-1,14
20	0,999	-2,29
30	0,998	-3,43
40	0,997	-4,57
50	0,995	-5,71
75	0,989	-8,53
100	0,981	-11,3

The filter gain at 50 Hz is 0.995, so calibration at this frequency is acceptable. There is no frequency dependent component in the voltage measurement module except low pass filter. Since the gain is near unity at lower frequencies the module measures the voltage correctly. In this thesis, frequency range of the system is 0-50Hz (motor speed is between 0 and 3000rpm). At higher frequencies phase shift increases and gain decreases. Filter must be redesigned to work correct at higher frequencies.

Input of the Analog Digital Converter is $\pm$ 10V. This input range must not be exceeded. While making the calibration, maximum obtainable output voltage is taken into account. Peak value of the maximum fundamental phase voltage that may be achieved in Space Vector Pulse Width Modulation (SVPWM) is:

$$\left|\vec{V}_{ref}\right|_{\max} = \frac{2}{3} V_d \frac{\sqrt{3}}{2} = \frac{1}{\sqrt{3}} V_d = \frac{1}{\sqrt{3}} 560 = 323V \tag{4.7}$$

In the voltage measurement module resistors are adjusted so that ADC input is 7V when the input of the LEM is 340 V. Safety margin is left. LEM module can read voltage up to 485 volts without damaging ADC. Calibration of the module is given in the following figures.

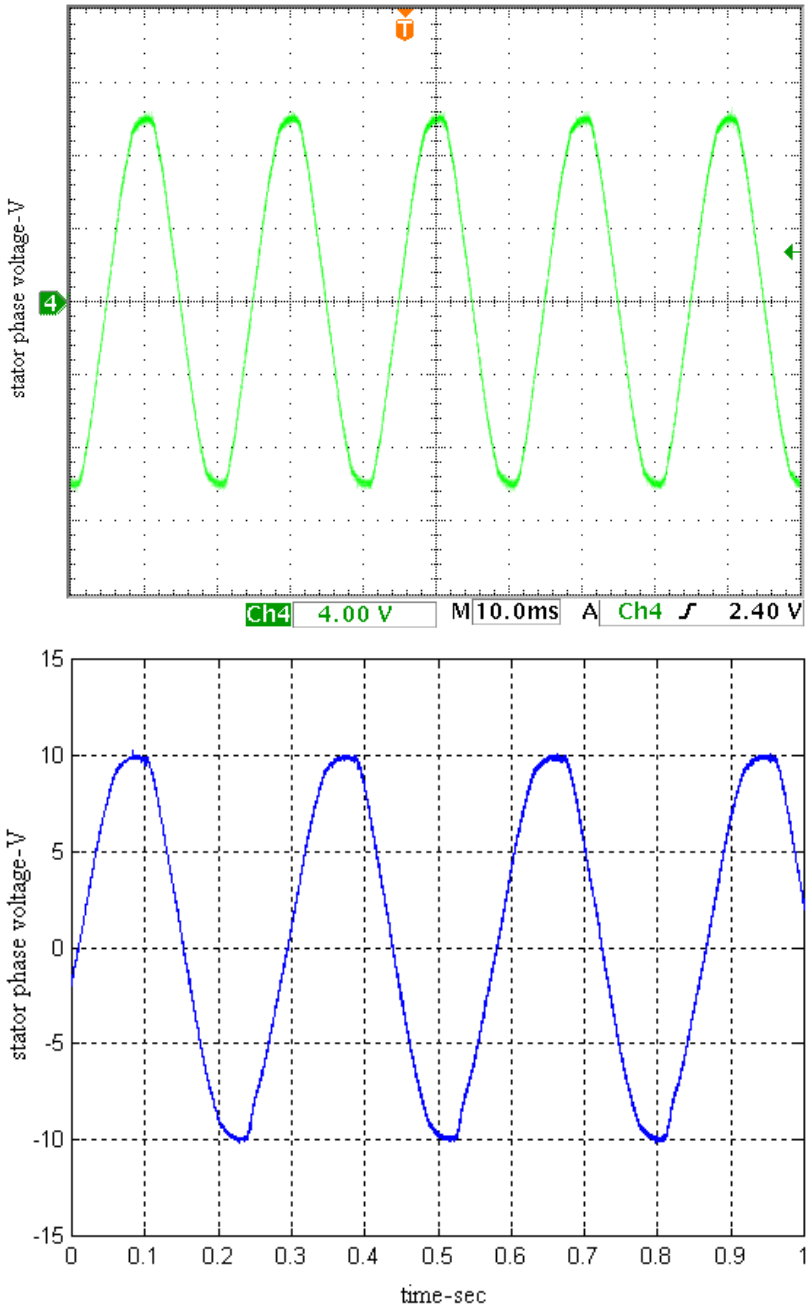

Figure 4.3. a - Stator phase voltage waveform obtained from scope
b - Stator phase voltage waveform obtained from TRACE for 10V peak at 50 Hz

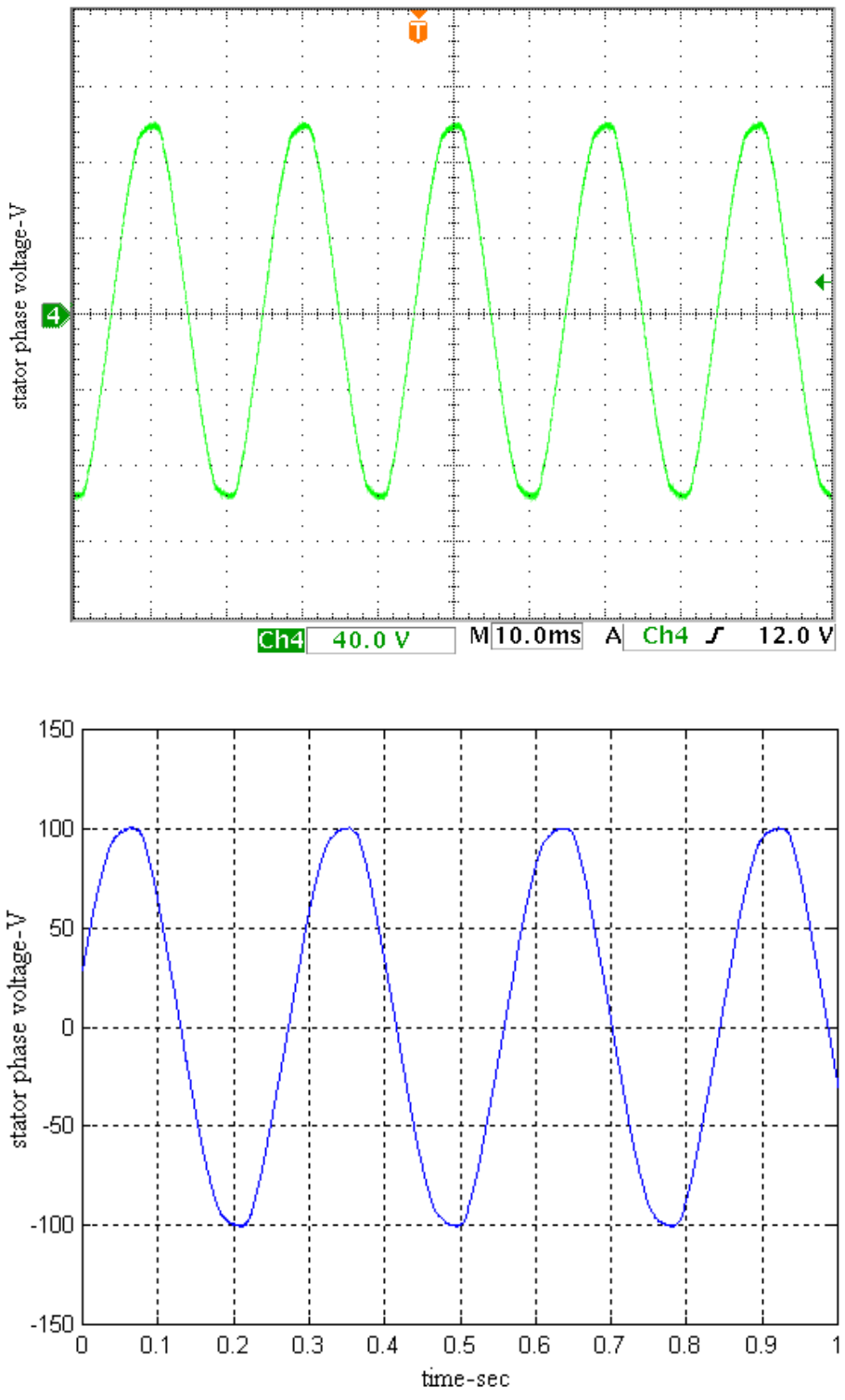

Figure 4. 4. a - Stator phase voltage waveform obtained from scope
b - Stator phase voltage waveform obtained from TRACE for 100V peak at 50 Hz

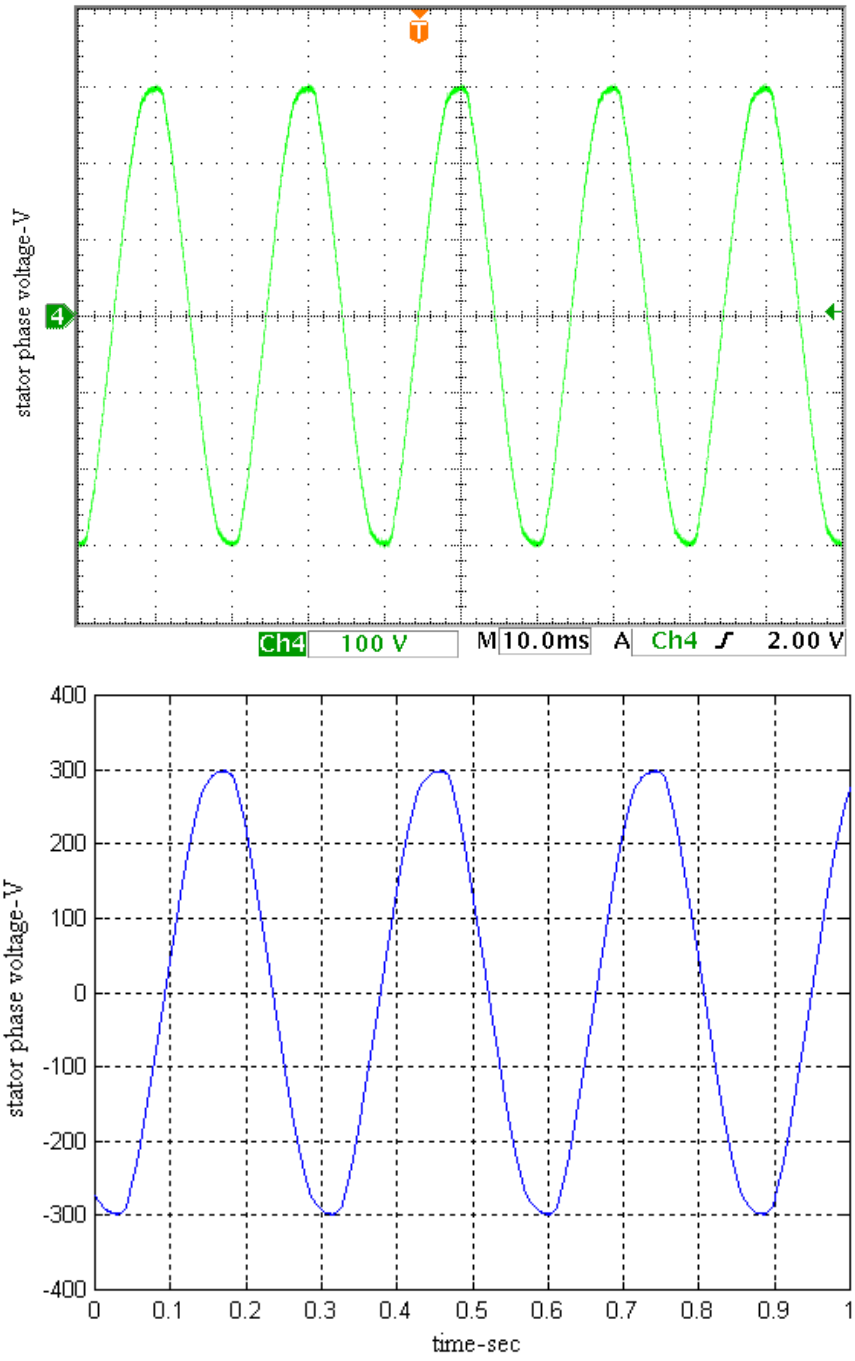

Figure 4. 5. a - Stator phase voltage waveform obtained from scope
b - Stator phase voltage waveform obtained from TRACE for 300V peak at 50 Hz

As may be seen from the figures TRACE data and oscilloscope data are the same. So calibration is performed successfully for voltage measurement module.

4.3. Calibration of the current measurement module

Motor is driven in V/f principle at different speeds and calibration of current measurement module is performed by comparing TRACE data with oscilloscope. Calibration of the module is given in the following figures.

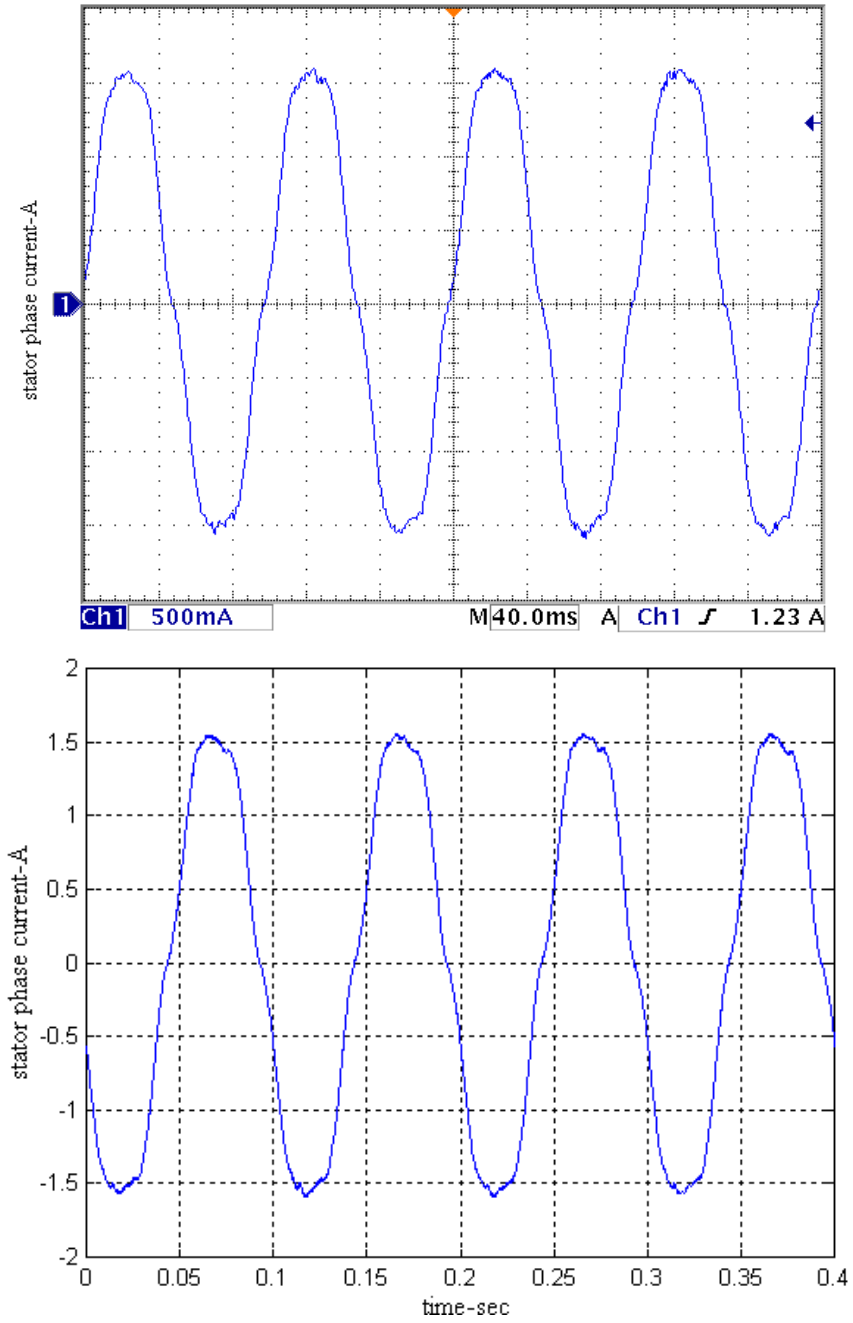

Figure 4. 6.a - Stator current waveform obtained from scope
b - Stator current waveform obtained from trace for 10Hz 60V reference

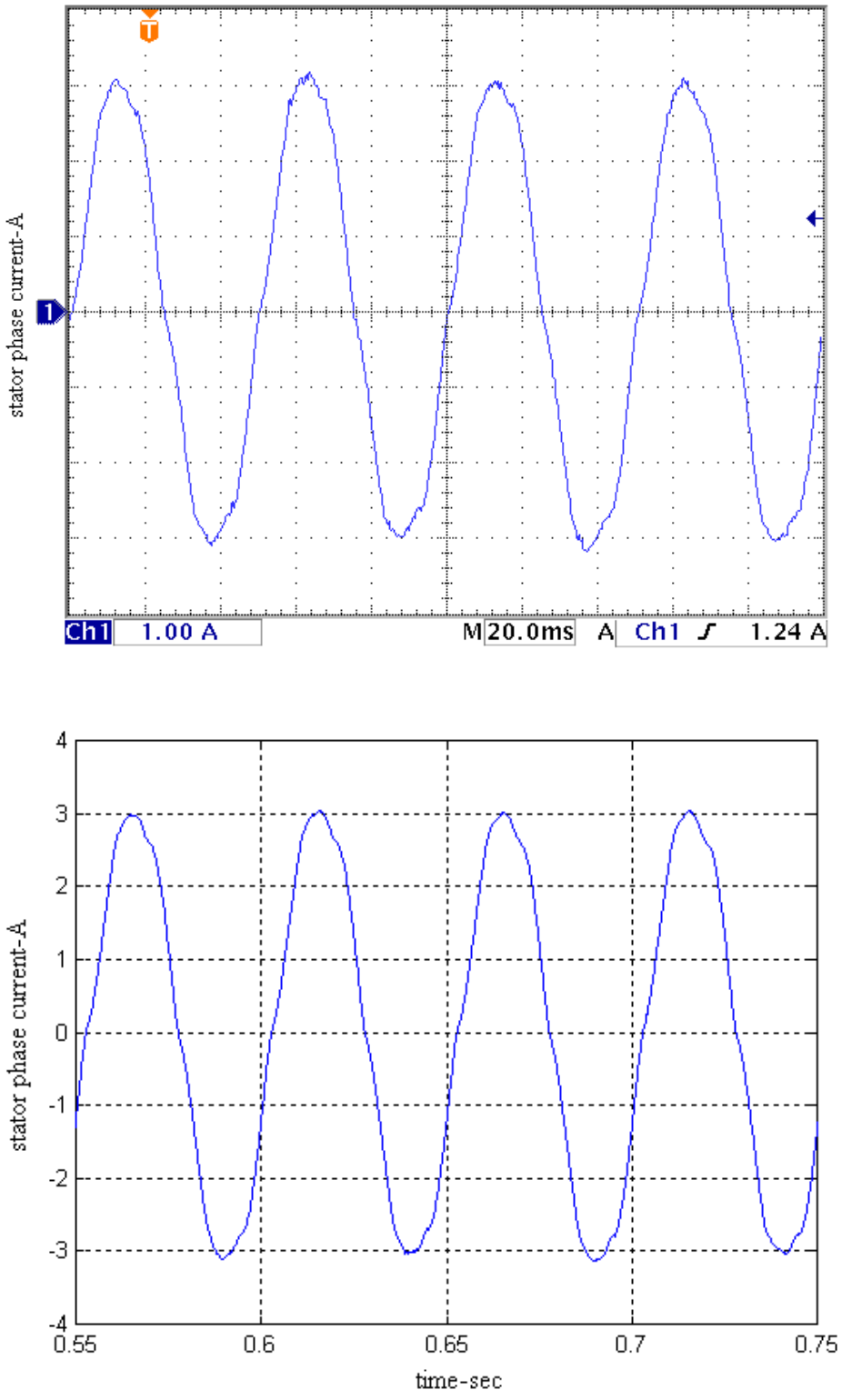

Figure 4. 7.a - Stator current waveform obtained from scope
b - Stator current waveform obtained from trace for 20Hz 120V reference

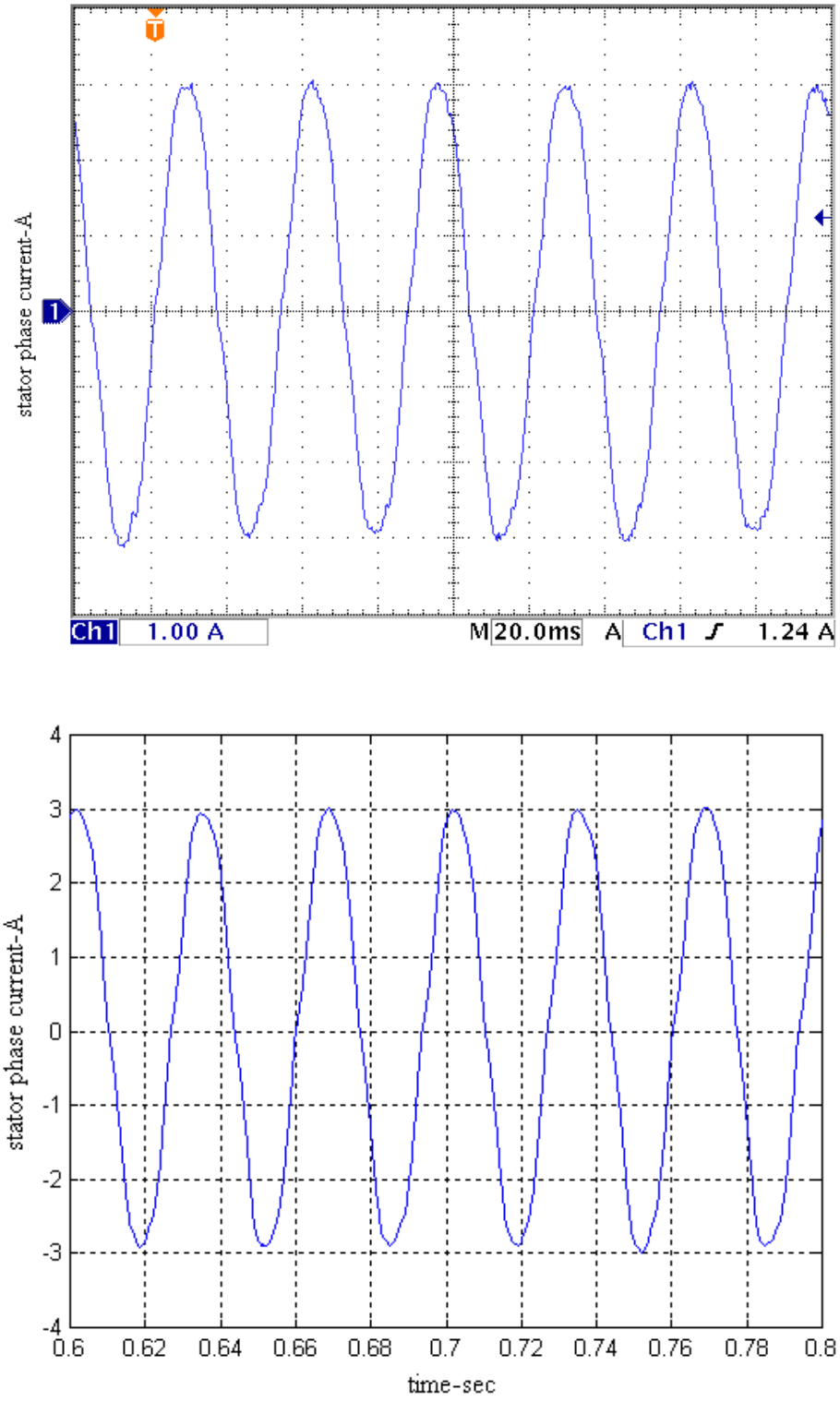

Figure 4. 8.a - Stator current waveform obtained from scope
b - Stator current waveform obtained from trace for 30Hz 180V reference

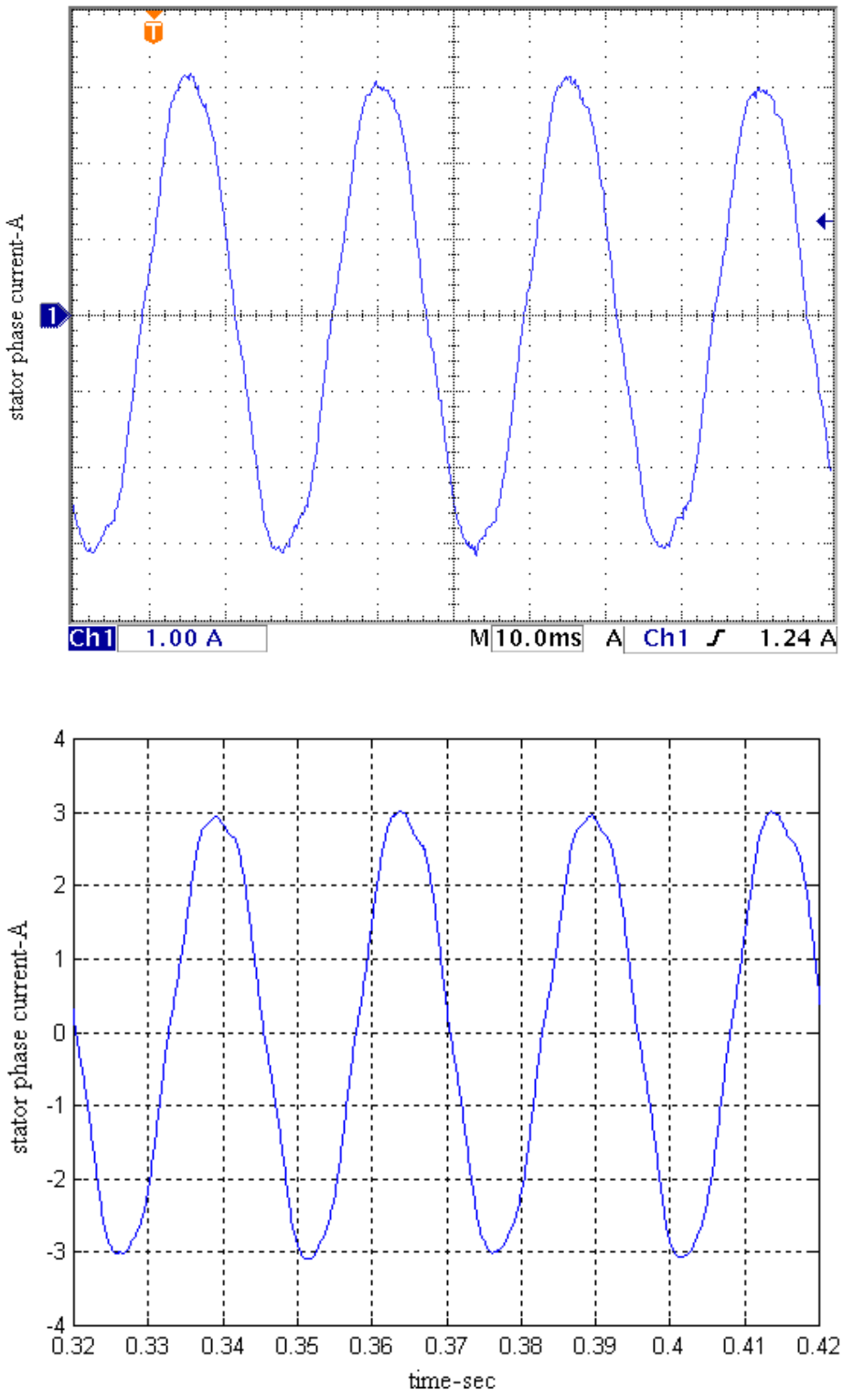

Figure 4. 9.a - Stator current waveform obtained from scope
b - Stator current waveform obtained from trace for 40Hz 240V reference

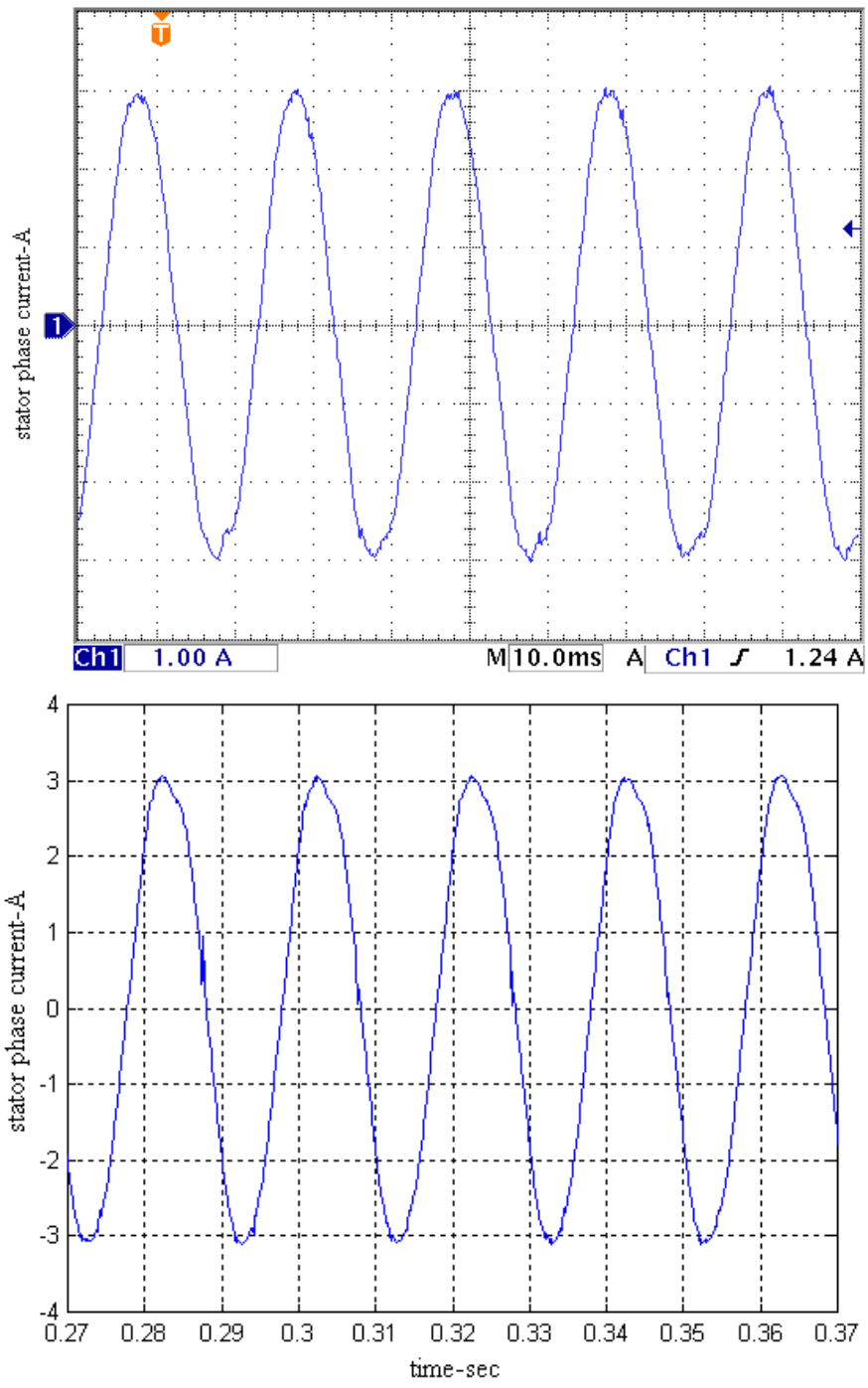

Figure 4. 10.a - Stator current waveform obtained from scope
b - Stator current waveform obtained from trace for 50Hz 300V reference

As seen from the figures, calibration is verified for different frequencies. TRACE data and oscilloscope data are the same for all frequencies, so the calibration is performed successfully.

4.4. Calibration tests performed on the lock-out module

Lock-out circuit provides the dead time delay between the upper and lower IGBT signals of the inverter. Dead time delay must be adjusted correctly not to cause short circuit in the inverter leg. Also IGBT turn on and turn off times must be checked to be sure that dead time duration is enough.

4.4.1. Verification of dead time durations between logic signals

For the calibration purpose of dead times, Lock-out module is disconnected from the isolation card. P1, P2, P3 input signals, which convey the inverter phase information are produced by DSP and sent to Lock-out circuit. Two oscilloscope channels are used to compare firstly P1(P2,P3) input signal and upper IGBT switching signal (UP) and then P1(P2,P3) input signal and lower IGBT switching signal (UN). POT1-POT6 which are delay calibration potentiometers on lock-out circuit are used to adjust dead time durations to 3 µsec. Dead time verification for one inverter leg is shown below. Same measurements are obtained for the other legs.

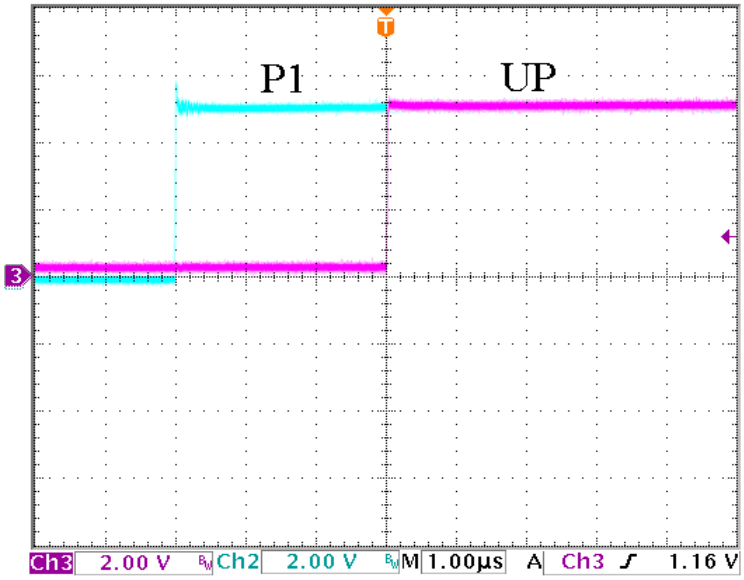

Figure 4. 11. P1 input signal and delayed signal UP

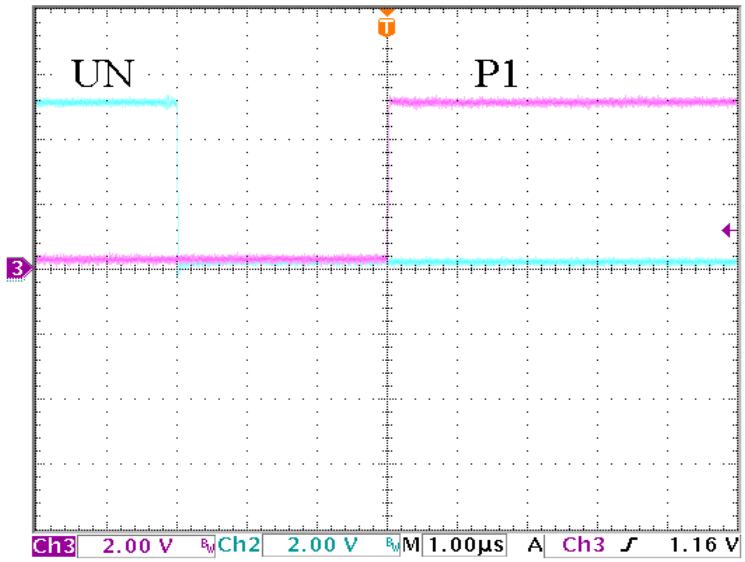

Figure 4. 12. P1 and delayed signal UN

3 µsec dead time durations between logic signals can be observed clearly from the figures 4.12 and 4.13. Also it is necessary to check dead times between upper IGBT switching signal (UP) and lower IGBT switching signal (UN). For this purpose UP and UN are observed at the same time as shown in the following figure. 3 µsec dead time duration between logic signals is seen clearly.

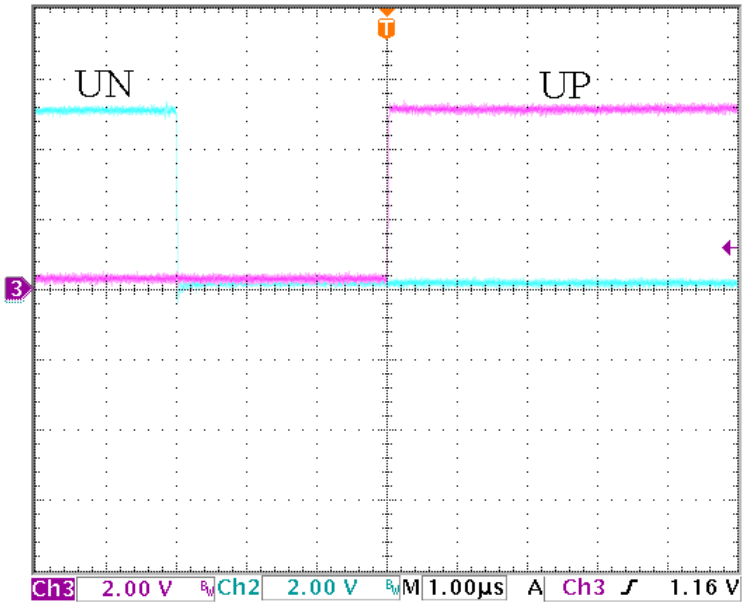

Figure 4. 13. Dead time between upper IGBT switching signal (UP) and lower IGBT switching signal (UN)

4.4.2. Measurement of IGBT turn on and turn off times

IGBT turn on and turn off times is measured to be sure that dead time delay is enough. For this purpose motor is driven at V/f control with 300V, 50Hz reference. Phase current is effective on the turn on and turns off times. Motor is loaded to make the measurements in worst case. Inverter is shown below.

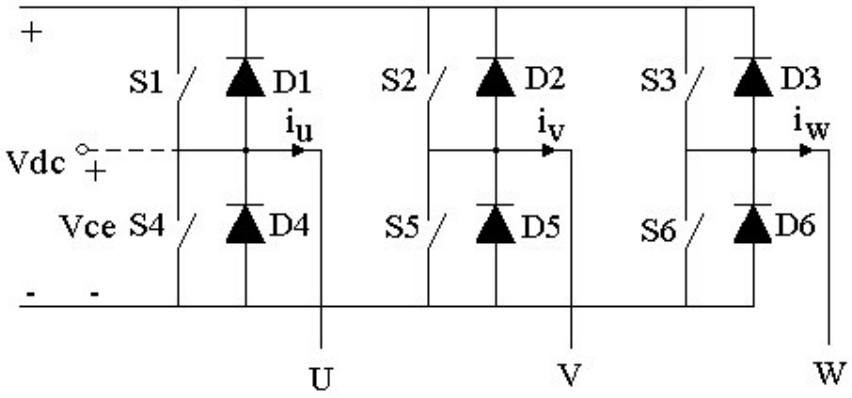

Figure 4. 14. Three phase inverter

In the figure S1, S2, S3, S4, S5 and S6 represents switches, D1, D2, D3, D4, D5 and D6 represents diodes, U,V and W represents inverter phases, Vdc represent DC link voltage, i_u, i_v and i_w represents phase currents and Vce represents collector-emitter voltage of switch S4.

Switching signals for one phase of the inverter is shown in Figure 4.15. There are four modes in the operation of inverter as depicted in the following figure.

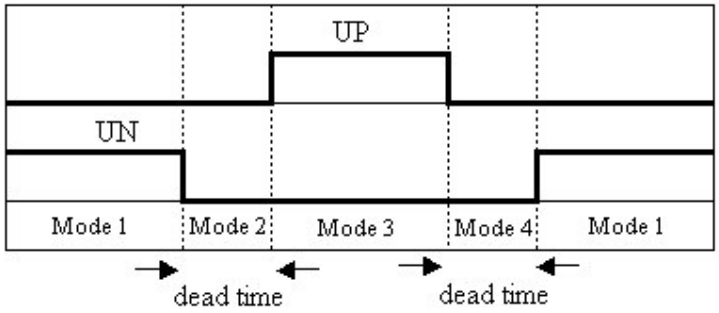

Figure 4. 15. Upper and lower switching signals for U phase of inverter

There are two possible polarities for phase current in each cycle. Phase current may be positive or negative. These two possible states must be explained first.

4.4.2.1. Analysis of the inverter operation with positive phase current

Inverter operation modes shown in Figure 4.15 are explained here in detail for positive phase current.

Mode 1:

In mode 1, lower switch (S4) is on and upper switch (S1) is off. Current path and states of switches are shown in the following figure. Collector-emitter voltage of S1 switch is at the level of DC link and collector-emitter voltage of S4 switch is nearly zero.

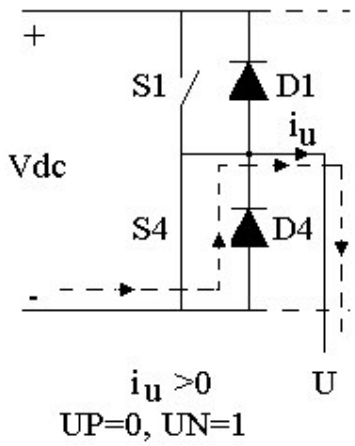

Figure 4. 16. Current path and switch positions for UP=0 and UN=1

Mode 2:

In Mode 2, S4 switch is turned off and current still flows through diode D4. During this period both switching signals UP and UN are zero. Collector-emitter voltages of S1 switch and S4 switch is the same with Mode 1.

Mode 3:

This mode can be divided into two parts. In the first part, Upper IGBT (S1) switching signal (UP) is logic 1 and switch starts to turn on. Diode D4 conducts and carries the current. Second part starts when S1 switch is turned on completely. Collector-emitter voltage of switch S1 becomes zero and collector-emitter voltage of S4 switch becomes to a level of DC link as soon as S1 switch is turned on. Inverter switches and current path are shown in the following figure for this mode

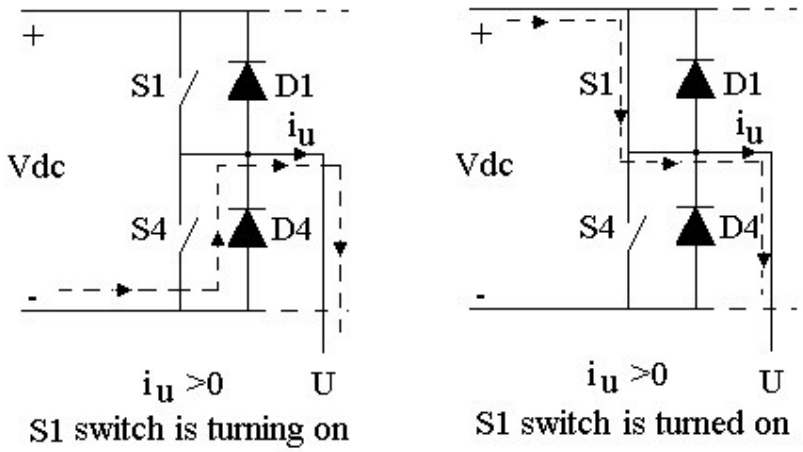

Figure 4. 17. Current path and switch states for UP=1 and UN=0

Mode 4:

This mode can be divided into two parts. In the first part, UP becomes zero and switch S1 starts to turn off. While Switch is turning off, collector-emitter voltage of S1 switch is nearly zero and collector emitter voltage of switch S4 is at the level of DC link. Second part starts when S1 switch is turned off completely. Diode D4 starts to conduct and collector-emitter voltage of S4 switch becomes zero while collector-emitter voltage of S1 switch reaches to the level of DC link. Current path and position of switches during this period are shown in the following figure

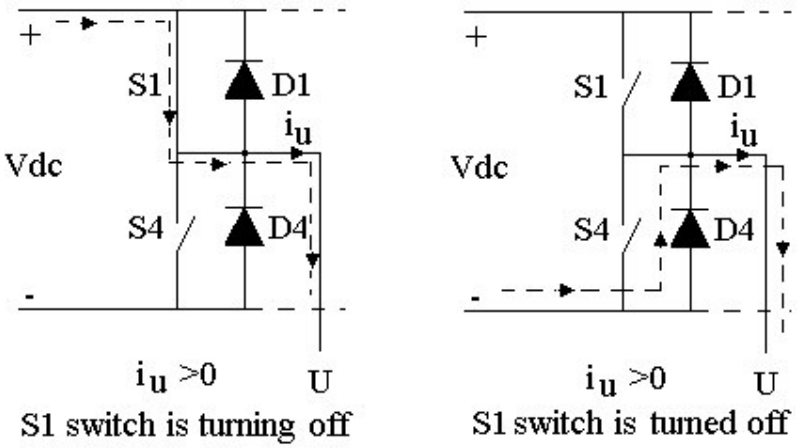

Figure 4. 18. Current path and switch states for UP=0 and UN=0

4.4.2.2. Measurement of IGBT turn on time when the phase current is positive

To measure turn on time of IGBT, collector-emitter voltage of S4 switch and upper IGBT switching signal (UP) is observed while the phase current is positive. When logic 1 signal is sent to switch S1, collector-emitter voltage of S4 switch remains zero until switch S1 is turned on completely. Voltage reaches to a level of DC link as soon as switch S1 is turned on completely as explained in Mode 3 of section 4.4.2.1.

Turn on time can be measured at this instant. Turn on time is measured as 1.1 μsec as shown in Figure 4.19.

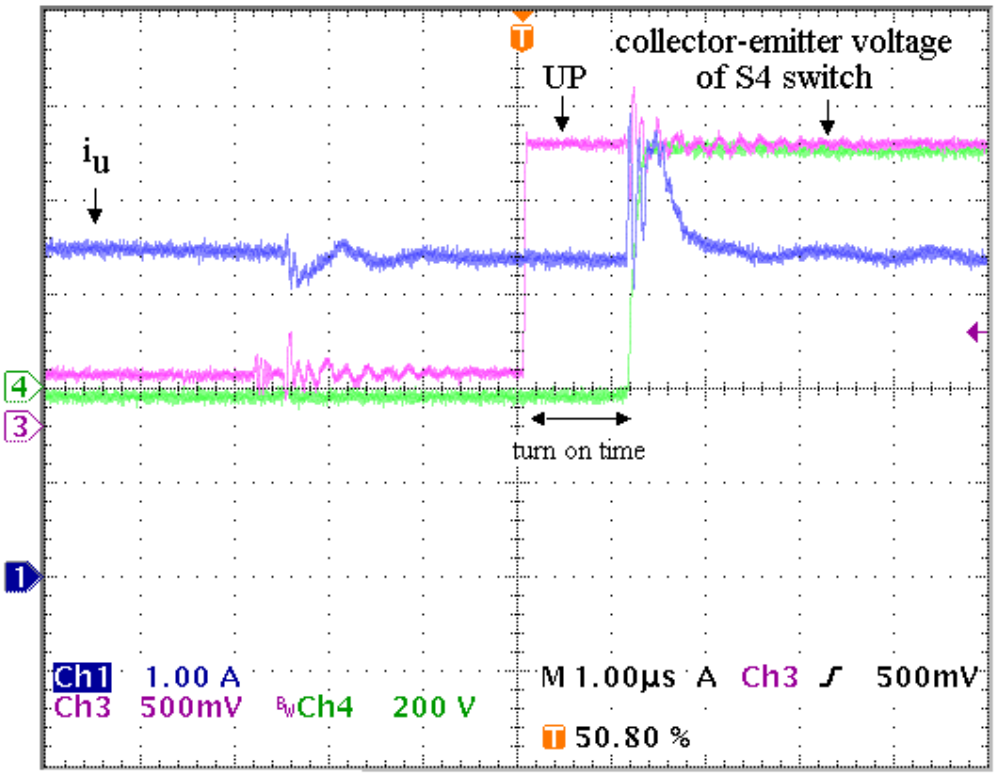

Figure 4. 19. Phase current, UP and collector-emitter voltage of S4 switch during turn on time measurement

4.4.2.3. Measurement of IGBT turn off time when the phase current is positive

To measure turn off time of IGBT, collector-emitter voltage of S4 switch and upper IGBT switching signal (UP) is observed while the phase current is positive. When UP goes from high to low, collector-emitter voltage of S4 switch remains at the level of Vdc until S1 switch turns off completely. When S1 switch is turned off, diode D4 starts to conduct and collector-emitter voltage of S4 switch becomes nearly zero as explained in mode 4 of section 4.4.2.1. Turn off time can be measured at this instant. Turn off time is measured as 2.2 µsec as shown in the following figure.

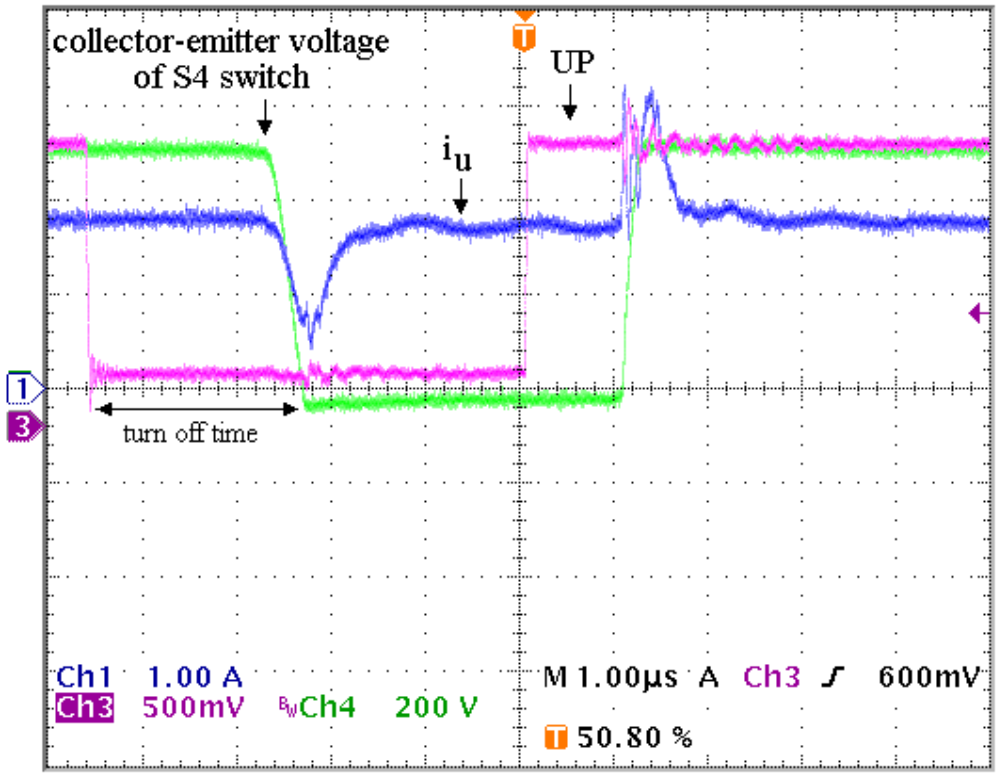

Figure 4. 20. Phase current, UP and S4 voltage during turn off time measurement

IGBT turn on and turn off times can also be measured when the phase current is negative.

4.4.2.4. Analysis of the inverter operation with negative phase current

Inverter operation modes shown in Figure 4.15 are explained here in detail for negative phase current.

Mode 1:

This mode can be divided into two parts. In the first part, UN becomes logic 1 and S4 switch starts to turn on. During turn on process, collector-emitter voltage of S4 switch is at the level of DC link, current flows through diode D1 consequently collector-emitter voltage of S1 switch is zero. Second part starts when S4 switch is turned on completely. Collector-emitter voltage of S4 switch becomes zero. Current path and inverter switch states are shown in the following figure

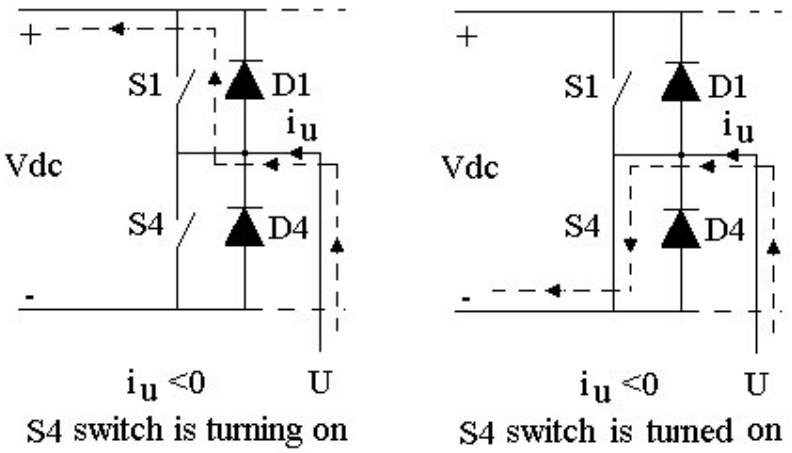

Figure 4. 21.Current path and switch positions for UP=0 and UN=1

Mode 2:

This mode can be divided into two parts. In the first part, UN is logic 0 and S4 switch starts to turn off. During turn off process, current flows through S4 switch and as a result collector-emitter voltage of S4 switch is zero. Second part starts when the S4 switched is turned off completely. Diode D1 starts to conduct and carry current and collector-emitter voltage of S4 switch reaches to the level of DC link. Inverter switches and current path are shown in the following figure for this stage

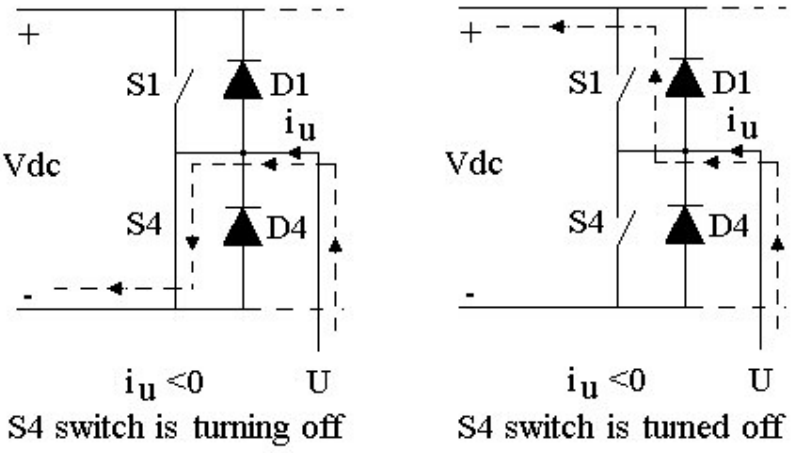

Figure 4. 22.Current path and switch positions for UP=0 and UN=0

Mode 3:

In this mode, S1 switch is turned on and current still flows through diode D1.

Mode 4:

In this mode, S1 switch is turned off. Current remains to flow through diode D1. At this stage both switching signals are zero. Current path and switch positions are shown below

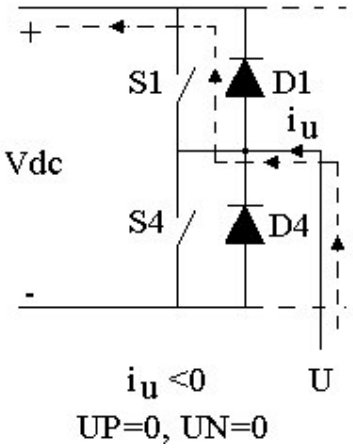

Figure 4. 23. Current path and switch positions for UP=0 and UN=0

4.4.2.5. Measurement of IGBT turn on and turn off times when the phase current is negative

To measure turn on time of the IGBT, Upper IGBT switching signal (UP) and collector-emitter voltage of S4 switch are observed while the phase current is negative. When UN goes from low to high which occurs a dead time duration later than transition of UP from high to low, S4 switch starts to turn on. During turn on process, collector-emitter voltage of S4 switch remains at the level of DC link. Voltage becomes zero as soon as S4 switch is turned on completely as explained in mode 1 of section 4.4.2.5. Turn on time is measured as 1.1 μsec as shown in Figure 4.24.

To measure turn off time of IGBT, collector-emitter voltage of S4 switch and UP signal are observed again while the phase current is negative. When logic 0 signal is sent to S4 switch, which is a dead time before than transition of UP from low to high, S4 starts to turn off. During turn off process S4 switch carries the phase current. Collector-emitter voltage of S4 switch remains zero until S4 switch is turned off completely. Voltage reaches to the level of DC link as soon as S4 switch is turned

off completely as explained in mode 2 of section 4.4.2.4. Turn off time can be measured at this instant.

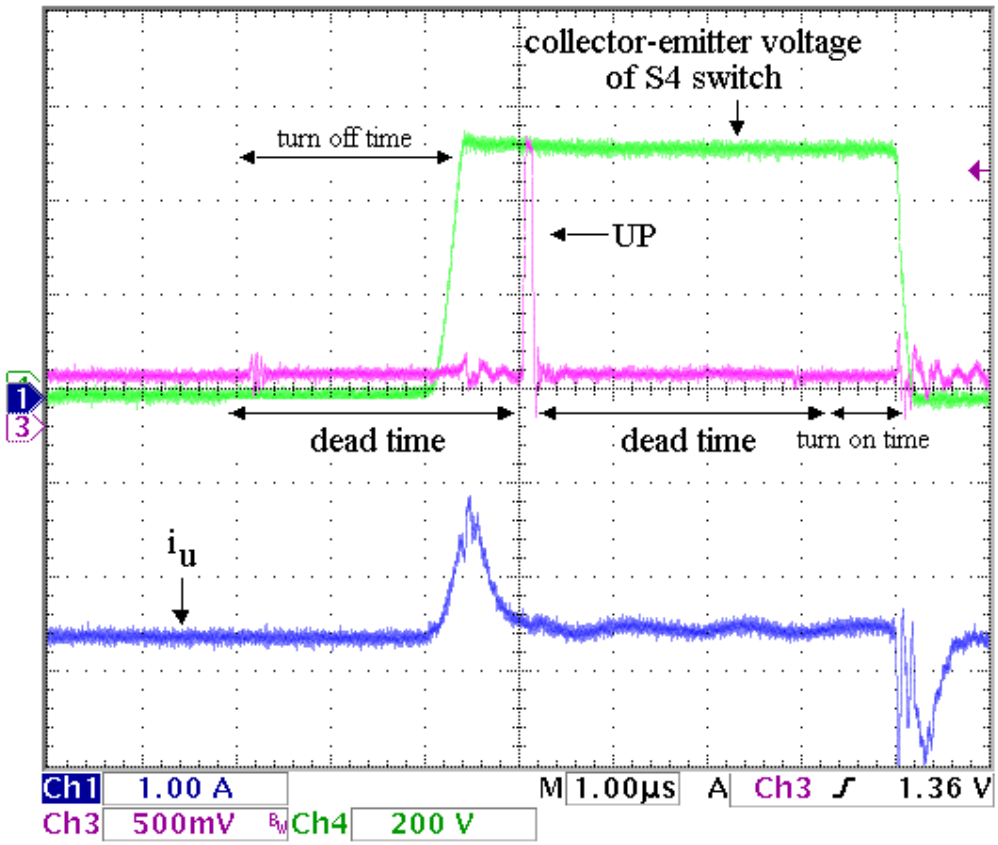

Figure 4. 24.Phase current, UP and collector-emitter voltage of S4 switch while the current is negative

Turn off time is measured as 2.2 µsec as shown in the following figure. IGBT turn on and turn off times are given in the datasheets as follows

Table 4. 2. IGBT turn on and turn off times taken from datasheets

Inductive load switching times	Min.	Typical	Max.	Units
turn on	0,5	1	2,5	µsec
turn off	-	2	3	µsec

As may be seen from Table 4.2, turn on and turn off time measurements performed in this section are nearly the same with data sheet typical values. For the safety, dead times are adjusted to 3 μsec in the circuit.

4.5. Rotor Flux Measurements

Reference value of rotor flux is calculated as 0.9 Wb from nameplate data of the motor in Appendix C. Measured stator phase voltages and phase currents are used in the estimation of rotor flux. Rotor flux estimation method is explained in detail in section 2.2.2.12. Rotor fluxes are observed in TRACE program while the motor is driven with vector control at 2 Nm torque reference. Rotor flux estimations in different motor speeds are given in the following figures.

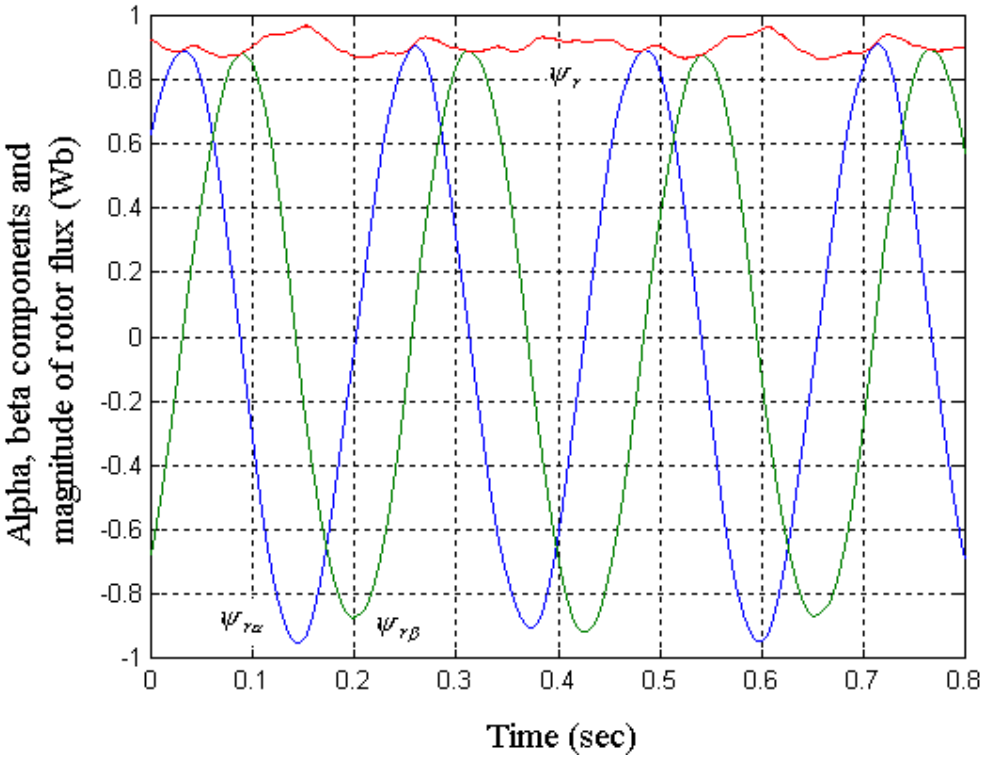

Figure 4. 25. α,β components and magnitude of rotor flux at 200 rpm

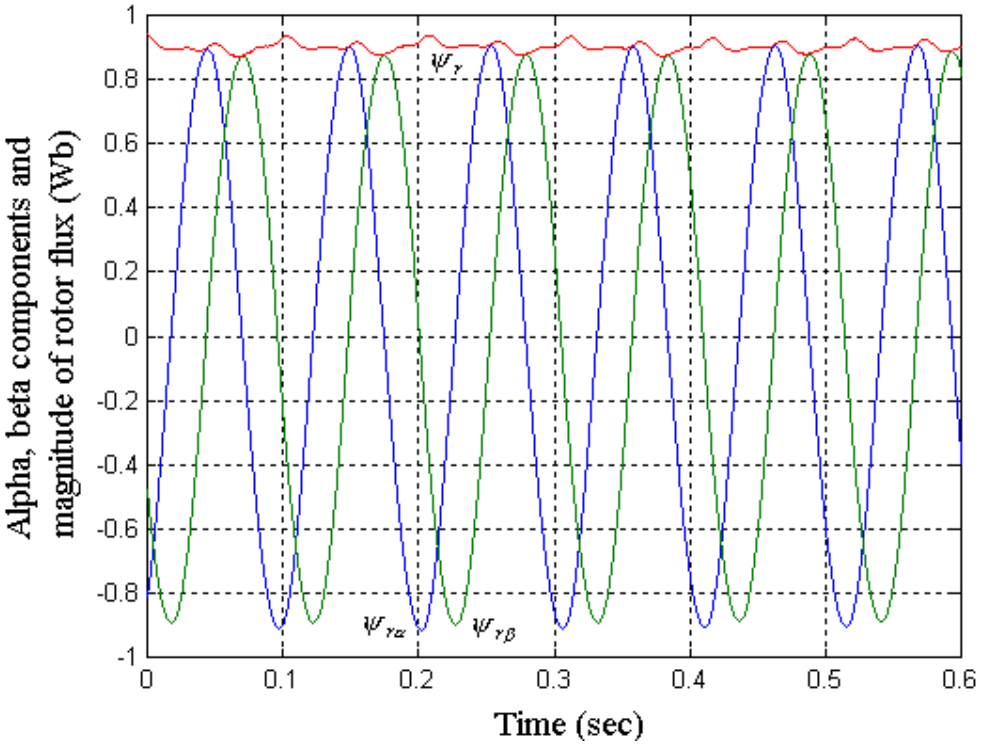

Figure 4. 26. α,β components and magnitude of rotor flux at 500 rpm

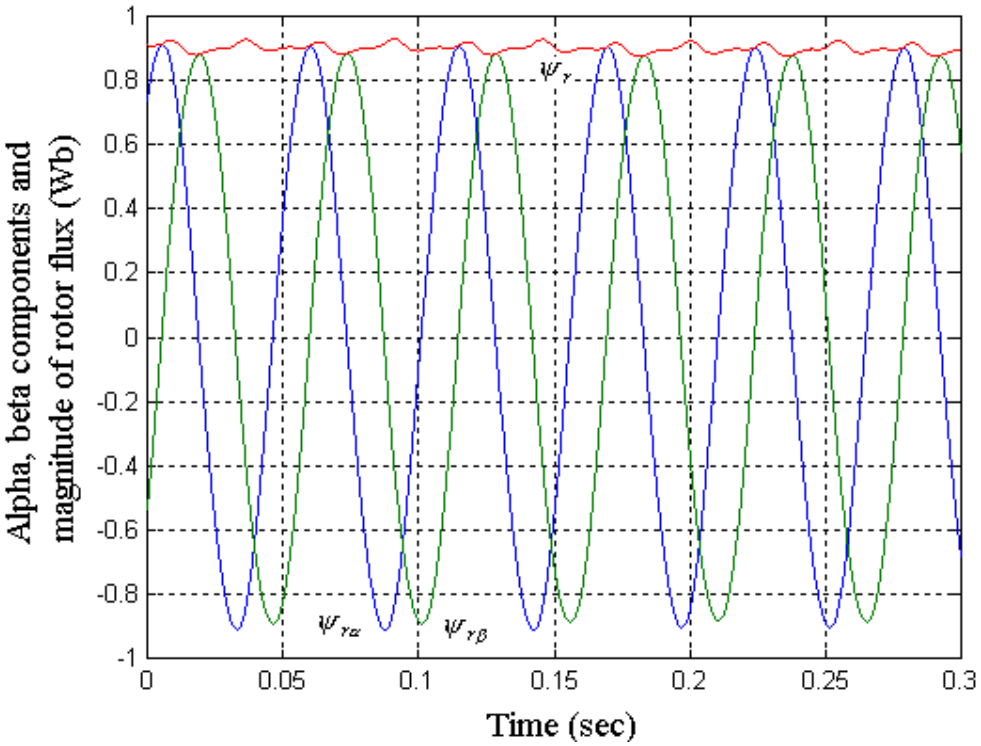

Figure 4. 27. α,β components and magnitude of rotor flux at 1000 rpm

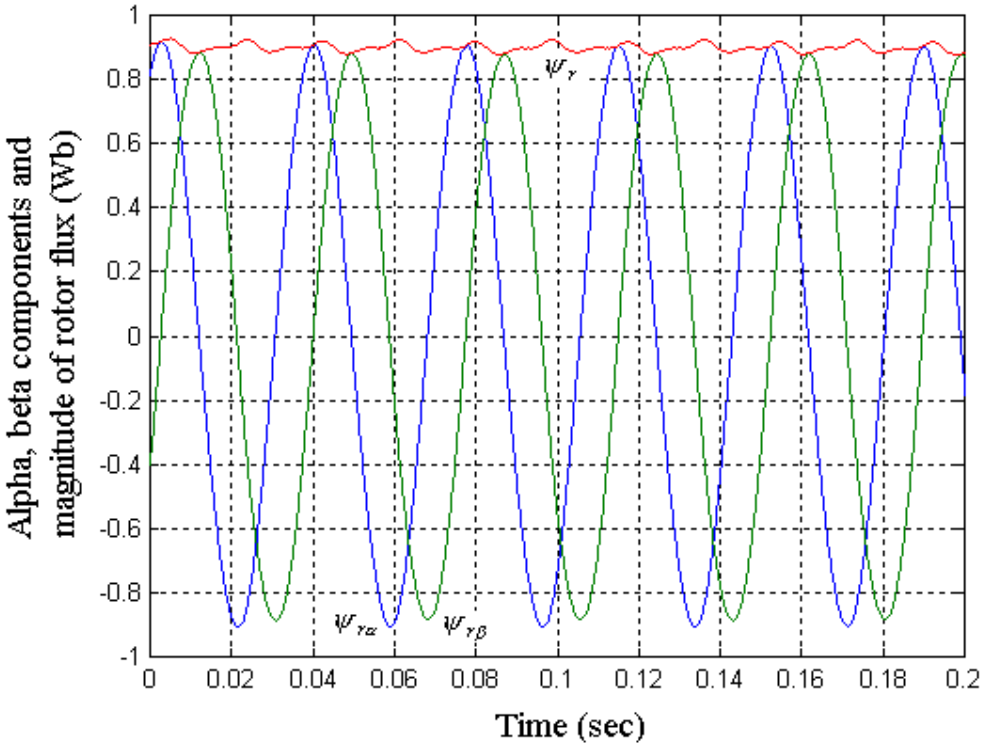

Figure 4. 28.α,β components and magnitude of rotor flux at 1500 rpm

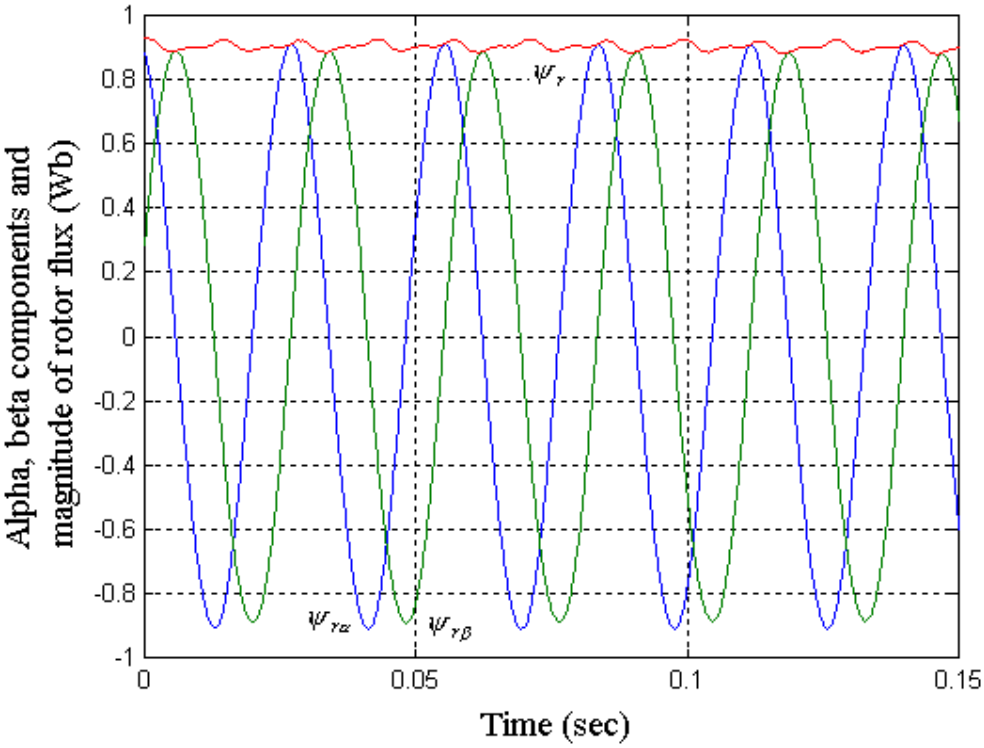

Figure 4. 29.α,β components and magnitude of rotor flux at 2000 rpm

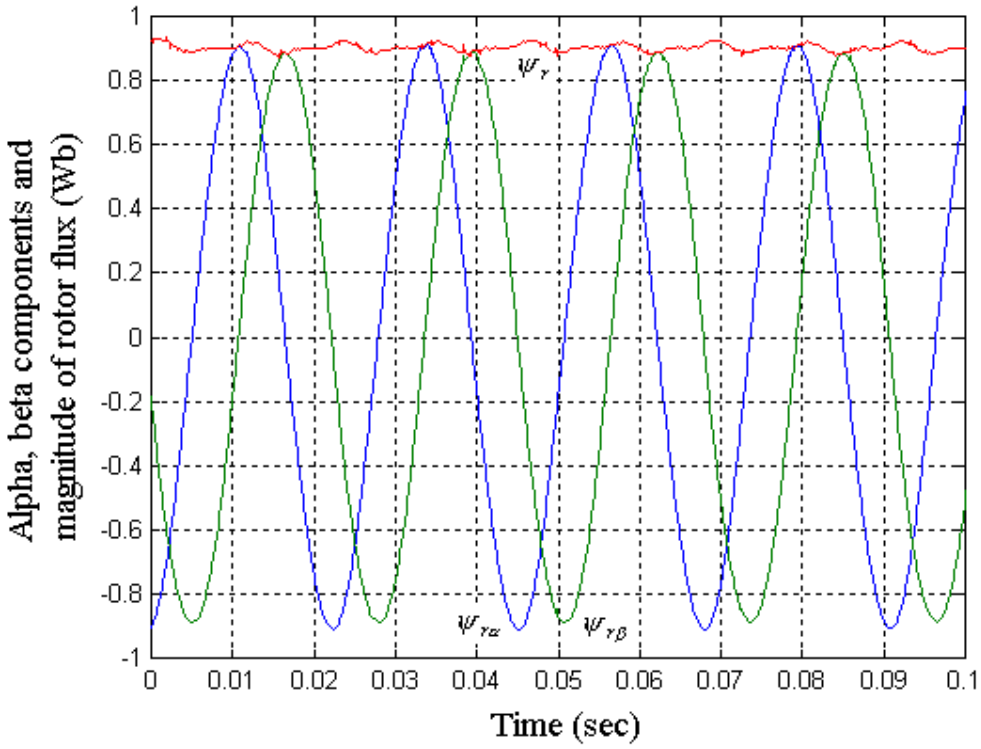

Figure 4. 30. α,β components and magnitude of rotor flux at 2500 rpm

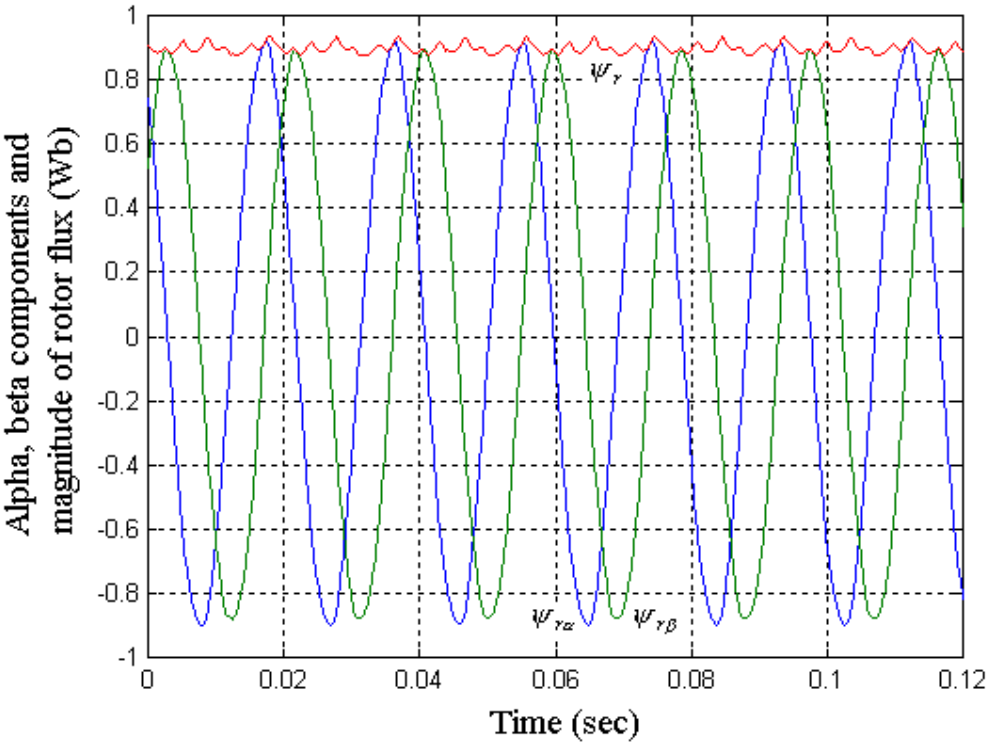

Figure 4. 31.α,β components and magnitude of rotor flux at 3000 rpm

A table can be formed with test results as follows

Table 4. 3. Minimum, maximum and average values of rotor flux magnitude with 0,9 Wb reference at different speeds

Rotor Speed (rpm)	$\psi_{r\,min}$ (Wb)	$\psi_{r\,max}$ (Wb)	ψ_{rmean} (Wb)	ψ_{ref} (Wb)
200	0,85	0,97	0,9	0,9
500	0,87	0,95	0,9	0,9
1000	0,87	0,93	0,9	0,9
1500	0,87	0,92	0,9	0,9
2000	0,88	0,92	0,9	0,9
2500	0,88	0,91	0,9	0,9
3000	0,87	0,92	0,9	0,9

As depicted in the table, rotor flux mean value is the same with the reference.

At low speed region, applied stator voltage decreases and voltage drop on stator resistance becomes comparable with applied stator voltage. Dead time and IGBT voltage drop compensation is not performed in the system, which becomes effective at low speed operation. Calculated reference voltage cannot be produced accurately at stator windings so rotor flux starts to fluctuate. It is observed from the table that fluctuations on rotor flux increases with decrease in rotor speed.

4.6. Steady state torque performance of the system

Block diagram of the experimental setup used in steady state torque measurements is given in the following figure.

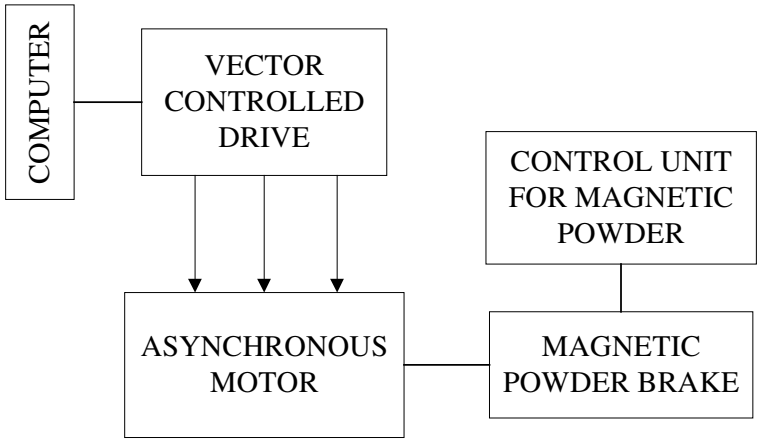

Figure 4. 32. Experimental setup used in vector control

Vector control software is written in C programming language, then compiled and downloaded to the DSP card, which is in the computer. Vector controlled drive was explained in Chapter 2.

In this setup, magnetic powder brake is used to load motor. Magnetic powder brake has two operation modes, which can be selected by using operation mode switch located on the control unit. These modes are n and m. In n mode, motor is loaded so that motor speed is constant at a preset value. Speed reference is selected by using set/start value potentiometer, which is located on the control unit. In m mode, constant torque is applied to the motor. Motor is loaded in n mode during steady state torque measurements. While making measurements set/start value potentiometer is changed and measurements are taken at different speeds.

Vector control software is operated at torque control mode. The motor should be able to produce same torque value independent of its speed. Measured torque values at different speeds are given in the following figure

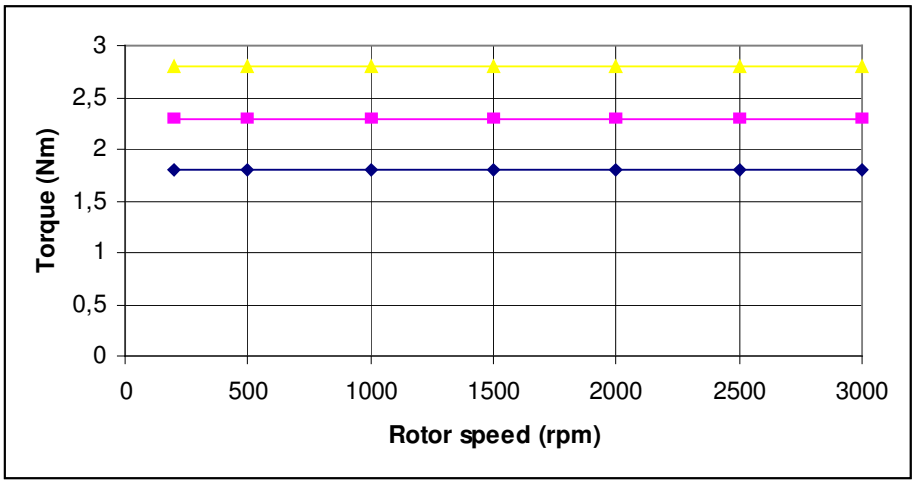

Figure 4. 33. Motor torque at different speeds

A table can be formed to view torque performance of the motor.

Table 4. 4. Motor torque at different speeds

TORQUE REFERENCE (NM)	SPEED (RPM)													
	200		500		1000		1500		2000		2500		3000	
	T_p	ERROR %	T_p	ERROR %	T_p	ERROR %	T_p	ERROR %	T_p	ERROR %	T_p	ERROR %	T_p	ERROR %
2	1,8	10	1,8	10	1,8	10	1,8	10	1,8	10	1,8	10	1,8	10
2,5	2,3	8	2,3	8	2,3	8	2,3	8	2,3	8	2,3	8	2,3	8
3	2,8	7	2,8	7	2,8	7	2,8	7	2,8	7	2,8	7	2,8	7

As seen from the table motor produces the torque with a maximum 10% error. Motor torque is constant at all speeds. Motor torque equation in rotor flux oriented system is given as follows

$$T_e = \frac{3}{2}\frac{p}{2}\frac{L_m^2}{L_r} i_{sd} i_{sq} \tag{4.8}$$

Error in produced torque may arise due to error in realizing reference current values. Figure 4.34. displays the results found at 1500 rpm with reference values of 1.56 for i_{sq} and 2.4 for i_{sd}. i_{sd} and i_{sq} values are observed with TRACE program from the measured current values and estimated rotor flux position(θ angle). It can be seen that these values are obtained with a little hysteresis band and have the correct magnitude. The same figure also displays the reference set with a solid straight line.

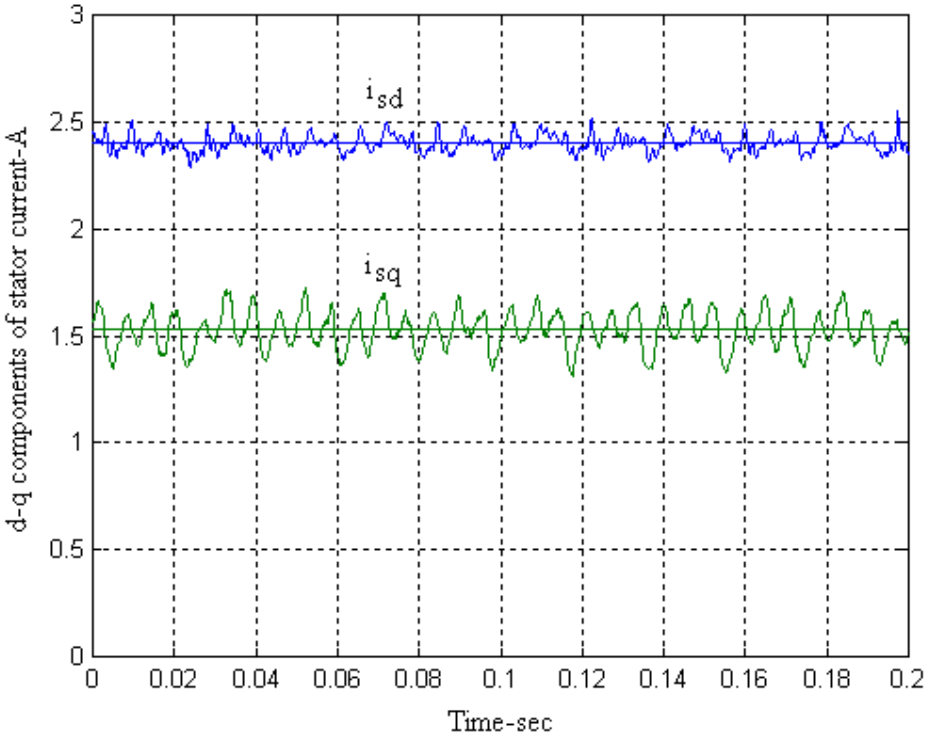

Figure 4. 34. d-q components of stator current with reference values

Same measurements are taken for other speeds and similar results are obtained. Since the findings show that i_{sd} and i_{sq} values are implemented correctly, the error observed in obtaining the desired torque is probably due to an error in the value of mutual inductance. However there wasn't enough time to investigate this issue. . So error between calculated and produced torque may occur due to error in mutual inductance value.

4.7.Estimated dynamic torque performance of the system

Motor is operated with vector control at no load condition and motor speed is estimated from the Equation (2.38), which uses estimated flux values. Initially motor torque reference is set to 2Nm. When the motor speed reaches to a value of 1500 rpm, motor torque is reversed by reversing the torque producing component of stator current (i_{sqref}). When the motor speed reaches to a level of 500 rpm motor torque is reversed again, so that motor speed increases and decreases between 500 and 1500 rpm. In this case the mechanical equations are as follows.

$$T_e = T_{f\&w} + j\frac{dw}{dt} \tag{4.9}$$

Since the test is performed at no load conditions T_L is eliminated from the equation. If friction and windage loss is neglected motor speed is expected to increase and decrease linearly. But here speed range is large and friction and windage loss may become effective. Following figure is obtained from TRACE program. Here the torque is also calculated from the measured i_{sd} and i_{sq} currents.

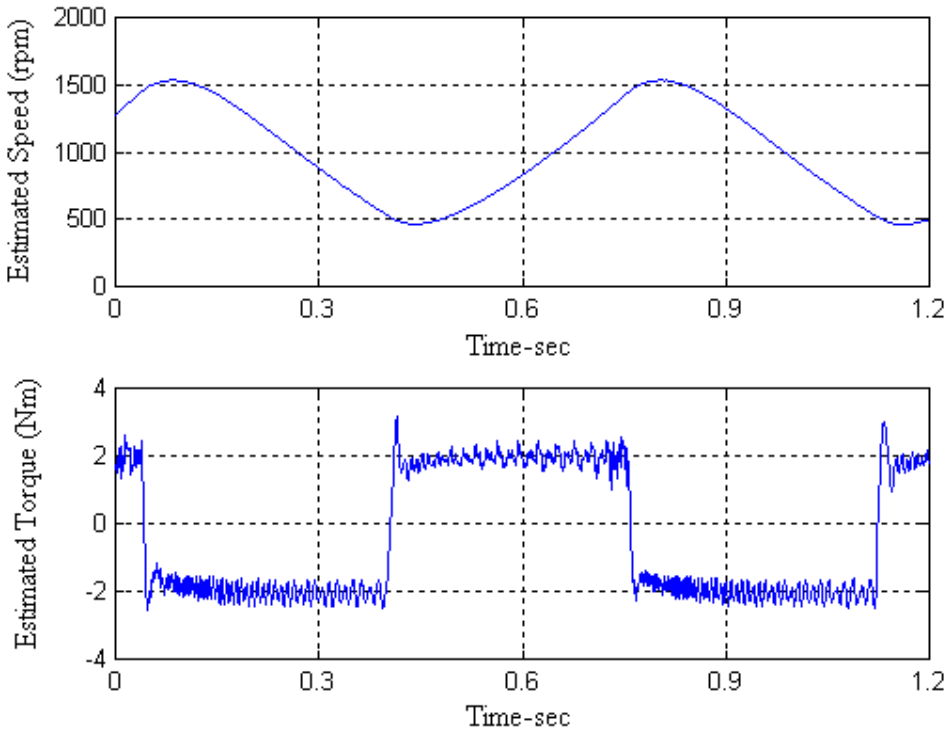

Figure 4. 35. Estimated dynamic torque response of the motor

CHAPTER 5

IMPLEMENTATION OF SELF COMMISSIONING ALGORITHMS

5.1. Introduction

The aim of this chapter is to explain the theory and give the experimental results of the implementation of self commissioning algorithms developed by Ertan Murat [7] . First the necessity for self commissioning is explained, then experimental results of the algorithms used in this thesis are presented and compared with the conventional test results.

All control algorithms use motor models which depend on motor parameters, so motor parameters should be measured accurately. Conventionally, IM parametes (Rs, Rr, Lıs, Lır, Lm) may be obtained directly from the conventional dc test, no load test and locked rotor test, but there are some disadvantages in obtaining the induction machine parameters by this way.

- First of all, the induction machine parameters determined by conventional tests are not directly applicable to sensorless Field Oriented Control (FOC) since the switching effects on the parameters are not taken into account by the conventional tests.

- A technical person should be present to perform the conventional tests during installation, which is inconvenient in some cases.

- The flux level used in locked rotor test is significantly lower than that during normal operation. The slip frequency is higher causing rotor skin depth effects.

- No consideration is made for the effects of converter harmonic.

In order to overcome these problems an automatic parameter measurement method is desired. Automatic determination of induction motor parameters prior to starting the drive system with the aid of motor driver itself is called self commissioning.

Stator winding resistance and rotor winding resistance are temperature dependent components. The value of these components increase with temperature. Also mutual inductance value depends on the flux level and distribution in the machine. These values should be measured and corrected online in the system. In this thesis online implementation is not performed but offline measurement of the parameters are given in detail.

In the following sections, self commissioning methods used in this thesis to obtain stator winding resistance (Rs), referred rotor resistance (Rr), leakege inductance (Lıs=Lır) and mutual inductance (Lm) are explained and also experimental results of these methods are given.

5.2. Automated Stator Winding Resistance Measurement

Performance of many sensorless vector control algorithms strictly depends on the accurate knowledge of stator winding resistance R_s. In this thesis to obtain stator winding resistance at standstill, a very well known method is used. This method depends on forcing a known dc current through the stator phase windings. State equations of the induction machine at stationary reference frame can be expressed as in equation (5.1).

$$\begin{bmatrix} \vec{U}_s \\ 0 \end{bmatrix} = \begin{bmatrix} R_s + pL_s & pL_m \\ (p - jw)L_m & Rr + (p - jw)L_r \end{bmatrix} \begin{bmatrix} \vec{I}_s \\ \vec{I}_r' \end{bmatrix} \tag{5.1}$$

At standstill, since speed terms are zero an induction machine is not different from a resistive inductive (R-L) load. In the steady state, stator voltage in the stationary reference frame can be written as follows [1]

$$U_s = R_s I_s \tag{5.2}$$

So if a dc current passes through the stator phase windings, winding resistance can be found by the ratio of applied dc voltage to the dc phase current. DC current value should not exceed the motor rated current during measurements.

In the experiment, a dc current was forced to pass through stator windings. For this purpose, direct axis reference current I_{sdref} is set to 2.4 A peak, which is rated value of I_{sdref} in this motor. Then motor torque is set to zero (Equation A.10) by setting quadrature axis reference current (I_{sqref}) and angle (θ) between α axis and rotor flux to zero, so motor remains stationary during this test. Motor currents are sampled and controlled with a PI controller, so that motor current references are achieved and stator windings are protected from over current. This is done by sampling the phase currents at each program loop and compare the currents with the reference currents. Then PI controller is used to obtain reference voltages from the error between motor currents and reference currents. SVPWM technique is used to calculate proper switching cycles for the inverter by using reference voltages. Program cycle is adjusted to be 100μs. In each program cycle motor two phase voltages and currents are read by using ADCs.

Three phase motor in dc test can be shown as follows

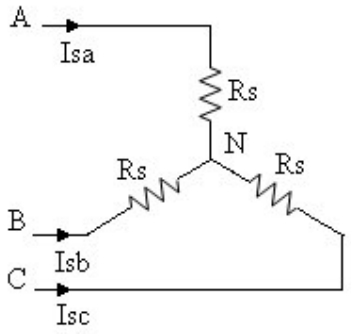

Figure 5. 1. Three phase motor equivalent circuit in dc test

Motor phase currents (I_{sa}, I_{sb}) and voltages (V_{AN}, V_{BN}) are sampled in every 100μs for 1 seconds duration. In each program cycle motor phase voltage V_{AN} and motor phase current I_{sa} are added to the previous sum of voltage and currents and at the end of 1 seconds stator winding resistance is calculated as the ratio of sum of motor voltages to sum of motor currents. Stator voltage and currents during stator winding measurement are shown in the following figures.

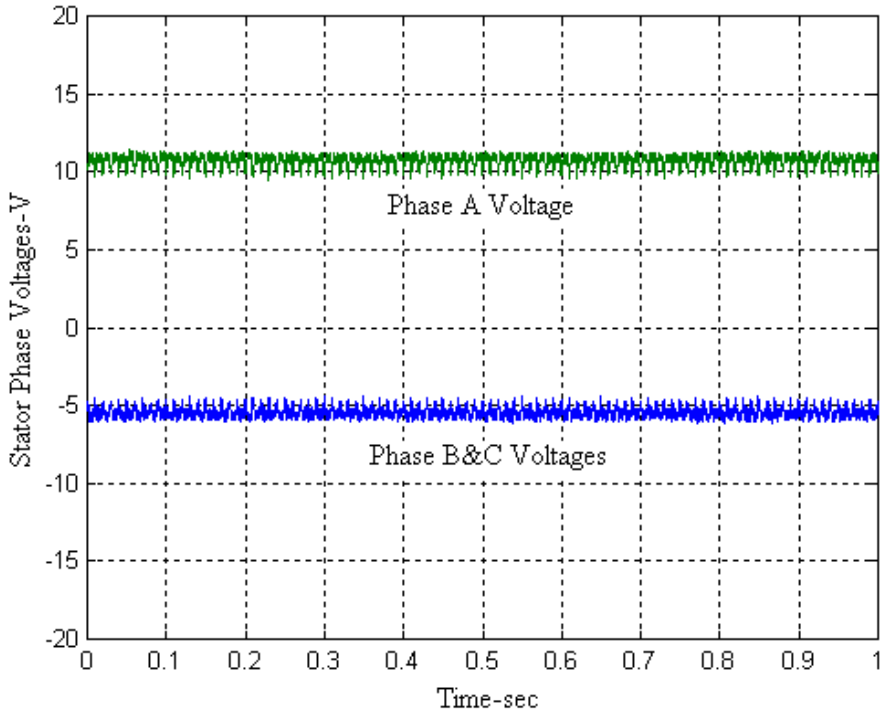

Figure 5. 2. Stator phase voltages during stator winding resistance measurement

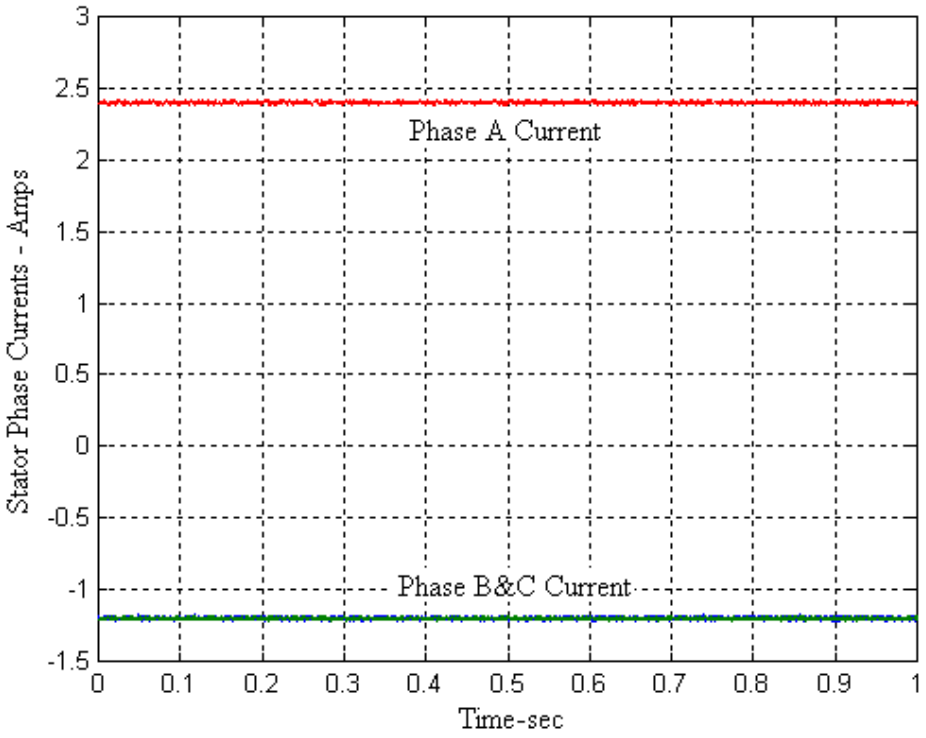

Figure 5. 3. Stator phase currents during stator winding resistance measurement

As seen from Figure 5.3 motor currents are balanced. Phase B and C currents are equal and half of the Phase A current in magnitude which is an expected result.

Stator winding resistance was measured as 4.57 Ω with this method. It was measured as 4.5 Ω in conventional tests.

5.3. Automated Leakage Inductance Measurement

Leakage inductance is the half of the stator transient inductance. In this thesis, stator transient inductance is measured with the method developed by Ertan Murat [7]. Then leakage inductance is calculated. In this section, first of all stator transient inductance is explained and then theory of the method is given, finally experimental results are presented.

Stator transient inductance term refers to the inductance value measured from the stator winding terminals and can be written as in Equation (5.3). Motor equivalent circuit is shown in the following figure.

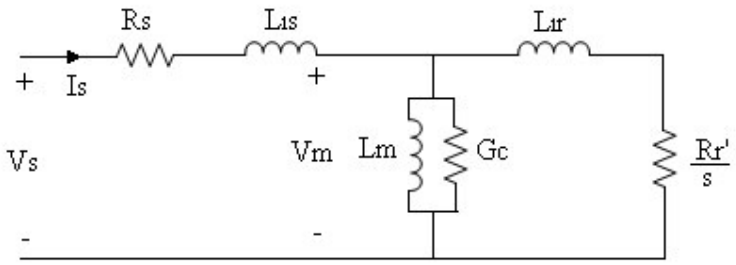

Figure 5. 4. Induction machine equivalent circuit

$$\sigma L_s = L_{ls} + L_{lr} \,//\, L_m \tag{5.3}$$

which yields

$$\sigma L_s = \frac{L_{ls} L_{lr} + L_m (L_{ls} + L_{lr})}{L_m + L_{lr}} \tag{5.4}$$

With the assumption of $L_m >> L_{lr}$ usually stator transient inductance is considered as $\sigma L_s = L_{ls} + L_{lr}$ [8]. Where L_m, L_{ls}, L_{lr} terms represents mutual inductance, stator leakage inductance and rotor leakage inductance respectively.

In stator transient inductance measurement, a dc current is forced to flow in stator windings and then suddenly stator windings are short circuited with the aid of inverter. As soon as the lower power switches of the inverter are turned on, stator phase voltages become zero and stator phase currents tend to be zero. At first, stator phase currents draws a trajectory that has very high rate of change of current, then stator phase current reaches to zero with a decreasing rate of change as shown in Figure 5.5.

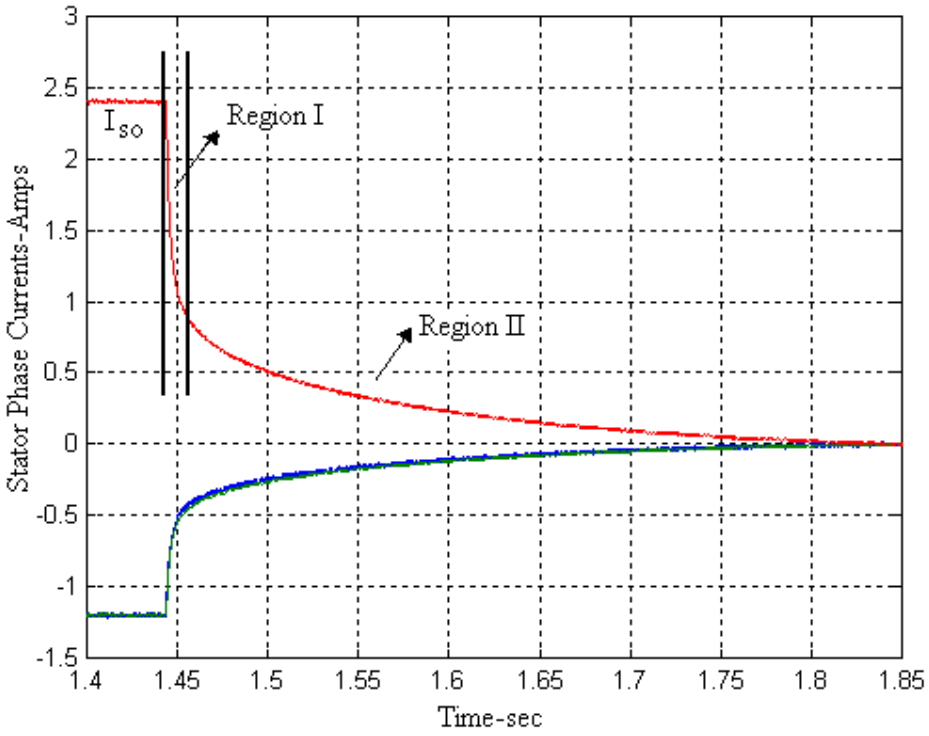

The trajectory of current, after the stator phase windings are short circuited, may be divided into two regions:

- Region I
- Region II

In region I, stator currents decrease with a high rate of change. However in region II, current reaches to zero in a very long time period compared to region I. In the region I, induction motor stator voltage is given by:

$$\vec{U}_s = R_s \vec{I}_s + \sigma L_s \frac{d\vec{I}_s}{dt} + (1-\sigma) L_s \frac{d\vec{I}_{mr}}{dt} \tag{5.5}$$

Since the mutual flux variation for the very small time duration is negligibly small, transient equation of the induction motor is given by:

$$\vec{U}_s = R_s \vec{I}_s + \sigma L_s \frac{d\vec{I}_s}{dt} \tag{5.6}$$

The solution of the stator current is given by:

$$I_s(t) = I_{so} e^{-t/\tau_{s'}} \tag{5.7}$$

Where I_{so} is the initial value of stator phase current, which is 2.4 A in this thesis, $I_s(t)$ is the instantaneous value of current at time t ,$\tau_{s'}$ is stator transient time constant and represented as follows:

$$\tau_s' = \frac{\sigma L_s}{R_s} \tag{5.8}$$

Stator transient time constant can be calculated by measuring I_{so}, I_s at time t and substituting in equation (5.7). In dc test, stator winding resistance was measured. Since stator transient inductance and stator winding resistance (R_s) are known, stator transient inductance can be calculated with equation (5.8). Then stator and rotor leakage inductance values are calculated as the half of the stator transient inductance.

In this test, firstly motor is driven with a dc current, which is set to 2.4 A in this thesis. Then inverter switching periods are adjusted to give zero voltage at the output of the inverter. In each control cycle, which is 100 μsec, stator phase current is measured and calculation for stator transient inductance is performed. Then leakage inductances for stator and rotor are taken to be equal and half of the stator transient inductance. Measurements must be performed in region I for the correct parameter calculation. In the software, first three measurements are taken and averaged. (Measurement1=0.0115, Measurement2=0.0116, Measurement3=0.0114)

Then the subsequent measured leakage inductances are compared with the average value of these first three measurements. When the error reaches to a level of 5% calculation is stopped and calculated leakage inductance values are averaged to find out leakage inductance. Voltage and current measurements are given in Figures 5.6 and 5.7

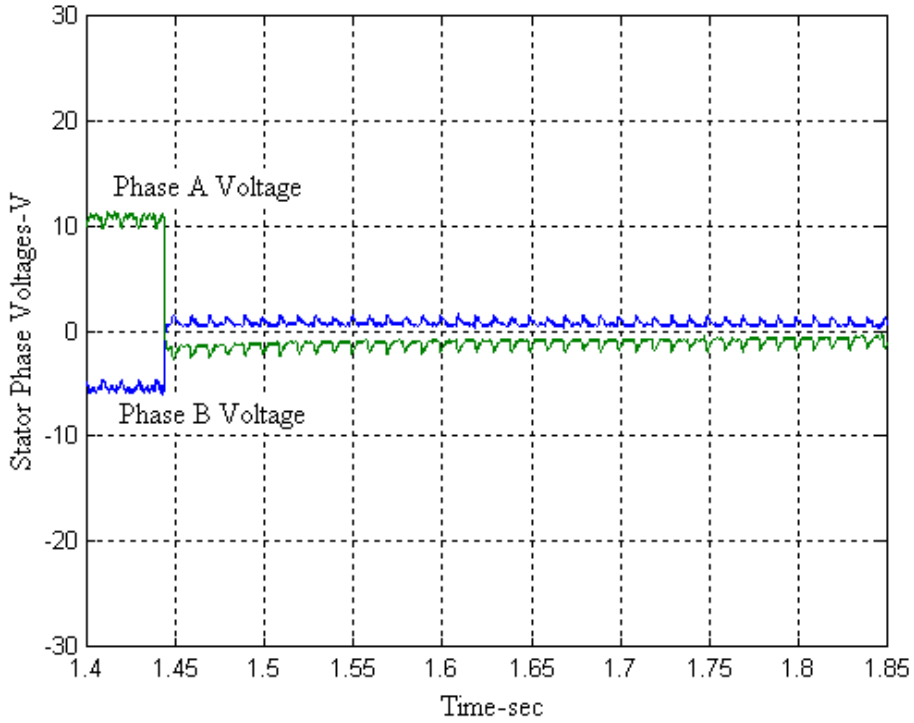

Figure 5. 6. Stator phase voltages during stator transient inductance measurement

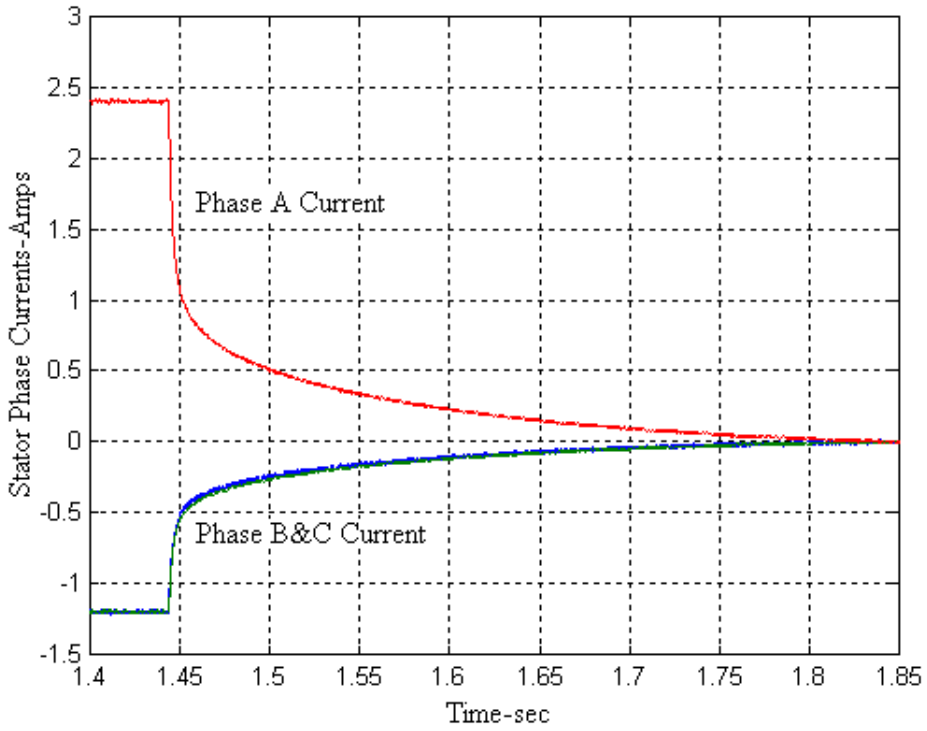

Figure 5. 7. Stator phase currents during stator transient inductance measurement

Calculated stator leakage inductance values for 2 msec time duration and 1 second time duration are shown in Figures 5.8 and 5.9 respectively.

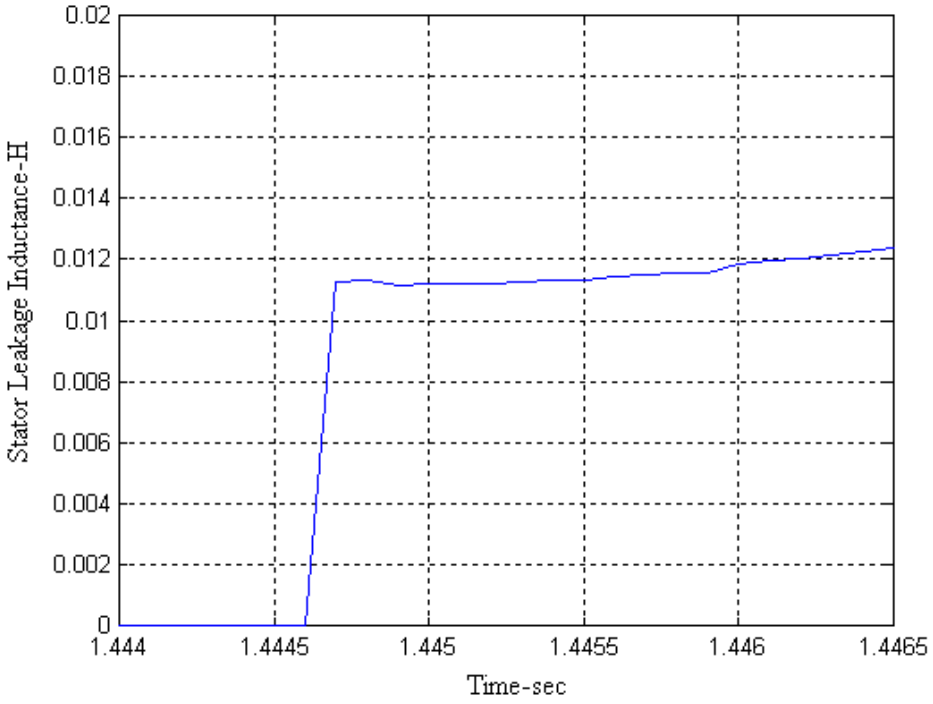

Figure 5.8.Calculated stator leakage inductance values for 2 msec time duration

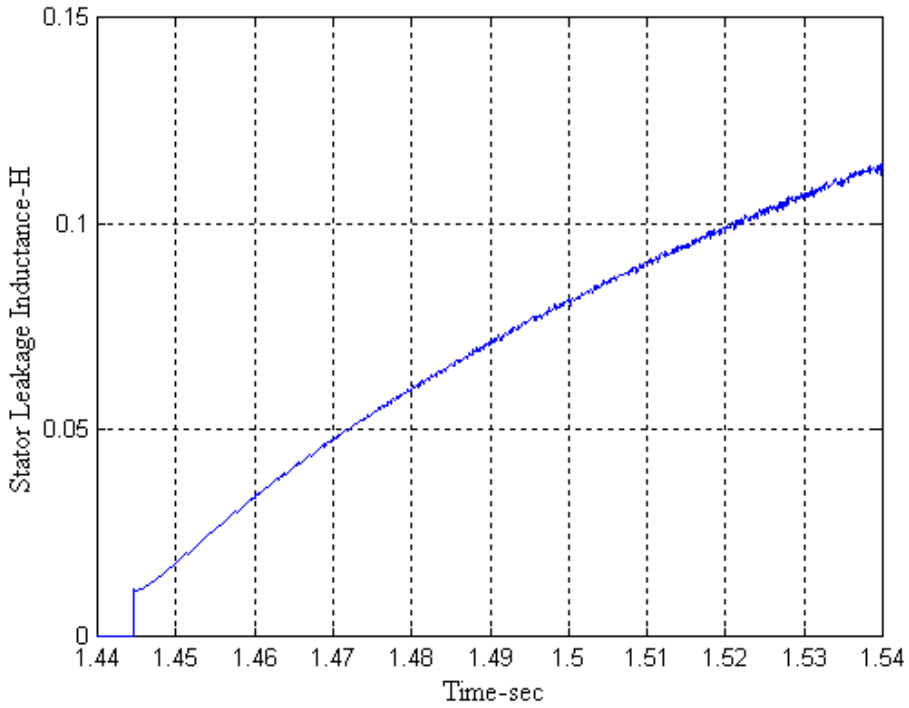

Figure 5. 9. Calculated stator leakage inductance values for 1-second duration

As can be seen from the Figure 5.8 the calculations for 1.5 msec time duration are nearly constant as expected. In Figure 5.9, calculated leakage inductance values are given for 1 second duration and change of inductance calculation is seen more clearly.

In the conventional locked rotor test stator leakage inductance value was calculated as 11.7 mH and with this method it is calculated as 11.9 mH. The error between the results is about 2% , but note that much depends on how the measurements are stopped.

5.4. Automated Referred Rotor Resistance Measurement

In this section, the theory of motor referred rotor resistance measurement method is explained and then experimental results of this method are presented.

Referred rotor resistance is calculated by measuring the power dissipation on resistances. Power dissipation on rotor resistance can be measured when a current flows in the rotor cage. To induce current in the rotor cage, varying airgap flux must be built-up. To built-up a varying air gap flux, the machine is operated at V/f ratio control principle. Voltage reference is given so small at rated frequency that rotor cannot rotate and motor remains stationary under three phase excitation. Motor model can be represented as follows

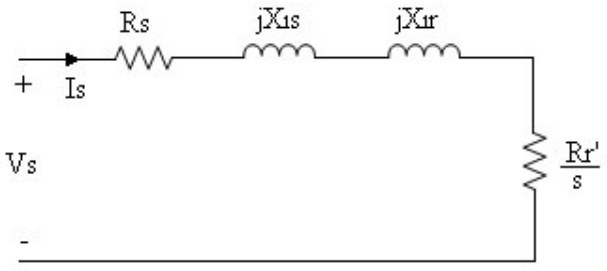

Figure 5. 9. Motor equivalent circuit during referred rotor resistance measurement

. Input power is measured. Since no electrical energy is converted to mechanical energy, the dissipated power is equal to stator and rotor resistance heat

losses at standstill. So rotor resistance is calculated by finding the rotor circuit power dissipation. The input power of the motor is calculated as follows

$$Power = \frac{3}{2}(U_{s\alpha} I_{s\alpha} + U_{s\beta} I_{s\beta}) \tag{5.9}$$

Stator winding resistance was measured in dc test. So power dissipation on stator winding resistance can be calculated if the rms value of stator current is known. In this thesis, two stator phase voltages and two stator phase currents are sampled in every 100 μsec. Assuming a set of balanced sinusoidal currents , the rms value, in terms of instantaneous quantities, can be written as [11]

$$I_{rms} = \sqrt{\frac{2}{3}} \sqrt{(i_{sa}(i_{sa} + i_{sb}) + {i_{sb}}^2)} \tag{5.10}$$

Power dissipation on rotor resistance is calculated as follows

$$P_{stator} = 3{I_{rms}}^2 R_s \tag{5.11}$$

Power dissipation on referred rotor resistance is the difference between input power and power dissipation on stator winding resistance

$$P_{rotor} = Power - P_{stator} \tag{5.12}$$

Finally referred rotor resistance is calculated as follows

$$R_r' = P_{rotot} / (3I_{rms}^2) \tag{5.13}$$

In this thesis, motor is driven at V/f ratio control. Reference voltage and frequency was given as 20V and 50 Hz respectively. In each program cycle, motor

two phase currents and voltages are sampled. Then α,β components of motor voltages and currents are obtained by using Clarke transformations as explained in 2.2.2.4. Input power is calculated for 0.3 second duration by using equation (5.9). At the same time rms value of stator current is calculated with equation (5.10). Then at the end of 0.3 seconds, average values of input power and rms current are calculated. Rs was measured in dc test. Referred rotor resistance is calculated by using equations (5.11)-(5.13).

Experimental results are given in the Figures 5.10 and 5.11.

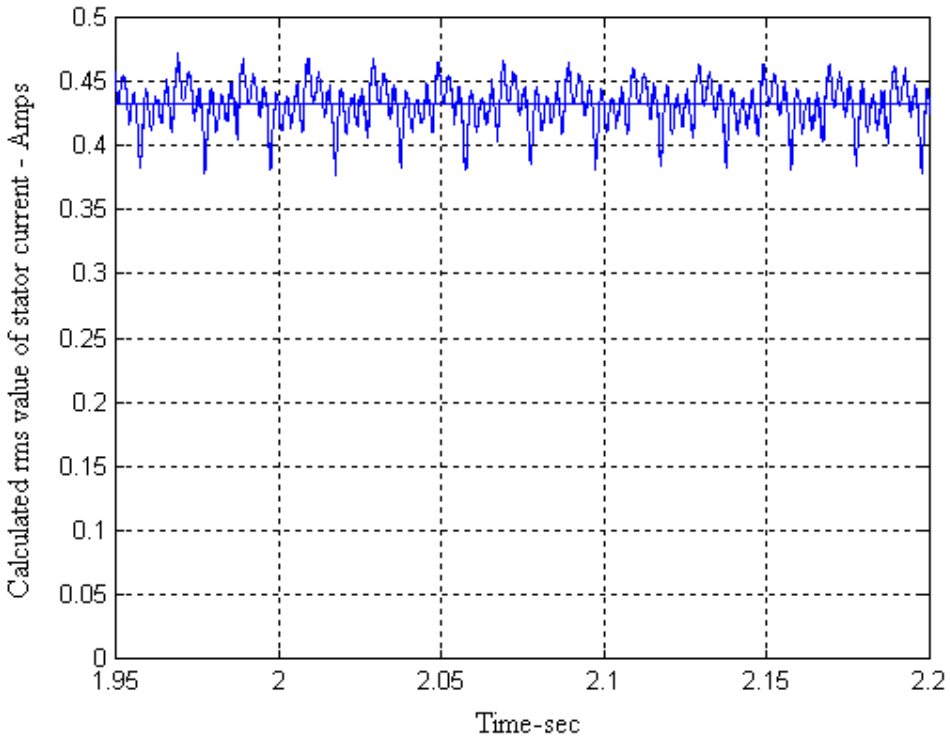

Figure 5. 10 .Calculated rms value of stator current during referred rotor resistance measurement

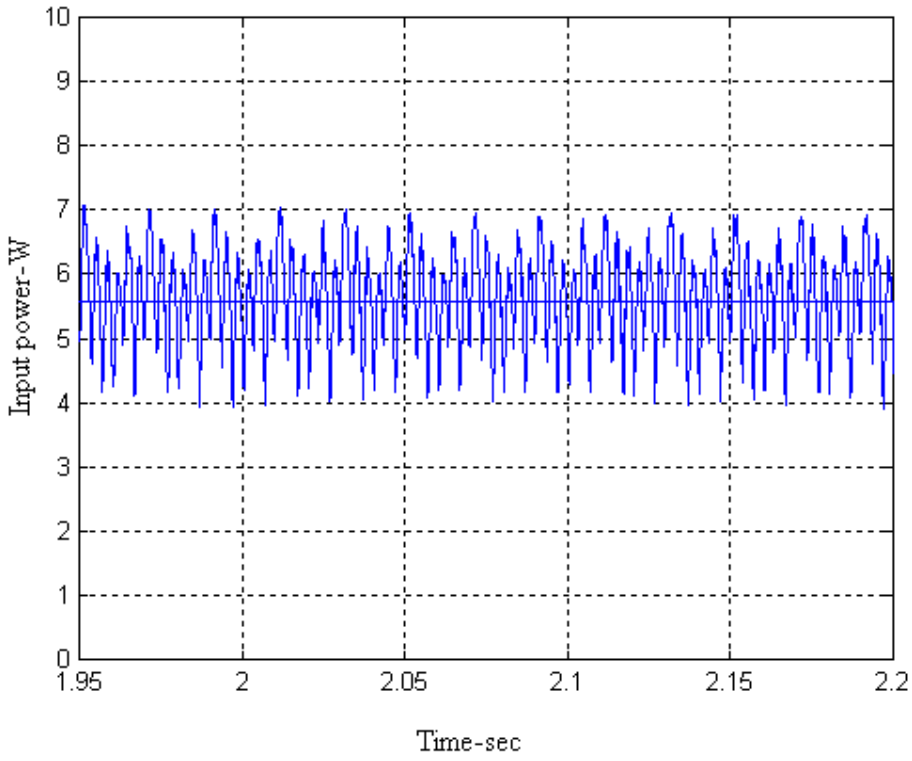

Figure 5. 11. Input power during referred rotor resistance measurement

Average input power and average of the stator current rms value is calculated in the software as shown below

Power = 5.56W

Irms=0.416A

Rs was measured as 4.57ohm in dc test

Following calculations are performed in the software to obtain referred rotor resistance value.

P_{rotor} = Power-3 I_{rms}^2 R_s = 5.56-3*0.416^2*4.57 = 3.19W

$R_r'=P_{rotor}/(3I_{rms}^2)=3.19/(3*0.416^2)=6.13\ \Omega$

Referred rotor resistance is measured as 6.13 ohms by using automated referred rotor resistance measurement algorithm. In conventional tests it was also measured as 6.02 ohms. Error between measured values is 1.8%.

5.5. Automated Mutual Inductance Measurement

In this section, theory of mutual inductance measurement is explained and experimental results are presented.

To measure mutual inductance, the motor is driven at no load condition in V/f control principle. So motor must be disconnected from its load in this test. The voltage and frequency are set to their rated values as in conventional tests. Induction machine equivalent circuit at no load condition is given in Figure 5.12

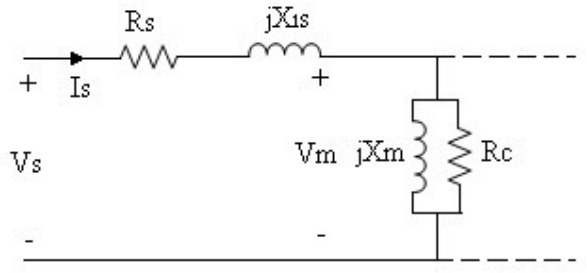

Figure 5. 12. Equivalent circuit of an induction machine

If the stator voltages and currents are measured. Input power can be calculated as given in equation 5.9. Then power dissipation on Rs is subtracted from input power to obtain power dissipation on Rc.

$$P_{core} = Power - 3I^2 R_s \tag{5.14}$$

Vm is obtained by substituting voltage drop on stator side. Then Rc can be calculated as follows

$$V_m = V_s - I(R_s + jX_{ls}) \tag{5.15}$$

$$R_c = \frac{P_{core}/3}{V_m^2} \tag{5.16}$$

Vm and Rc are known so ic can be calculated and im can be obtained as follows

$$i_c = \frac{V_m}{R_c} \tag{5.17}$$

$$i_m = \sqrt{(I_s - i_c)} \tag{5.18}$$

Since im and Vm are knowm Xm and then Lm may be calculated as follows

$$X_m = \frac{V_m}{i_m} \tag{5.19}$$

$$L_m = \frac{X_m}{2\pi f} \tag{5.20}$$

In the experiments, rated voltage and rated frequency are set to 220V and 50 Hz respectively. Motor is driven at no load in V/f principle. Motor two phase currents and two phase voltages are measured in each program cycle.Input power is calculated as in equation 5.9. Then rms voltage and rms currents are calculated for from two instantaneous values as given in equation 5.10. In each cycle these calculated values are added to their previous sums and at the end of one period,which is 20 msec for 50 Hz, these values are averaged. Then to find Lm, calculations as given in equations from (5.14) to (5.20) are performed. Test results are as follows

V_s=225V

I_s=1.865A

Power=130W

Rs=4.57Ω (Measured in dc test)

Pcore=Power-3 I_s^2 Rs=82.3W

$V_m = V_s - I(R_s + jX_{ls})$ =225-1.865*5.97=214V

Rc = Vm^2 /(Pcore/3) = 214^2/(82.3/3)= 1669Ω

ic=Vm/Rc=214/1669=0.13A

$i_m = \sqrt{(I_s - i_c)}$ = 1.86A

Xm=Vm/im=214/1.86=116.1Ω

Lm=Xm/(2*pi*f)= 116.1/(2*pi*50)=370mH

In conventional tests it was also measured as 0.375H.

5.6. Conclusions

In Table 5.1, The results obtained from the self tuning algorithm are compared with the results found from conventional tests.

Table 5. 1. Comparison of automated self commissioning algorithms test results with conventional test results

Mesured Parameter	Conventional Test Result	Automated Self Commissioning Algorithm Result	Error %
Stator Winding Resistance (Rs)	4,5 ohm	4,57 ohm	1,56
Leakage Inductance (Lıs,Lır)	11,7 mH	11,9 mH	1,7
Mutual Inductance (Lm)	0,375 H	0,370 H	1,33
Referred Rotor Resistance (Rr')	6,02 ohm	6,13 ohm	1,8

As can be seen from the table parameters are estimated within the error range of 2%. This shows that the procedures adopted work well. A further effort however is needed to seek a way of determining mutual inductance (Lm) without decoupling the motor from the load.

CHAPTER 6

CONCLUSION

6.1. General

The purpose of this study was to integrate various hardware and software developed in different studies. With this purpose, firstly the problems on the available hardware are analyzed and located. Then some improvements are made on the hardware as explained in Chapter 3. Dead time circuit and protection circuit on the lock-out module are properly operated after the modifications. Calibration of the system is performed and given in Chapter 4. After the reliable hardware is obtained, parameter estimation and vector control algorithms are implemented.

The parameter estimation techniques previously developed are embedded into vector control. It is shown that, the stator winding resistance, leakage inductance and referred rotor resistance measurement algorithms lead to accurate results, within 5% of values experimentally obtained using well established method.

Next using the parameters found during the tuning operation, the motor is operated with vector control algorithm in the torque control mode . The purpose was to verify earlier measurements and establish reliability of the algorithms used. It is found that indeed the motor was capable of following the torque reference at steady state throughout the 0-50 Hz. Range with some constant error. The source of this error is studied and it is found out that the reason was not the currents driving the motor but perhaps the errors between the parameters used by the algorithm and their effective values during operation.

Limited dynamic operating condition tests are performed on the motor by continuously altering the torque applied to the motor under no load conditions. It is found that the motor torque almost instantly reverses direction as instructed and that the PI parameters of the software are well tuned.

Further work:

In this thesis a sound understanding of the existing hardware and software for vector control of induction motors is studied. The reliability of the existing approach is verified. However there remains much to be done

a) The filter design of current and voltage sensing circuits must be improved to achieve a wider speed range.
b) The reason for the constant error at the motor torque with respect to reference torque must be identified.
c) A better set up must be prepared for dynamic tests and acceptability of the performance must be studied.
d) The dynamic tests should be extended to speed reversal to study the vector control algorithm behavior.
e) The very low speed and high speed performance of the drive system must be studied in detail.
f) Online resistance measured algorithm developed previously must be integrated into the software.
g) The tuning procedure of the software must be improved to respond to unusual operating conditions that may be encountered in practice.

At the level of understanding of the subject matter the author achieved these tasks could be accomplished in several months. These tasks could not be completed earlier as this research was initially conducted while working. This was followed by a several month's hard work during which several unfortunate incidents took place. The first set used for the study was accidentally damaged. The second test has had a

bad accident in another study and identifying and eliminating these took a long time. But working on these problems led to complete understanding of the system operation and was very useful.

REFERENCES

[1] : Vas, P. , " Sensorless Vector And Direct Torque Control " , Oxford University Press, 1998.

[2] : Novotny, D. W. , Lipo, T.A. , "Vector Control And Dynamics Of AC Drives", 1992.

[3] : Fitzgerald , A. E. , Kingsley C. , D. Umans Jr. Stephen , " Electric Machinery" , McGraw-Hill, 1983

[4] : Akın, E. , "Stator Alan Akısı Üzerinden Asenkron Motorun Rotor Akısı Yönlendirmesi İçin Bir Yöntem" ,Doktora Tezi, Fırat Üniversitesi, 1994.

[5] : Can , H. , "Implementation Of Vector Control For Induction Motors" , Msc. Thesis, METU, 1999.

[6] : Akın, M. , "Bir Vektör Kontrol Yönteminin Uygulama Hız Sınırlarının Genişletilmesi İçin Yöntem Geliştirme", Msc. Thesis, METU, 2002.

[7] : Murat, İ. E. , "Self Commissioning And Online Parameter Identification Of Induction Motors", METU, 2002.

[8] : Silvino, J. L., Rabelo, B.C. , "An Improved Estimation Of The Induction Machine Leakage Inductances " , IEEE Transactions On Industrial Electronics, Letter to the editor, Vol. 46, No.5, October 1999.

[9] : " Field Oriented Control Of 3-Phase AC Motors" , Texas Instruments

Europe Application Note, Literature Number: BPRA073, 1998.

[10] : "Implementing Space Vector Modulation With the ADMC401" , Analog Devices, AN401-18, January 2000.

[11] : Munoz- Garcia, A. , Lipo, A.T. , Novotny W.D. , " A new Induction Motor V/f Control Method Capable Of High Performance Regulation At Low Speeds" , IEEE Transactions on Industry Applications. Vol. 34, No.4, July/August 1998.

[12] : Lai Yen-Shin, Chang Ye-Then "Design And Implementation Of Vector Controlled Induction Motor Drives Using Random Switching Technique With Constant Sampling Frequency" , IEEE Transactions on Power Electronics, Vol.16, No.3 , May 2001.

[13] : DS1102 Software Environment, dSPACE reference guide

[14] : Bimal K.Bose, NitinR. Patel " A Programmable Cascaded Low-Pass Filter Based Flux Synthesis for a Stator Flux-Oriented Vector Controlled Induction Motor Drive" , IEEE Transactions on Industrial Electronics, Vol.44.

[15] : "Squirrel Cage Induction Motor Control with DS1102 Controller Board, January 1999, Application Note, dSPACE

[16] : Chang, T.Y., Pan, C.T. "A practical Vector Control Algorithm for DSP Based Induction Motor Drives Using a New Space Vector Current Controller, IEEE Transactions on Industrial Electronics, Vol.41

[17] : Bonanno, F., Consoli, A. , Raciti, A. , Testa A."An innovative Direct Self Control Scheme For Induction Motor Drives", IEEE Transactions On Power Electronics, Vol.12

[18] : Vas, P. , “Parameter Estimation, Condition Monitoring, and Diagnosis Of Electrical Machines” , Clarendon Press, Oxford, 1993

[19] : Leonhard, W. , “Control Of Electrical Drives” , Springer Verlag, Berlin 1985.

[20] : David J.Atkinson, Paul P. Acarnley and John W. Finch, “Observers for Induction Motor State and Parameter Estimation” , Vol.27

[21] : Ohtani, T. , Takada, N. , Tanaka, K. “Vector control of an induction motor without shaft encoder”, IEEE Transactions on Industry Applications, Vol.28

[22] : Robert D. Lorenz, “Tuning of Field-Oriented Induction Motor Controller for High Performance Applications”, Vol. IA-22,1986

[23] : Chang, T.Y., Pan, C.T., “ A Microcomputer Based Vector Controlled Induction Motor Drive ” , IEEE Transactions on Energy Conversion, Vol.8, 1985.

[24] : Capolino , G.A. , Boussak , M. , “ Induction Machine Parameters Identification : A Comparison Of Different Algorithms” , ICEM 1990 pp 940-945.

[25] : Khambadkone , A. M. , Holtz , J. , “Vector Controlled Induction Motor Drive With a Self Commissioning Scheme ” , IEEE Transactions on Industrial Electronics, Vol. 38, No:5, October 1991.

[26] : Lindsay , J.F. , Barton , T.H. , “ A Modern Approach to Machine Parameter Identification” , IEEE Transactions PAS, col. PAS-51, 1972 , pp 1493-1500.

[27] : Ermiş, M. , Ersak, A. , " Notes on Principles Of Electromechanical Energy Conversion" , 2nd Edition, November 1986, METU.

[28] : Nilsson , J., " Electric Circuits Fourth Edition " , Addison Wesley Publishing Company, 1993.

[29] : Krishnan, R. , "Electric Motor Drives: Modeling, Analysis, and Control" Prentice Hall. Inc. , 2001

APPENDIX A

Motor d-q Model

Motor d-q model is explained in detail in [4]. Here a summary of d-q model is given. Motor mathematical model contains nonlinear and time variant terms. When the motor model is represented in an arbitrarily rotating reference frame, time variant terms can be eliminated. Motor model represented in a rotating reference frame is called as d-q motor model. d-q motor model is given as in the following equations.

$$\psi_{sd} = L_s i_{sd} + L_m i_{rd} \tag{A.1}$$

$$\psi_{sq} = L_s i_{sq} + L_m i_{rq} \tag{A.2}$$

$$\psi_{rd} = L_r i_{rd} + L_m i_{sd} \tag{A.3}$$

$$\psi_{rq} = L_r i_{rq} + L_m i_{sq} \tag{A.4}$$

$$V_{sd} = R_s i_{sd} - w_s \psi_{sq} + p\psi_{sd} \tag{A.5}$$

$$V_{sq} = R_s i_{sq} + w_s \psi_{sd} + p\psi_{sq} \tag{A.6}$$

$$0 = R_r i_{rd} - w_{sl} \psi_{rq} + p\psi_{rd} \tag{A.7}$$

$$0 = R_r i_{rq} - w_{sl} \psi_{rd} + p\psi_{rq} \tag{A.8}$$

Electrical torque equation of the motor is given as follows

$$T_e = \frac{3}{2}\frac{P}{2}(\psi_{md} i_{rq} - \psi_{md} i_{rd}) = \frac{3}{2}\frac{P}{2} L_m (i_{sq} i_{rd} - i_{sd} i_{rq}) \qquad \text{(A.9)}$$

q component of the rotor flux is zero when the rotor flux orientation is used. Rearranging the torque equation by taking into account $\Psi_{rq}=0$ yields

$$T_e = \frac{3}{2}\frac{P}{2}\frac{L_m^{\ 2}}{L_r} i_{sd} i_{sq} \qquad \text{(A.10)}$$

Motor torque equation also can be defined as follows

$$T_e - T_L = j\frac{dw_r}{dt} \qquad \text{(A.11)}$$

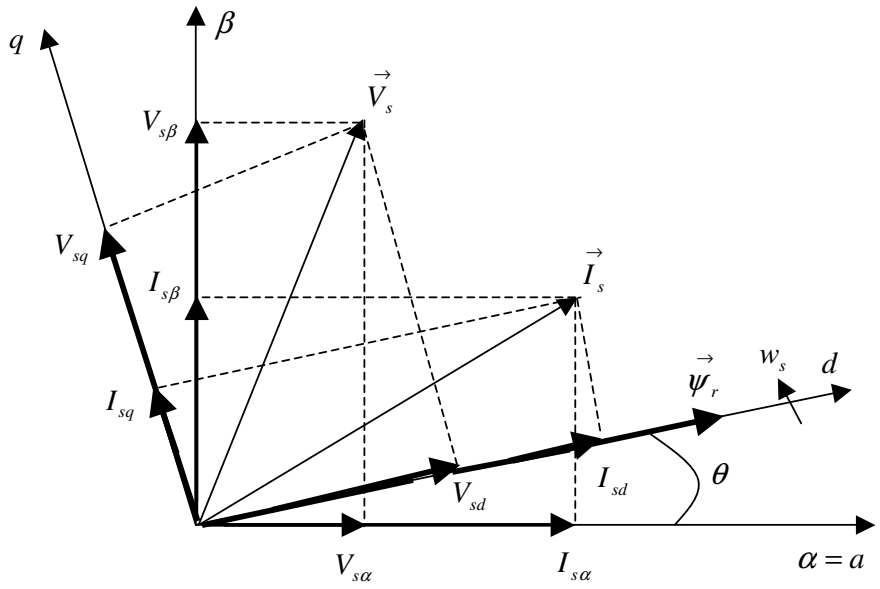

Figure A. 1. Current, voltage and rotor flux vectors in the stationary and rotating reference frames for rotor flux oriented control

Projections on stationary reference frame (α, β) are obtained with w_s=0

$$\begin{bmatrix} I_{s\alpha} \\ I_{s\beta} \end{bmatrix} = \begin{bmatrix} \cos\theta & -\sin\theta \\ \sin\theta & \cos\theta \end{bmatrix} \begin{bmatrix} I_{sd} \\ I_{sq} \end{bmatrix} \tag{A.12}$$

$$\begin{bmatrix} I_{sa} \\ I_{sb} \\ I_{sc} \end{bmatrix} = \begin{bmatrix} 1 & 0 \\ -\frac{1}{2} & \frac{\sqrt{3}}{2} \\ -\frac{1}{2} & -\frac{\sqrt{3}}{2} \end{bmatrix} \begin{bmatrix} I_{s\alpha} \\ I_{s\beta} \end{bmatrix} \tag{A.13}$$

These transformations are applicable to flux and voltage as well as current. d,q and α,β components can be obtained from measured three phase quantities with inverse transformations.

APPENDIX B

Calculation of PI Controller Parameters

The controller design under consideration of high dynamic performance induction motor drive is based on [12].

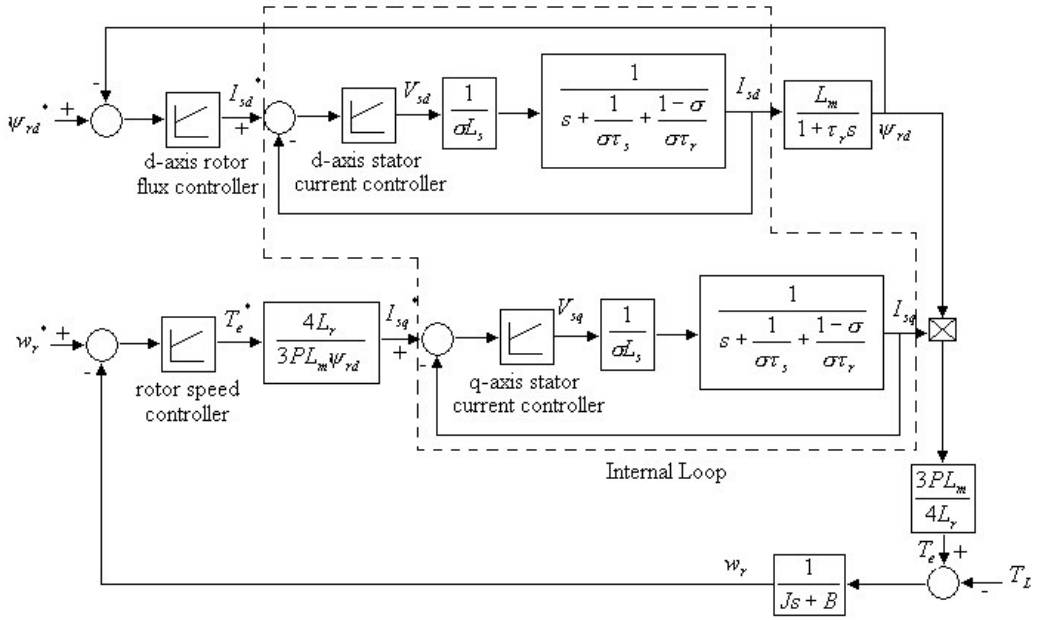

Figure B. 1. Control system of vector controlled induction motor drives

The dynamic model of induction motors for rotor flux oriented vector control applications can be written as follows

$$p\begin{bmatrix} I_{ds} \\ I_{qs} \\ \psi_{rd} \\ \psi_{rq} \end{bmatrix} = \begin{bmatrix} -\frac{1}{\sigma\tau_s} - \frac{1-\sigma}{\sigma\tau_r} & w_e & \frac{L_m}{\sigma L_s \tau_r L_r} & \frac{L_m w_r}{\sigma L_s L_r} \\ -w_e & -\frac{1}{\sigma\tau_s} - \frac{1-\sigma}{\sigma\tau_r} & -\frac{L_m w_r}{\sigma L_s L_r} & \frac{L_m}{\sigma L_s \tau_r L_r} \\ \frac{L_m}{\tau_r} & 0 & -\frac{1}{\tau_r} & w_s \\ 0 & \frac{L_m}{\tau_r} & -w_s & -\frac{1}{\tau_r} \end{bmatrix} \begin{bmatrix} I_{ds} \\ I_{qs} \\ \psi_{rd} \\ \psi_{rq} \end{bmatrix} + \frac{1}{\sigma L_s} \begin{bmatrix} V_{sd} \\ V_{sq} \\ 0 \\ 0 \end{bmatrix} \tag{B.1}$$

Substituting the condition of rotor flux oriented vector control

$$\psi_r = \psi_{rd} + j\psi_{rq} = \psi_{rd} \tag{B.2}$$

$$\psi_{rq} = 0 \tag{B.3}$$

into (B.1) yields

$$p\begin{bmatrix} I_{sd} \\ I_{sq} \\ \psi_{rd} \end{bmatrix} = \begin{bmatrix} -\frac{1}{\sigma\tau_s} - \frac{1-\sigma}{\sigma\tau_r} & w_e & \frac{L_m}{\sigma L_s \tau_r L_r} \\ -w_e & -\frac{1}{\sigma\tau_s} - \frac{1-\sigma}{\sigma\tau_r} & -\frac{L_m w_r}{\sigma L_s L_r} \\ \frac{L_m}{\tau_r} & 0 & -\frac{1}{\tau_r} \end{bmatrix} \begin{bmatrix} I_{sd} \\ I_{sq} \\ \psi_{rd} \end{bmatrix} + \frac{1}{\sigma L_s} \begin{bmatrix} V_{sd} \\ V_{sq} \\ 0 \end{bmatrix} \tag{B.4}$$

and the torque equation becomes

$$T_e = \frac{3}{2}\frac{P}{2}\frac{L_m}{L_r} I_{sq}\psi_{rd} \tag{B.5}$$

Rewriting the Equation (B.1) in the form of decoupling as shown in Equation (B.6), the nonlinearity can be separated from the consideration of controller design.

$$p\begin{bmatrix} I_{sd} \\ I_{sq} \\ \psi_{rd} \end{bmatrix} = \begin{bmatrix} -\frac{1}{\sigma\tau_s} - \frac{1-\sigma}{\sigma\tau_r} & 0 & 0 \\ 0 & -\frac{1}{\sigma\tau_s} - \frac{1-\sigma}{\sigma\tau_r} & 0 \\ \frac{L_m}{\tau_r} & 0 & -\frac{1}{\tau_r} \end{bmatrix} \begin{bmatrix} I_{sd} \\ I_{sq} \\ \psi_{rd} \end{bmatrix} + \frac{1}{\sigma L_s} \begin{bmatrix} V_{sd}^{*} \\ V_{sq}^{*} \\ 0 \end{bmatrix} \quad \text{(B.6)}$$

where

$$\begin{bmatrix} V_{sddecoup} \\ V_{sqdecoup} \end{bmatrix} = \begin{bmatrix} w_e I_{sq} + \frac{L_m}{\sigma L_s \tau_r L_r} \psi_{rd} \\ -w_e I_{sd} - \frac{L_m}{\sigma L_s \tau_r L_r} \psi_{rd} \end{bmatrix} \quad \text{(B.7)}$$

The transfer function of the plant for the controllers of the vector controlled induction motor drives can be derived and shown as follows

d-Axis Current Controller:

$$G_{Id}(s) = \frac{I_{sd}}{V_{sd}} = \frac{\frac{1}{\sigma L_s}}{s + \frac{1}{\sigma L_s} + \frac{1-\sigma}{\sigma\tau_r}} = \frac{\frac{1}{\sigma L_s}}{s + \frac{\tau_r + \tau_s - \sigma\tau_s}{\sigma\tau_s\tau_r}} \quad \text{(B.8)}$$

q-Axis Current Controller:

$$G_{Iq}(s) = \frac{I_{sq}}{V_{sq}} = \frac{\frac{1}{\sigma L_s}}{s + \frac{1}{\sigma L_s} + \frac{1-\sigma}{\sigma\tau_r}} = \frac{\frac{1}{\sigma L_s}}{s + \frac{\tau_r + \tau_s - \sigma\tau_s}{\sigma\tau_s\tau_r}} \quad \text{(B.9)}$$

Flux Controller:

$$G_{\psi}(s) = \frac{\psi_{rd}}{I_{sd}} = \frac{\frac{L_m}{\tau_r}}{s + \frac{1}{\tau_r}} \tag{B.10}$$

Speed Controller:

$$G_s(s) = \frac{w_r}{T_e} = \frac{\frac{1}{J_m}}{s + \frac{B}{J_m}} \tag{B.11}$$

Since the motor plants of q-axis current control, d-axis current control, flux control, and speed control are all first order systems, the design process for these four controllers are similar.

Transfer function of current control system is given below

$$G_I(s) = \frac{I_s}{V_s} = \frac{\frac{1}{\sigma L_s}}{s + \frac{\tau_r + \tau_s - \sigma\tau_s}{\sigma\tau_s\tau_r}} \tag{B.12}$$

For a proportional-integral controller, the controller, C(s), is

$$C(s) = \frac{k_p\left(s + \frac{k_i}{k_p}\right)}{s} \tag{B.13}$$

By using the pole-zero cancellation method, the parameters of the controller are derived and shown as follows

$$k_p = BW \cdot \sigma L_s \tag{B.14}$$

$$k_i = \frac{\tau_r + \tau_s - \sigma\tau_s}{\sigma\tau_s\tau_r} \cdot BW \cdot \sigma L_s \tag{B.15}$$

where BW=bandwidth of the controller.

Calculations performed upto now are valid in continuous time domain. But in real time applications, system is controlled in discrete time domain, so parameters of the controller must be calculated in discrete time domain also. Block diagram of the current controller in discrete time domain is shown in Figure B.2.

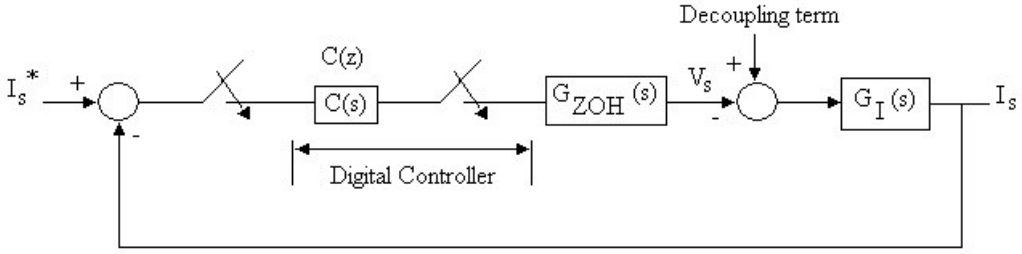

Figure B. 2.Block diagram of the current control system in discrete time domain

The proportional-integral controller in terms of "Z" transforms in the discrete time domain can be derived as shown

$$C(z) = \frac{(k_p + k_i T)z - k_p}{z - 1} \tag{B.16}$$

The controller design in discrete time domain includes the following steps:

1) Calculating the open loop transfer function of the plant
2) Deriving the loop gain of the control system using a pole-zero cancellation method.
3) Deducing the parameters of the controller for the specified bandwidth.

Step 1- Calculating the open loop transfer function of the plant:

The open loop transfer function of the plant in discrete time domain can be derived as

$$\frac{I_s(z)}{\Delta I_s(z)} = C(z) \cdot Z\left[G_{ZOH}(s) \cdot G_I(s)\right]$$

$$= \frac{(k_p + k_i T)\tau_r \tau_s}{L_s(\tau_r + \tau_s - \sigma\tau_s)} \cdot \frac{\left(z - \frac{k_p}{k_p + k_i T}\right)\left[1 - \exp\left(-\frac{\tau_r + \tau_s - \sigma\tau_s}{\sigma\tau_r\sigma_s}T\right)\right]}{(z-1)\left[z - \exp\left(-\frac{\tau_r + \tau_s - \sigma\tau_s}{\sigma\tau_r\tau_s}\right)\right]} \quad \text{(B.17)}$$

Step 2- Deriving the loop gain of the control system using a pole-zero cancellation method:

The relationship between the proportional and integral constants for pole-zero cancellation can be derived as

$$k_p = \frac{\exp\left(-\frac{\tau_r + \tau_s - \sigma\tau_s}{\sigma\tau_r\sigma_s}T\right) \cdot k_i T}{1 - \exp\left(-\frac{\tau_r + \tau_s - \sigma\tau_s}{\sigma\tau_r\sigma_s}T\right)} \quad \text{(B.18)}$$

Substituting Equation (B.18) into Equation (B.17), the transfer function shown in Equation (B.17) becomes

$$\frac{I_s(z)}{\Delta I_s(z)} = \frac{(k_p + k_i T)\tau_r \tau_s}{L_s(\tau_r + \tau_s - \sigma\tau_s)} \cdot \frac{\left[1 - \exp\left(-\frac{\tau_r + \tau_s - \sigma\tau_s}{\sigma\tau_r\sigma_s} T\right)\right]}{(z-1)} \tag{B.19}$$

Step 3- Deducing the parameters of the controller for the specified bandwith:

The closed loop transfer function of the system can be derived as

$$\frac{I_s(z)}{I_s^*(z)} = \frac{\frac{(k_p + k_i T)\tau_r \tau_s \left[1 - \exp\left(-\frac{\tau_r + \tau_s - \sigma\tau_s}{\sigma\tau_r\sigma_s} T\right)\right]}{L_s(\tau_r + \tau_s - \sigma\tau_s)}}{z - 1 + \frac{(k_p + k_i T)\tau_r \tau_s \left[1 - \exp\left(-\frac{\tau_r + \tau_s - \sigma\tau_s}{\sigma\tau_r\sigma_s} T\right)\right]}{L_s(\tau_r + \tau_s - \sigma\tau_s)}} \tag{B.20}$$

By specifying the bandwidth of the first order system, the corresponding representation in discrete time-domain is

$$Z\left[G_{ZOH}(s)\frac{BW}{s + BW}\right] = \frac{1 - \exp(-BW \cdot T)}{z - \exp(-BW \cdot T)} \tag{B.21}$$

Comparing Equation (B.20) and Equation (B.21) yields

$$k_p + k_i T = \frac{\left[1 - \exp(-BW \cdot T)\right] L_s(\tau_r + \tau_s - \sigma\tau_s)}{\tau_r \tau_s \left[1 - \exp\left(-\frac{\tau_r + \tau_s - \sigma\tau_s}{\sigma\tau_r\sigma_s} T\right)\right]} \tag{B.22}$$

$$k_i = \frac{\left[1 - \exp(-BW \cdot T)\right] L_s(\tau_r + \tau_s - \sigma\tau_s)}{\tau_r \tau_s T} \tag{B.23}$$

$$k_p = \frac{\exp\left(-\frac{\tau_r + \tau_s - \sigma\tau_s}{\sigma\tau_r\sigma_s}T\right)\left[1-\exp(-BW\cdot T)\right]L_s(\tau_r+\tau_s-\sigma\tau_s)}{\tau_r\tau_s\left[1-\exp\left(-\frac{\tau_r+\tau_s-\sigma\tau_s}{\sigma\tau_r\sigma_s}T\right)\right]} \tag{B.24}$$

Flux Controller:

$$k_i = \frac{\left[1-\exp(-BW\cdot T)\right]}{L_m T} \tag{B.25}$$

$$k_p = \frac{\exp\left(-\frac{1}{\tau_r}T\right)\left[1-\exp(-BW\cdot T)\right]}{\left[1-\exp\left(-\frac{1}{\tau_r}T\right)\right]L_m} \tag{B.26}$$

Speed Controller:

$$k_i = \frac{\left[1-\exp(-BW\cdot T)\right]B_m}{T} \tag{B.27}$$

$$k_p = \frac{\exp\left(-\frac{B_m}{J_m}T\right)\left[1-\exp(-BW\cdot T)\right]B_m}{\left[1-\exp\left(-\frac{B_m}{J_m}T\right)\right]} \tag{B.28}$$

PI controller parameters of the vector controlled system for different bandwidth values are given in Table B.1. In the application, PI controller parameters calculated for 314 rad/sec are used.

Table B. 1. PI controller parameters for different bandwidth values

Bandwidth of PI controller parameters (rad/sec)	k_i	k_p
314	3195	6,97
500	5041	10,99
1000	9837	21,45

APPENDIX C

Calculation of Motor Parameters And Reference Currents for Vector Control

No load and locked rotor tests are performed to obtain motor parameters. In no load test, motor is driven with three phase voltage in no load condition. Motor voltage is increased until its rated value. Motor current and three phase real power are measured for different voltage levels. In locked rotor test, motor shaft is locked mechanically and voltage is increased so that rated current flows in the motor. Motor phase to phase voltage and motor currents are measured. As a result of these tests; leakage inductance, mutual inductance and rotor resistance are calculated.

No load test:

Input power and motor current are measured at different voltage levels. Motor input power for different voltage levels are given in the following figure.

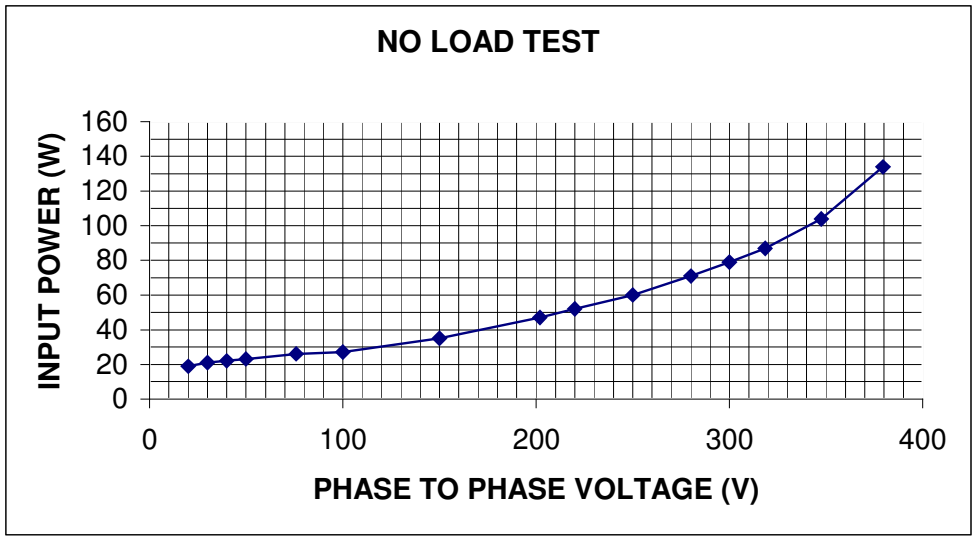

Figure C. 1. Input power at different voltage levels for no load test

As seen from the figure motor rotational loss is 20 W. Motor current and input power at rated voltage are called as no load current (I_{nl}) and no load power (P_{nl}) respectively. Following measurements are taken in test

$$Vnl = 380\ V \tag{C.1}$$

$$Inl = 1.8\ A \tag{C.2}$$

$$Pnl = 134\ W \tag{C.3}$$

Motor no load resistance, no load impedance and no load reactance can be calculated as follows

$$R_{nl} = \frac{P_{nl} - P_{rot}}{3 \cdot I_{nl}^{\ 2}} = \frac{134 - 20}{3 \cdot 1.8^2} = 11.73\Omega \tag{C.4}$$

$$Z_{nl} = \frac{V_{nl}}{\sqrt{3} \cdot I_{nl}} = \frac{380}{\sqrt{3} \cdot 1.8} = 121.885\Omega \tag{C.5}$$

$$X_{nl} = \sqrt{\left(Z_{nl}^{\ 2} - R_{nl}^{\ 2}\right)} = \sqrt{\left(121.885^2 - 11.73^2\right)} = 121.29\Omega \tag{C.6}$$

Locked Rotor Test:

Motor phase to phase voltage and input power at rated current are called as locked rotor voltage (V_{lr}) and locked rotor power (P_{lr}) respectively. Following measurements are taken in test

$$V_{lr} = 60 \text{ V} \tag{C.7}$$

$$I_{lr} = 2.7 \text{ A} \tag{C.8}$$

$$P_{lr} = 230 \text{ W} \tag{C.9}$$

Motor locked rotor resistance, locked rotor impedance and locked rotor reactance can be calculated as follows

$$R_{lr} = \frac{P_{lr}}{3 \cdot I_{lr}^{\ 2}} = \frac{230}{3 \cdot 2.7^2} = 10.517\Omega \tag{C.10}$$

$$Z_{lr} = \frac{V_{lr}}{\sqrt{3} \cdot I_{lr}} = \frac{60}{\sqrt{3} \cdot 2.7} = 12.83\Omega \tag{C.11}$$

$$X_{lr} = \sqrt{\left(Z_{lr}^{\ 2} - R_{lr}^{\ 2}\right)} = \sqrt{\left(12.83^2 - 10.517^2\right)} = 7.349\Omega \tag{C.12}$$

Stator and rotor leakage reactance values are equal to each other and calculated as follows

$$X_{lstator} = X_{lrotor} = \frac{X_{lr}}{2} = \frac{7.349}{2} = 3.675\Omega \tag{C.13}$$

Mutual reactance can be calculated by using no load reactance and stator leakage reactance as follows

$$X_m = X_{nl} - X_{lstator} = 121.29 - 3.675 = 117.615\Omega \quad \text{(C.14)}$$

Stator winding resistance is measured with a micro ohm meter and found to be 4.5 Ω.

Rotor winding resistance is the difference between locked rotor resistance and stator winding resistance and can be calculated as follows

$$R_r = R_{lr} - R_s = 10.517 - 4.5 = 6.017\Omega \quad \text{(C.15)}$$

Stator and rotor leakage inductances can be calculated from stator and rotor leakage reactance values as follows

$$L_{ls} = L_{lr} = \frac{X_{lstator}}{2 \cdot \pi \cdot f} = \frac{X_{lrotor}}{2 \cdot \pi \cdot f} = \frac{3.675}{2 \cdot \pi \cdot 50} = 11.7mH \quad \text{(C.16)}$$

Mutual inductance is calculated from mutual reactance as follows

$$L_m = \frac{X_m}{2 \cdot \pi \cdot f} = \frac{117.615}{2 \cdot \pi \cdot 50} = 375mH \quad \text{(C.17)}$$

Rotor and stator self inductance values are calculated with the following formula

$$L_s = L_r = L_{ls} + L_m = L_{lr} + L_m = 11.7 + 375 = 386.7mH \quad \text{(C.18)}$$

The flux reference (I_{sd}) must be adjusted to the value which corresponds to maximum non-saturated flux value [5]. This flux value is calculated by using nameplate data of the motor as shown below

$$E_{lm} = \sqrt{\left[(V_{1n}\cos\varphi_n - R_s I_{sn}) + (V_{1n}\sin\varphi_n - w_s \sigma L_s I_{sn})\right]} \quad \text{(C.19)}$$

$$\psi_{mn} = \frac{E_{lm}\sqrt{2}}{w_s} \quad \text{(C.20)}$$

$$I_{sdref} = \frac{\psi_{mn}}{L_m} \quad \text{(C.21)}$$

The variables used in the equations are defined in variables and symbols section.

$$E_{lm} = \sqrt{\left[(220 \cdot 0.76 - 4.35 \cdot 2.7)^2 + (220 \cdot 0.65 - 314 \cdot 0.0233 \cdot 2.7)^2\right]} = 198.4V \quad \text{(C.22)}$$

$$\psi_{mn} = \frac{198.4 \cdot \sqrt{2}}{314} \cong 0.9Wb \quad \text{(C.23)}$$

$$I_{sdref} = \frac{0.9}{0.375} = 2.4A \quad \text{(C.24)}$$

Reference value of torque producing component can be calculated by using torque equation as shown below

$$T_{eref} = \frac{3}{2}\frac{P}{2}\frac{{L_m}^2}{L_r} I_{sdref} I_{sqref} \quad \text{(C.25)}$$

Following equation is obtained for the torque producing component of the current

$$I_{sqref} = 0.78 \cdot T_{eref} \quad \text{(C.26)}$$

Reference current for different torque values are given in the following table

Table C. 1. Torque producing component of current for different torque references

T_{eref} (Nm)	I_{sqref} (A)
1	0,78
1,5	1,17
2	1,56
2,5	1,95
3	2,34
3,5	2,73
4	3,12